POLITECNICO
MILANO 1863

SCUOLA DI INGEGNERIA INDUSTRIALE
E DELL'INFORMAZIONE

Analysis and modelling of natural gas grids in presence of biomethane and hydrogen injections

TESI DI LAUREA MAGISTRALE IN
ENERGY ENGINEERING
INGEGNERIA ENERGETICA

Author: **Marco Sapienza**

Student ID: 964416
Advisor: Giulio Guandalini
Co-advisor: Paolo Colbertaldo
Academic Year: 2021-22

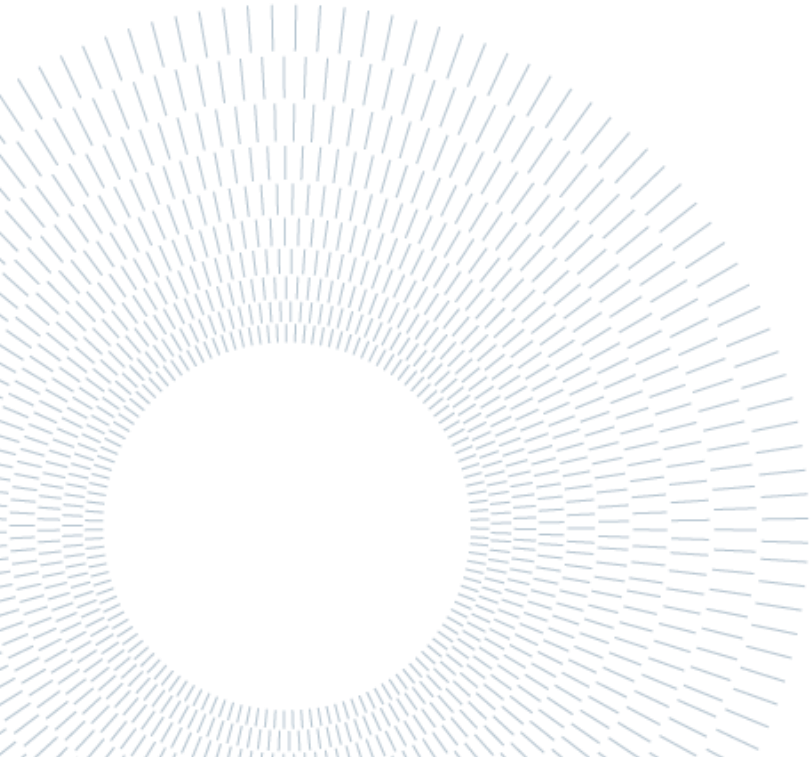

Abstract

In last decades, the global energy scenario has faced multiple changes that include the transition from conventional fossil to more sustainable fuels. In the projections, natural gas is expecting to have an increasing role, and sustainable fuels, like biomethane and hydrogen, can represent a valid alternative. In this new scenario of the gas system, modelling and simulation of gas networks, in particular in the presence of alternative sources, is essential for gas companies. This work analyses the current biomethane scenario and the testing projects for grids transporting natural gas – hydrogen blends or pure hydrogen at experimental or pilot level in Europe and the world, determining the main critical aspects of the technology and its potential development in the future. Furthermore, a model for the simulation of gas networks is studied and applied to a distribution network. As model applications, biomethane and hydrogen decentralized injections in different positions of the grid and with different flow rates have been studied, as well as different natural gas-hydrogen blends and a grid supplied by pure hydrogen. Particular attention has been paid to the critical network operating conditions: pressure levels, maximum velocity, flow rate introduced. Finally, in the case of hydrogen injections, the concept of gas quality tracking is introduced to study the composition of the gas in the nodes of the network and the energy supplied to each of them.

Key-words: Alternative gas injection; Biomethane; Hydrogen; Distribution grid simulation.

Abstract in italiano

Negli ultimi decenni, lo scenario energetico mondiale ha affrontato molteplici cambiamenti che includono il passaggio dalle risorse energetiche convenzionali a quelle sostenibili. In questa prospettiva, il gas naturale avrà un ruolo sempre più significativo, e i gas sostenibili, come biometano e idrogeno, potranno rappresentare una valida alternativa. In questo nuovo scenario, la modellazione e la simulazione delle reti gas, soprattutto in presenza di fonti alternative, sono essenziali per le compagnie di gas. Questo lavoro analizza lo scenario corrente del biometano e i progetti di prova per reti che trasportano miscele di gas naturale e idrogeno a livello sperimentale in Europa e nel mondo, individuando i principali aspetti critici della tecnologia e il suo potenziale per il futuro. Successivamente, un modello per la simulazione di reti gas è studiato e applicato a una rete di distribuzione. Come applicazioni del modello, sono state studiate le immissioni decentralizzate di idrogeno e biometano in posizioni diverse della rete e con quantità diverse di gas, oltre a reti con diverse miscele di gas naturale e idrogeno e una rete alimentata da idrogeno puro. È stata data particolare attenzione alle condizioni critiche operative: livelli di pressione, velocità massima, quantità di gas introdotto. Infine, nel caso di immissioni di idrogeno, il concetto di "gas quality tracking" (tracciamento della qualità del gas) è stato introdotto al fine di analizzare la composizione del gas nei vari nodi della rete e l'energia fornita a ciascuno di loro.

Parole chiave: Iniezione di gas alternativi; Biometano; Idrogeno; Simulazione di una rete di distribuzione.

Contents

1 Introduction

Due to climate change, the global energy market is in the middle of a sustainable transformation. In the last years, sustainable policies of countries, climate actions and commission strategies have led to substitute hydrocarbon fuel, such as oil and coal, with natural gas, that is a lower carbon fuel. The use of natural gas as primary energy provides a halving of CO_2 emissions with respect to oil and coal. However, this solution is not able to satisfy the high targets defined by the EU 2050 long term strategy [1].

Therefore, the introduction in the energy market of alternative green fuels, such as biomethane and hydrogen, is necessary to achieve zero-carbon emission and mitigate climate effects.

Figure 1.1 shows the primary energy consumption by sources in 2050 for the different world regions according to the Net Zero Emissions scenario, in which natural gas and renewable sources will replace high-carbon fuels.

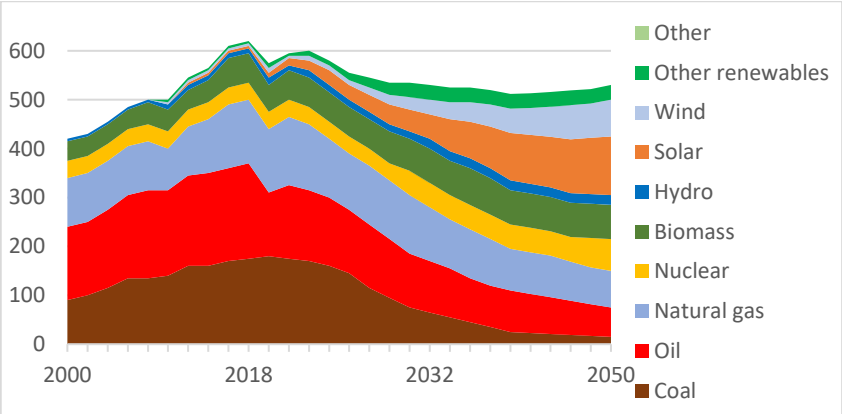

Figure 1.1: Total Energy supply in the Net Emission Zero scenario [2]

The fluctuation of wind and solar sources generates the loss of a large amount of energy. The surplus of electricity generated can be used by power-to-gas facilities to produce green pure hydrogen gas. The injection of the resulting fuel into gas networks would contribute to decarbonise the gas system and mitigate climate

change. However, due to its characteristics, hydrogen highly impacts on behaviour of gas networks and properties of the gas delivered to users.

In this new scenario of the gas system, modelling and simulation of gas networks, in particular in the presence of alternative sources, is essential for gas companies.

1.1. Current and future gas distribution systems

Natural gas helps to reduce atmospheric emissions by replacing polluting fossil fuels and reducing problems of air quality, acid rain and greenhouse emissions. It is mainly composed of methane and the main products releasing from its combustion are carbon dioxide (CO_2) and water vapour.

For the same energy input, the carbon dioxide produced by the combustion of natural gas is 25-30% less than oil products and 40-50% less than coal. The combustion of natural gas releases small amounts of sulphur dioxide and nitrogen oxides, it does not generate ash emissions or particulates and emits low levels of carbon dioxide, carbon monoxide and other reactive hydrocarbons. The decrease in emissions per unit of energy is further accentuated by the possibility of using natural gas in high-performance applications and technologies, such as condensation boilers, co-generation plants and combined cycles for producing electricity.

Natural gas resources are widely distributed around the world (figure 1.2). However, the main gas reserves are located in the Commonwealth of Independent States (CIS), Middle East and North America. Africa and Latin America, even if they do not have the bigger reserves, are the regions with the largest number of years of technically recoverable resources. As a consequence of gas reservoirs and customers located around the world, gas trade flows between countries and regions are massive. From production sites to the places of use, the natural gas can be transported by LNG carriers or onshore/offshore pipelines.

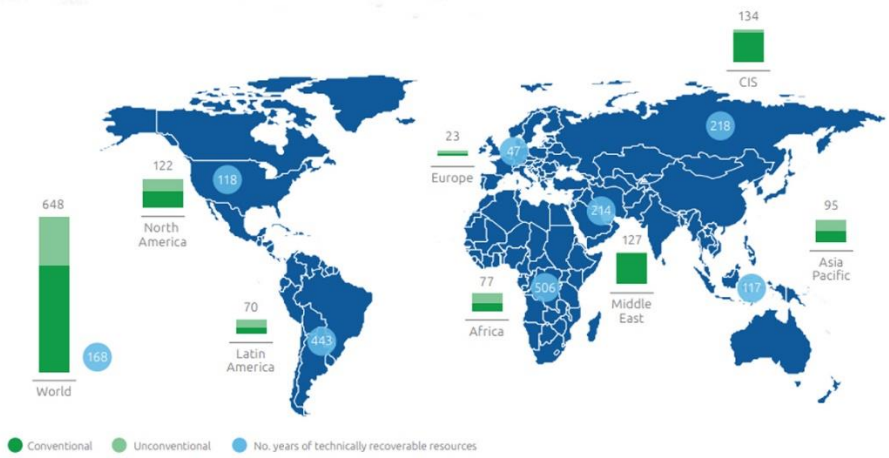

Figure 1.2: Natural gas technically recoverable resources by region (10^3 m^3) [3]

Decarbonising the gas system is a potential and essential solution to reduce greenhouse gas emissions and especially CO_2 emissions. This goal can be achieved partly (1st step) and fully (2nd step) substituting the traditional natural gas flowing into gas networks with green gases. In particular, biomethane and hydrogen will play a crucial role in the decarbonisation of the gas network and so to achieve the zero-carbon emission objective.

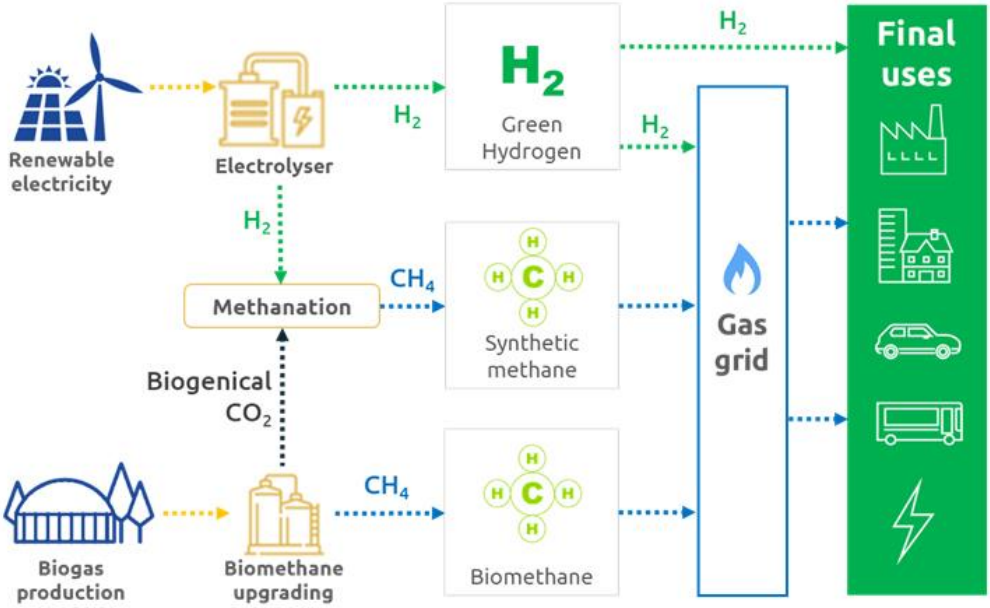

Figure 1.3: Alternative gases processes for energy transition [3]

1.1.1. Present scenario

Natural gas systems are very large complex structures, which aim to treat, transport, storage, distribute the gas and lastly increase/decrease gas pressure. The first stage of the supply chain is the production stage, where natural gas plants extract the gas situated in underground reserves, remove contaminants (CO_2, H_2S, heavy hydrocarbons, etc.) and sometimes liquify the gas. After that, long onshore/offshore pipelines and LNG carriers are responsible for moving and transferring the natural gas from one country to another (supply stage). In Italy, pipes are classified in seven species depending on their maximum operating pressure (MOP).

Table 1.1: Pipeline classification (based on MOP) [4]

Species	I	II	III	IV	V	VI	VII
MOP [bar]	> 24	12-24	5-12	1,5-5	0,5-1,5	0,04-0,5	<0,04

National and regional transmission adopts generally high-pressure pipes (MOP > 5 bar; I-III species), while at the distribution level medium-pressure pipes (IV-VI species) are applied. Low-pressure levels (MOP < 0,04 bar; VII species) are reached only at the final customer reduction.

Pipeline networks consist of supply and withdrawal nodes, connected by pipelines with different diameters and lengths. Supply nodes are the ones where the inlet pressure is defined, giving at least one boundary condition on the working pressure for the whole network. In the transmission grid, high pressure levels are needed to transport high gas flow rates, and supply nodes are coupled with compression stations. Moreover, other than maximum operating pressure requirements (due to mechanical resistance issues), the minimum one may be also constrained at some withdrawal points to secure the gas supply. To satisfy these requirements, some compressors may be disposed throughout the network to compensate for frictional pressure losses.

The distribution grid, on other hand, is connected to the main line by means of a reducing and metering station (REMI). The gas flow needs to be expanded up to a pressure level suitable for the supply to the final customer. Compressors are not displaced at this level, and simulation models are applied.

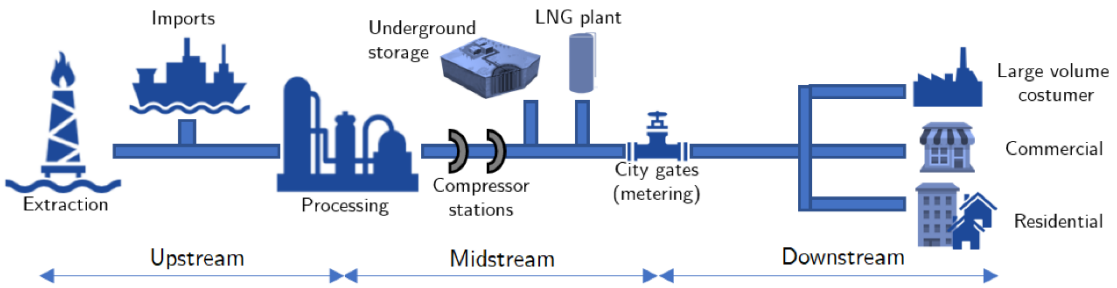

Figure 1.4: Scheme of a generic whole gas system [3]

1.1.2. Role of biomethane

Biomethane can answer to emission reduction goals by exploiting existing gas networks and contributing to increase domestic methane production.

Biomethane is a renewable energy source derived from agricultural biomass (dedicated crops, by-products and agricultural waste and animal waste), agro-industrial (waste from the food processing chain) and the Organic Fraction Municipal Solid Waste (OFMSW). It is obtained in two-phases: raw biogas production, predominantly through anaerobic digestion of biomass, and subsequent removal of non-compatible components (CO_2).

Biomethane can already be injected into the network and used in all sectors where the gas is present.

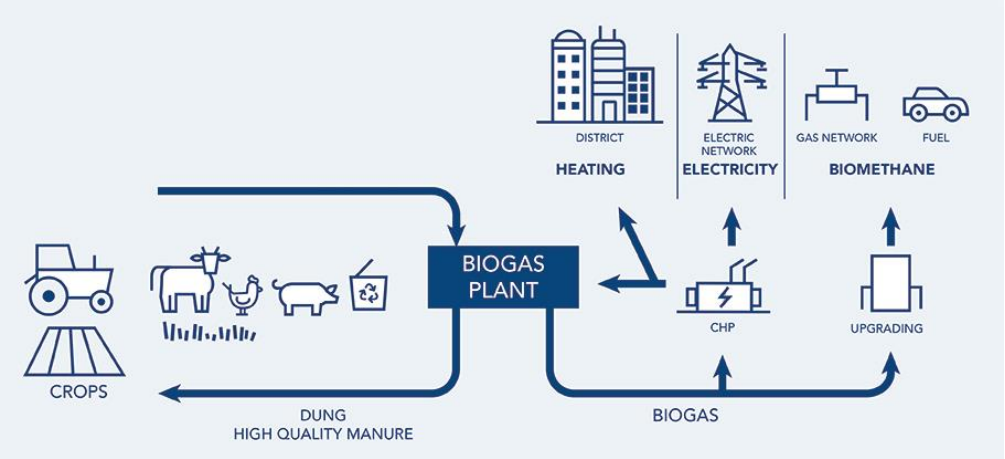

Figure 1.5: Biomethane production process [3]

1.1.3. Role of hydrogen

The most significant aspect of hydrogen is that it does not generate, in the final uses, carbon dioxide emissions or other climate-changing gases, nor does it produce emissions that are harmful for humans and the environment. It is the first element of periodic table and the most abundant in the universe and it is present, combined with other elements, in compounds such as water or minerals, hydrocarbons and biological molecules.

Hydrogen is not present in nature in its essential form. However, it can be produced through a wide range of chemical and physical processes. Currently, it is mainly obtained from natural gas for industrial uses, through a thermochemical conversion process with CO_2 production ("grey hydrogen"). CO_2 capture and storage (CCS) technology can be added to this to obtain decarbonised hydrogen ("blue hydrogen"). Another method is electrolysis, which involves the use of renewable electricity to "break down" the water into hydrogen and oxygen, without producing CO2, thus obtaining "green hydrogen". To date, approximately 4 to 5% of global hydrogen is obtained in this way [3]. However, in light of the progressive reduction in the cost of solar and wind power and electrolysers, this mode of production could prove to be a key for energy transition.

Hydrogen is suitable to be transported in the existing gas pipelines, to act as an efficient and cheaper mean than batteries for energy storage and to favour the decarbonisation of various industrial and heavy transport sectors. It is already used for industrial purposes across the steel, petrochemical and food sectors, but it now also being used in mobility. In the future, it could also replace natural gas to heat residential and commercial buildings and it could be transformed into clean electricity by injecting it into fuel cells.

The pathway to net zero emissions by 2050 requires substantially wider hydrogen use in existing applications and a significant uptake of hydrogen fuels.

1.2. Thesis outline

This thesis has the objective of (1) analyse the testing projects for grids transporting natural gas – hydrogen blends or pure hydrogen at experimental or pilot level in Europe and the world; (2) identify critical aspects in the development of such grids and outline relevant elements for experimental assessments; (3) simulate the expected behaviour of a pilot-scale grid using a simulation model in Matlab and analyse the effects of the injection of biomethane and hydrogen in the distribution

network. Particular attention will be paid to the physical properties of the gas flowing in the grid (pressure, velocity) and on the composition of the gas supplied to the withdrawal nodes of the network, introducing the concept of gas quality tracking.

2 Alternative gases State of the Art

As mentioned above, natural gas and renewable sources will replace high-carbon fuels in the next future. For many of the world regions, natural gas will dominate the energy market with a percentage between 25 and 57 of the total energy produced [2]. In 2033, natural gas will provide to users the maximum amount of energy (5500 Gm^3/year), which corresponds to an increment of 19% than today (figure 2.1). The main natural gas customers are and will be power generation, followed by residential users and manufacturing industries. In the next ten years, a significant increment of the natural gas demand, by these three principal sectors, is expected. Thereafter, the consumption of natural gas will be substantially constant or slightly decreasing until 2050.

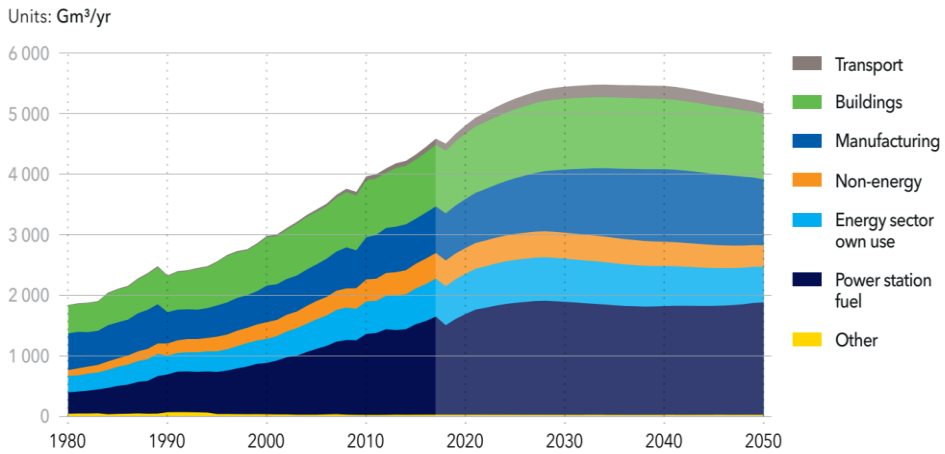

Figure 2.1: World natural gas demand by sector [2]

The injection of biomethane and green hydrogen is currently seen as the next step towards the decarbonization of the gas sector in several countries. However, the introduction of these gases in existent infrastructure has energetic, material and operational implications that should be carefully looked at. Furthermore, the adequate performance of end-use equipment connected to the grid must be accounted for. Throughout the world, several projects are already underway to assess the impact of small injections of hydrogen on pipelines and on end consumption, whereas biomethane is already widely used in some countries. This

chapter analyses the state of the art of the exploitation of these gases for energy uses, reporting the current scenario and the future projects, as well as their impact on existent infrastructure, with hydrogen presenting the most significant bottlenecks due to its material and energetic impacts.

2.1. Biogas production and outlook

Biogas production can contribute significantly to CO_2 emission reduction and its injection in the natural gas infrastructure, after an upgrading process (biomethane), is one of the most suitable pathways for enhancing biogas use.

Raw biogas is a mixture of CH_4 (40-75%), CO_2 (15-60%), H_2O (5-10%) and traces of other gases (namely H_2S and NH_3). The precise composition of biogas depends on the type of feedstock and the production pathway. This variation means that the energy content can vary; the lower heating value is between 16 and 28 MJ/m^3. Almost two-thirds of biogas production in 2018 was used to generate electricity and heat (with an approximately equal split between electricity-only facilities and co-generation facilities) [5]. Around 30% was consumed in buildings, mainly in the residential sector for cooking and heating, with the remainder upgraded to biomethane and blended into the gas networks or used as transport fuel [5]. In 2018, around 18 GW of installed power generation capacity were running on biogas around the world, most of which is in Germany, the United States and the United Kingdom [5]. Capacity increased on average by 4% per year between 2010 and 2018.

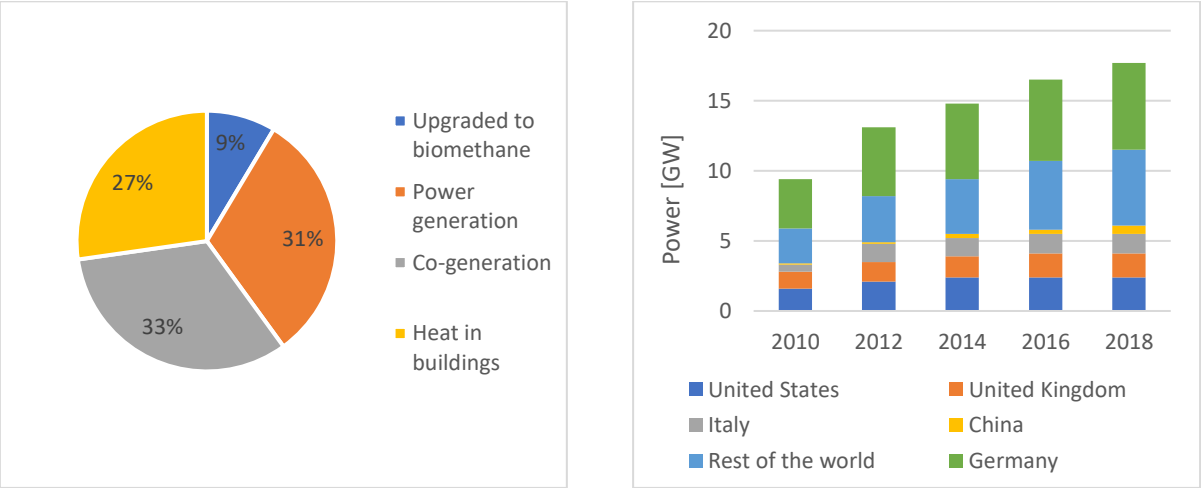

Figure 2.2: Biogas consumption by end use, 2018 (left); biogas power generation capacity, 2010-2018 (right) [5]

In the Sustainable Development Scenario (SDS) [6], developed by IEA, biogas provides a source of clean cooking to an additional 200 million people by 2040, half of which in Africa (figure 2.3).

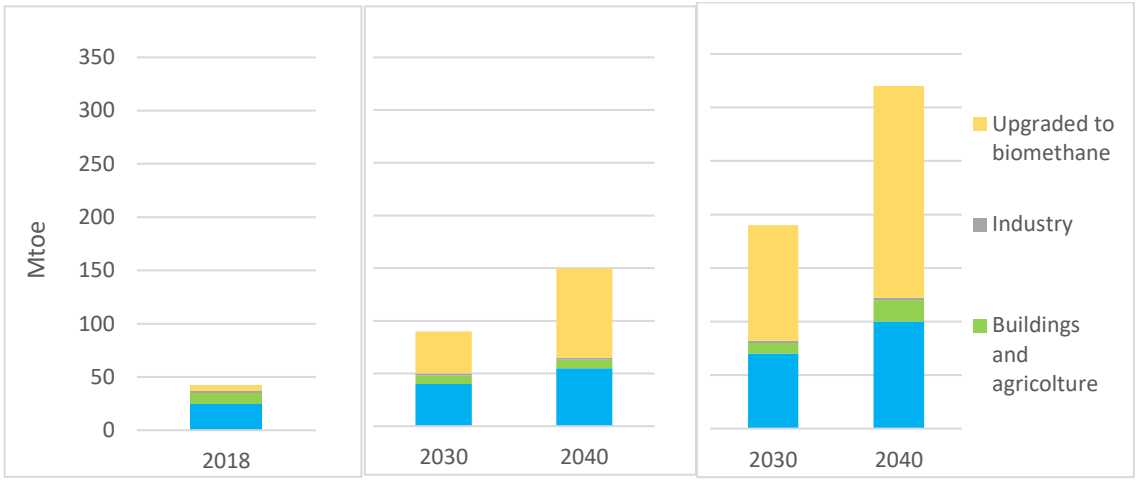

Figure 2.3: The outlook for biogas consumption by sector [6]: 2018 (left); 2030-2040 in the stated policies (middle); 2030-2040 in the SDS (right) (note: 1 Mtoe = 11,63 TWh)

2.2. Biomethane current scenario and outlook

Biomethane is a near-pure source of methane produced either by "upgrading" biogas (a process that removes CO_2 and other contaminants present in the biogas) or through the gasification of solid biomass followed by methanation.

Biomethane has an LHV around 36 MJ/m^3. It is indistinguishable from natural gas and so can be used without the need for any changes in transmission and distribution infrastructure or end-user equipment and is fully compatible for use in natural gas vehicles.

The biomethane industry is currently very small, although it is generating growing amount of interest in several countries for its potential to deliver clean energy to a wide array of end users, especially when this can be done using existing infrastructures. Currently, most of the production lies in European and North American markets, with some countries such as Denmark and Sweden boasting more than 10% shares of biogas/biomethane in total gas sales, while countries outside Europe and America are catching up quickly, with the number of upgrading facilities in Brazil and India tripling since 2015 [5].

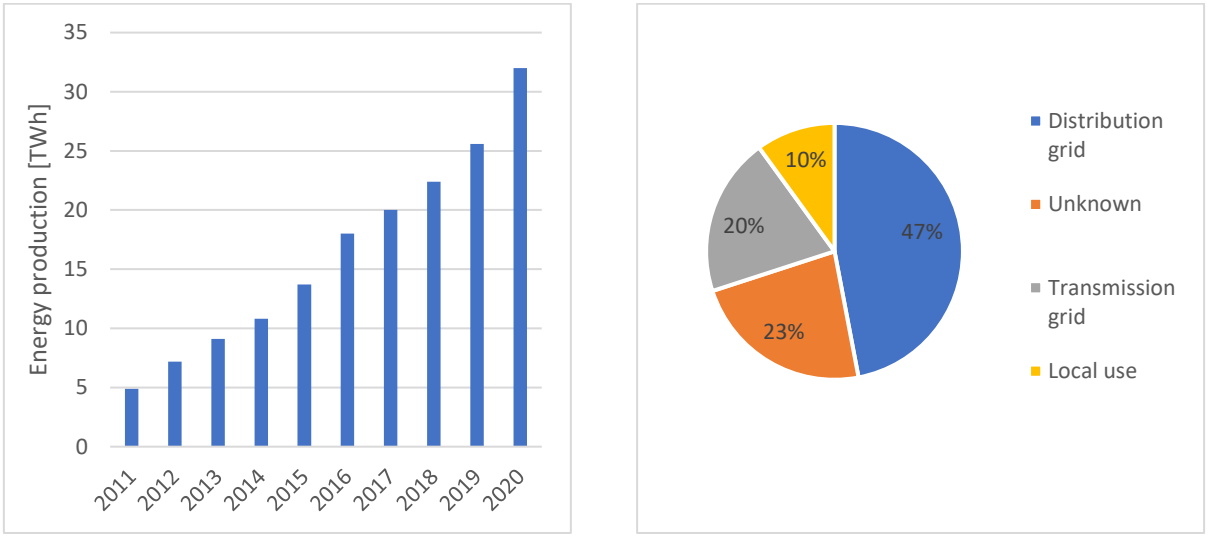

Figure 2.4: Evolution of biomethane production in Europe (left); distribution of biomethane plants per grid connection type, 2021 (right) [7]

Biomethane represents about 0,1% of natural gas demand today [5]; however, an increasing number of government policies are supporting its injection into natural gas grids for decarbonising transport. For example, Germany, Italy, the Netherlands and the United Kingdom have all introduced support for biomethane in transport [5]. Brazil's RenovaBio programme has a target of reducing the carbon intensity of fuels in the transport sector by 10% by 2028 [5]. Subnational schemes are also emerging, such as low-carbon fuel standard in the US state of California and in British Columbia, Canada [5].

In the SDS scenario, biomethane avoids around 1000 million tonnes of greenhouse gases emissions in 2040 [6]. This includes the CO_2 emissions that would have occurred if natural gas had been used instead, as well as the methane emissions that would otherwise have resulted from the decomposition of feedstocks.

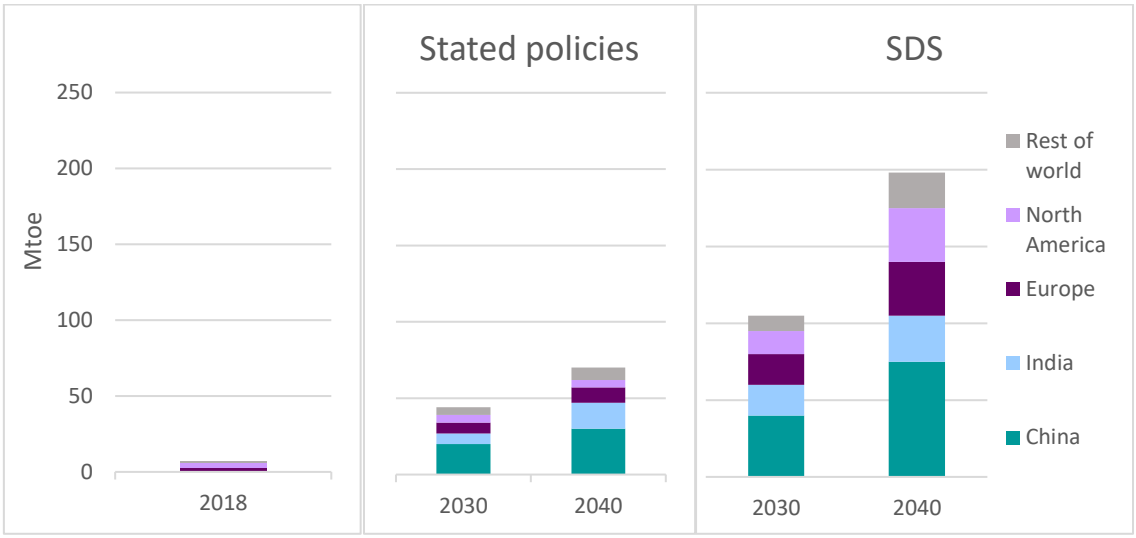

Figure 2.5: The outlook for global biomethane consumption by region [6]

2.3. Hydrogen production

Hydrogen is currently used mainly in the chemical industry for the production of ammonia and methanol and in the refinery sector, but the diversity of energy sources that can produce it makes hydrogen a promising energy carrier.

Steam reforming is currently one of the most widespread and at the same time least expensive processes for hydrogen production. Its advantage arises from the high efficiency of its operation and the low operational and production costs. The most frequently used raw materials are natural gas and lighter hydrocarbons, methanol and other oxygenated hydrocarbons. The network of reforming reactions for hydrocarbons and methanol used as feedstock is the following:

$$C_mH_n + mH_2O\ (g) \rightarrow\ mCO + (m + 0{,}5n)H_2$$

$$C_mH_n + 2mH_2O\ (g)\ \rightarrow\ mCO_2 + (2m + 0{,}5n)H_2$$

$$CO + H_2O\ (g) \rightarrow CO_2 +\ H_2$$

$$CH_3OH + H_2O\ (g) \rightarrow CO_2 +\ 3H_2$$

A promising method for the production of hydrogen in the future could be water electrolysis. The electrolysis of water or its breaking into hydrogen and oxygen is a well-known method which began to be used commercially already in 1890. It is a

process in which a direct current passing through two electrodes in a water solution results in the breaking of the chemical bonds present in water molecule into hydrogen and oxygen:

$$Cathode: 2H_2O\ (l) + 2e^- \rightarrow\ H_2\ (g) +\ +2OH^-$$

$$Anode: 4OH^-\ \rightarrow\ O_2\ (g) +\ +2H_2O\ (l) +\ 2e^-$$

$$Overall: 2H_2O \rightarrow\ 2H_2 +\ O_2$$

The most common electrolysis technology is alkaline-based but proton exchange membrane (PEM) and solid oxide electrolysis cells (SOEC) have been developed.

Electrolysis is a process that is becoming of interest by gas, electricity and hydrogen companies thanks to the possibility to use electricity generated by renewable sources (power-to-gas, P2G). In fact, fluctuating and intermittent renewable sources, such as wind and solar, produce electricity which is only partially used by the electric grid; the surplus of energy can be used by power-to-gas systems to produce, by water electrolysis, hydrogen gas that could be injected into the natural gas grid, as an alternative to develop a dedicated new infrastructure.

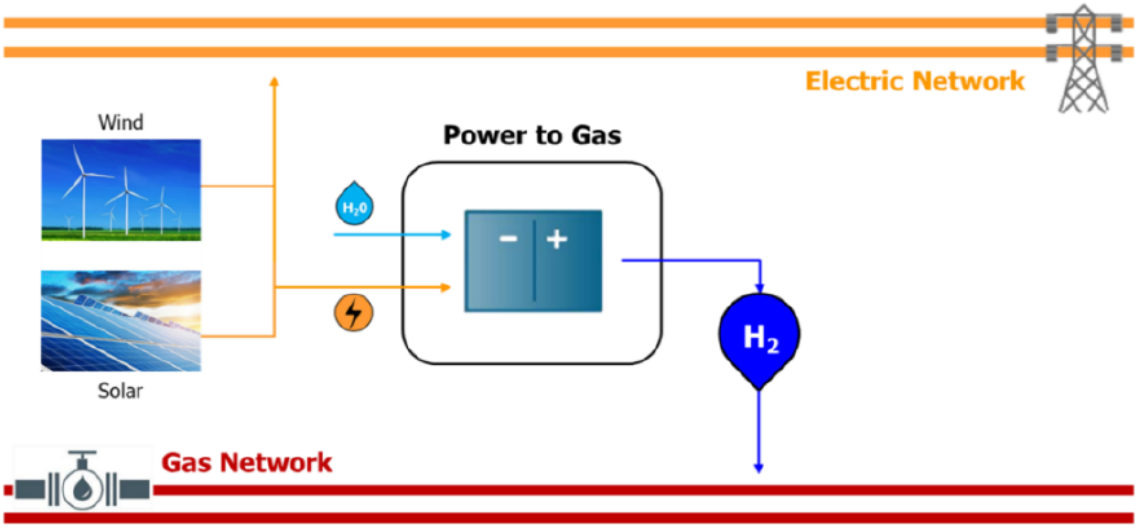

Figure 2.6: Scheme of a power-to-gas solution to produce hydrogen fuel

2.4. Hydrogen blending projects

Though the concept of blending hydrogen with natural gas is not new (IGT 1972 [8]), the rapid growth in installed wind power capacity has increased the interest in the power-to-gas initiatives. Blending hydrogen into the existing natural gas pipeline network has been proposed as a mean of increasing the output of renewable energy systems. As a hydrogen delivery method, blending can avoid the cost of building dedicated hydrogen pipelines or other costly delivery infrastructure during the early market development phase.

In table 2.1, a list of projects and initiatives regarding the injection of hydrogen into the grid in Europe and in the world is reported.

Table 2.1: Projects of hydrogen blending into the grid

Project name	Location	Status	Expected start-up date	% H_2 max	H_2 source	Size
H21	Leeds (UK)	Feasibility studies	2029	100	4 SMRs	1025 MW
HyDeploy [10]	Keele University (UK)	Completed	From Oct '19 to Spring '21	20	Electrolyzer	0,5 MW
	Winlaton (UK)	Operational	From August '21 to late '22			668 homes, several businesses
	UK and Ireland	Preparation	By the end of 2023			1 GW by 2025, 5 GW by 2030
Avacon [11]	Germany	Operational	2021	20	Electrolyzer	350 customers
Fort Saskatchewan [12]	Alberta (Canada)	Preparation	Fall 2022	5	Electrolyzer	2000 customers
MosaHYc [13]	Germany/ France/ Luxembourg border	Preparation	2026	100	Electrolyzer	60 MW
Snam project [14, 15]	Contursi Terme (Italy)	Completed	019	5 and 10	Electrolyzer	$70 * 10^9$ m^3/year
Snam project [16]	Rho (Italy)	Completed	2021	30	Electrolyzer	-
HyBRIDS [17]	Pescara (Italy)	Preparation	2025	1	Electrolyzer	Up to 72 ton/y
HyP SA [18]	Tonsley (Australia)	Operational	2021	5	Electrolyzer	1,25 MW
H100 Fife [19]	Buckhaven and Methil (Scotland)	Preparation	2023	100	Electrolyzer	300 local houses
GRHYD [20]	Dunkirk (France)	Completed	2020	20	Electrolyzer	200 houses
Enbridge project [21]	Markham (Canada)	Operational	2022	2	Electrolyzer	8 MW

One of the most relevant projects that is taking place today is the HyDeploy project [10] in the UK. It is the UK's first practical project to demonstrate that hydrogen can

be safely blended into the natural gas distribution system without requiring changes to appliances and the associated disruption. HyDeploy is structured into three distinct phases:

- Phase 1 – Keele University Trial

  In October 2019, a testing of a blend of fossil gas and hydrogen on part of the private gas network at Keele University campus, Staffordshire, took place. During the 18-month trial, 100 homes and 30 university buildings received the blended gas up to 20% by volume of hydrogen. Laboratory testing was conducted on a range of gas appliances and materials, confirming that blended hydrogen up to 20% by volume does not interact negatively on existing infrastructures. This phase concluded in Spring 2021.

- Phase 2 – Winlaton Trial

  A larger trial was conducted in Winlaton, near Gateshead, from August 2021 for 10 months, until June 2022. It involved 668 houses, a school, several small businesses and a church with a 20% hydrogen blend, supplying more evidence to support the safety of blending hydrogen into the gas network across the UK and demonstrating that hydrogen can be used safely in the public gas network.

- Phase 3 – Enabling Government Policy

  The UK Government has committed to allowing the use of hydrogen blending across the gas distribution network, if a positive economic and safety case can be made by the end of 2023.

Another UK project is the H21 Leeds City Gate project [9], that is studying the feasibility of a 100% hydrogen grid. It has the purpose of showing that the conversion of the UK gas distribution network is technically possible and economically feasible and it would enable a dramatic reduction in UK emissions with circa 73% reduction from heat but also from transport and power generation. Leeds was selected as the city on which to undertake the project because its gas grid is large and complex enough to provide a blueprint for all UK cities, and it is located in the north near the east coast, where the geology is suitable for the construction of the salt cavern storage required to manage demand profile variations.

The headline design parameters for a city of the size of Leeds are:

- Hydrogen would be provided through a production capacity of 1025 MW via four steam methane reformers (SMRs) located at Teesside due to its access to carbon capture and storage (CCS) plants.
- Total annual demand in a peak year would be 6,4 TWh.
- Intraday storage of circa 4000 MWh (120 tons of H_2) will be provided via salt caverns on Teesside.
- Inter-seasonal storage of 700000 MWh (21000 tons of H_2) will be provided through salt caverns in the Humber region.
- 1500 tonnes of CO_2 would be sequestered each year.
- The total cost to convert Leeds including hydrogen production and storage, all associated infrastructure and appliance conversions would be in the region of £2bn.

Since the Leeds City Gate report proved that a hydrogen gas conversion was technically possible and economically viable, the scope of H21 has expanded to include multiple projects which tackle the many different challenges of a hydrogen gas conversion. Current projects include testing hydrogen on a purpose-built micro-grid, which represents a typical UK distribution network at Spadeadam and it tests and makes recommendations to amend the operational and maintenance procedures required to operate a network on 100% hydrogen. The project will also include a 100% hydrogen trial on a section of the gas network in the South Bank area of Middlesbrough, with several months of rigorous testing of gas operations and maintenance activities.

In Italy, Snam has launched its experiment of introducing a 5% hydrogen and natural gas blend into the gas transmission network in April 2019 [14]. The experiment was conducted in Contursi Terme, in the province of Salerno, and involves the supply of the blended gas to two industrial companies in the area: a pasta factory and a mineral water bottling company. The experiment was then repeated successfully with 10% of hydrogen in the gas [15]. In 2021, Snam also successfully carried out the world's first test of a 30% hydrogen/natural gas blend in the forging processes used in industrial steelmaking in Rho (province of Milan) [16].

Another italian pilot project is Hybrid [17], that will be conducted by SGI ("Società Gasdotti Italia") in agreement with SCB ("Società Chimica Bussi"). The contract, signed in June 2021, establishes to blend 1% hydrogen, produced by electrolysis, in the methane, with a possible increase in the decarbonised percentage as soon as legislation allows.

Other European countries that are developing projects on injection of hydrogen in the gas grid are France, Germany and Netherlands. The MosaHYc [13] infrastructure project, realised by the distribution network operators Creos (Germany) and GRTgaz (France) in cooperation with the energy company Encevo (Luxembourg), wants to establish an approximately 100-kilometre-long hydrogen pipeline at the border between the three countries. About 70 kilometres of existing gas pipelines, some of which are out of service, are to be converted into hydrogen pipelines, with an additional construction of about 30 kilometres of hydrogen pipelines. The pipeline network is scheduled to be commissioned in 2026; in 2030, the transport of about 60000 t of hydrogen per year is expected. Gasunie, a dutch energy operator, has published the report of the project HyWay27 [11] in 2021, showing the possibility of producing up to 3,5 GW of electrolysis capacity in Netherlands by 2030, building new hydrogen pipelines and using already existing natural gas pipelines.

In United States, SoCalGas is implementing some new hydrogen blending demonstration projects, starting from a 5% level of hydrogen in the grid [12]. In Canada, the Fort Saskatchewan project [12] started in fall 2022, delivering a blend of natural gas containing 5% hydrogen by volume into a section of the Canadian natural gas distribution system that is addressed to 2000 costumers.

In Australia, the South Australian Government is supporting the project HyP SA [18], that produces renewable hydrogen, using a 1,25 MW electrolyser, that is blended with natural gas at volumes up to 5% and supplied to nearby homes via the existing gas network.

2.5. Critical aspects of hydrogen blending

Gas network elements and combustion devices of users connected to the grid were designed and realized to operate with natural gas. Although the composition and properties of natural gas change according to the source's origin, values are usually included in a limited range. Due to the different characteristics of the pure hydrogen gas (hydrogen is a fuel with very low density and specific energy that is about one-third of the natural gas), a mixture of natural gas and hydrogen can have properties very far from those of natural gas. Therefore, transport, storage and use of green hydrogen produced by power-to-gas facilities into gas networks are a great and difficult challenge.

2.5.1. Combustion parameters

An index used to evaluate the fuel gas interchangeability is the Wobbe Index (WI).

$$WI = \frac{H_s}{\sqrt{d}} \tag{2.1}$$

If two gases have the same Wobbe Index and are burned with the same burner nozzle and with the same nozzle pressure, they will release the same amount of heat [22].

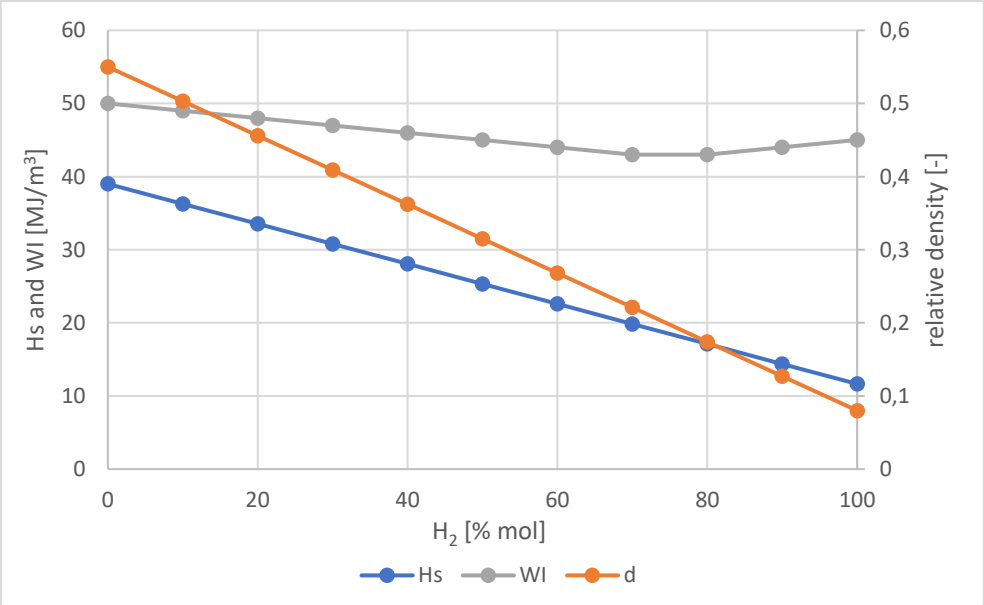

Figure 2.7: Relative densities, gross calorific values, Wobbe Indices for CH_4/H_2 blends [22]

As figure 2.7 shows, while both d and H_s decline linearly with higher levels of H_2, the reduction of the Wobbe Index is far less pronounced, and also non-linear.

Other combustion-related aspects should be considered as well. One of the main concerns in the context of H_2 admixture into natural gas and its impact on end-use equipment relates to expected higher combustion temperatures. With higher levels of hydrogen, the adiabatic combustion temperature of the fuel blend increases (figure 2.8), as long as the other operational parameters like the air excess ratio λ remain constant, that may cause local overheating of components and increased emissions of nitrogen oxides (NO_x).

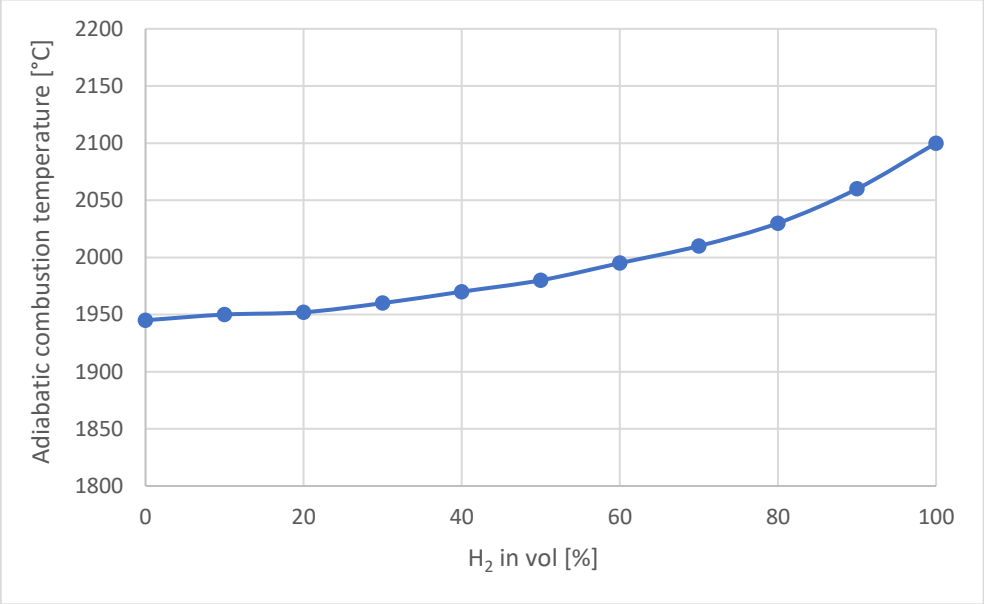

Figure 2.8: Adiabatic combustion temperature of CH_4/H_2 blends at stoichiometric conditions [22]

Another issue to consider is an increase in the laminar combustion velocity S_L. Combustion velocities are crucial for flame stabilization in premixed burners. Most residential and commercial appliances use premixed or partially premixed burners, in contrast to industrial burner systems where non-premixed systems are more common [22]. As combustion processes in residential appliances are usually laminar [22], the laminar combustion velocity is the relevant property for this application. As figure 2.9 shows, S_L increases significantly once H_2 is admixed to CH_4. As a consequence, there are concerns that higher levels of hydrogen in natural gas may cause flashbacks in appliances that are not designed for it, especially at partial load when flow speeds are lower anyway. In a flashback, the flame moves upstream into the burner itself because the local combustion velocity is higher than the local flow speed, leading to a safety shutdown or, in the worst case, to damage the burner.

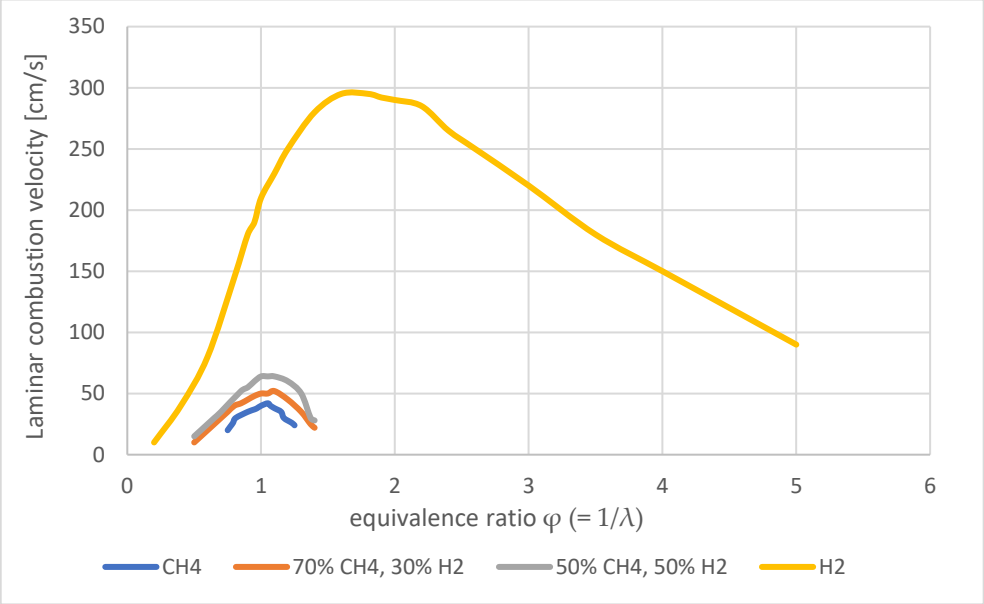

Figure 2.9: Laminar combustion velocity for different CH_4/H_2 blends as a function of the equivalence ratio [22]

The air excess ratio λ is a crucial operational parameter for all kinds of combustion processes. Changes in the air excess ratio can impact temperatures, efficiency, heat transfer and pollutant formation, but also safety-related aspects such as flame stability. One consequence of the admixture of hydrogen to natural gas is that the minimum amount of air that is necessary to achieve complete combustion is reduced. In an appliance with combustion control, this is, in theory, counteracted by reducing the volume flow of air accordingly, but in an uncontrolled system, where the volume flow of air remains constant, an increased H_2 concentration will lead to an increase of the air excess ratio λ.

Thus, if an appliance was adjusted to a gas with a given Wobbe Index and is then supplied with a fuel gas with a lower WI (as in the case of hydrogen admixture), the air excess ratio will increase and vice versa. This means that if an uncontrolled appliance was originally adjusted with natural gas and is then supplied with a natural gas/hydrogen blend, it will operate at a higher air excess ratio and is thus even less likely to produce carbon monoxide (CO).

In an uncontrolled system, the increase in S_L due to the presence of hydrogen will be mitigated by the shift of λ, so that the net change of S_L (and thus the propensity for flashback) is significantly reduced if the appliance is operated with air excess ratio higher than unity.

Combustion temperatures in uncontrolled appliances are also affected by the shifting air excess ratio: although hydrogen admixture leads to higher combustion temperatures of the fuel blend, this will be largely compensated if the air excess ratio is not actively controlled. Therefore, NO_x emissions in premixed uncontrolled appliances tend to decline as they are very much dependent on local temperatures.

In conclusion, theoretical considerations and first measurements indicate that the effects of hydrogen admixture on combustion temperatures (relevant for potential thermal overheating of components and NO_x emissions) and the laminar combustion velocities (important for flame stabilisation) are often largely mitigated by a shift towards higher air excess ratios, at least in residential premixed gas appliances. This shift occurs when a combustion process was adjusted for a fuel gas and is then supplied with another fuel gas with a lower Wobbe Index and is inevitable in an appliance without combustion control but can also occur in controlled systems.

2.5.2. Impact on existing infrastructures

Durability and integrability of the existing natural gas pipeline network in presence of hydrogen blending is an open question because hydrogen greatly degrades mechanical properties of steel (figure 2.10). This phenomenon is called hydrogen embrittlement (HE).

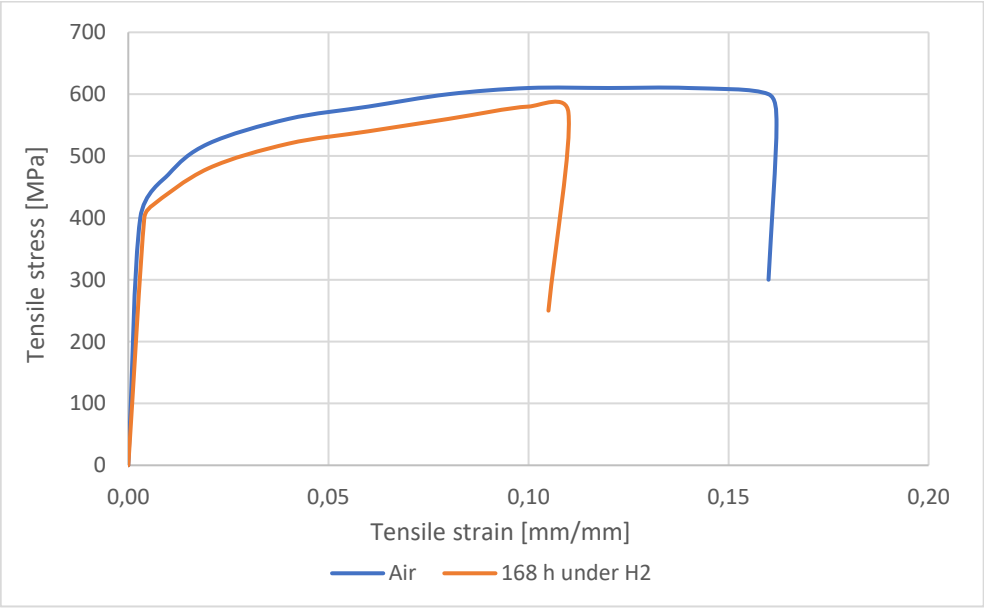

Figure 2.10: Tensile test on API L X52 pipe steel with specimens loaded in air and after hydrogen introduction by electrolytic process under a potential of V = - 1 Volt [23]

Elongation at failure is greatly reduced (38%) and yield stress (3,8%) and ultimate strength (7,4%) are less affected. This embrittlement is associated with a reduction of fracture resistance.

ASME B31.12 [24] is currently the most widely recognized standard for hydrogen pipeline systems. It applies to pure or blended hydrogen piping systems with a hydrogen content greater than 10% by volumes, pressures less than 21 MPa, temperatures between -62 °C and 232 °C and a moisture content lower than 20 ppm. In terms of material selection, the parameter requirements include minimum impact energy, maximum tensile strength and carbon equivalent to ensure fracture resistance and its weldability for hydrogen service.

Regarding the thickness requirements in pipeline design, by ASME B31.12 the wall thickness th at design pressure P could be determined by equation (2.2) [25]:

$$th = \frac{P\ D}{2\ S\ F\ E\ G\ H_f} \tag{2.2}$$

The coefficient H_f decreases with increases yield strength and design pressure. Therefore, the method described by equation (2.2) is to guard against hydrogen embrittlement by increasing the wall thickness.

Some studies (such as [26]) show that gases such as CO and O_2 could effectively inhibit embrittlement. If it is proven to be a universal effect for different grades of steel, it may well provide an interesting mitigation solution for the high-pressure hydrogen pipelines.

The polymer pipes are widely used in the distribution system, and the data showed that the working pressure was typically lower than 0,69 MPa, with diameters between 120 mm and 200 mm or less [25]. Hydrogen permeability through the polymer pipe is a potential concern, especially in the enclosed space: due to the smaller molecular size of hydrogen with respect to the methane, the leakage rate of H_2 through pipe walls and joints may be larger. NaturalHy [27] found that hydrogen permeability is about five times higher than that of methane in PE pipes, and it increases with pressure. Moreover, the contaminants may cause deterioration inside pipes, and the risk of leakage in the welding region of the polyethylene is an unsafety issue to consider.

In summary, hydrogen has no significant degradation on PE materials, but strength, stiffness and pressure-bearing capacity of plastic pipes are much less than steel pipes and are not suitable for transporting high-pressure hydrogen. Regarding the transportation pipelines, the critical aspect to analyse is the steel embrittlement, that

can be limited by the increase of wall thickness and by the addition of gases such as O_2 and CO.

Regarding the compressors in the gas infrastructure, for hydrogen blends up to 5% no problems are expected. Up to approximately 10% H_2, the compressor can usually continue to be used without major modifications. Up to 40% H_2, the compressor housing can be retained; impellers and recirculation stages as well as gearboxes must be adapted. Above 40% H_2, the compressor must be replaced [28].

2.5.3. Impact on appliances

In case of a high hydrogen blend level, adaption of end-use systems is required. Studies carried out during the development of the NaturalHy project concluded that hydrogen concentrations up to 28% ([29]) may be safely used with properly serviced existing domestic appliances although long term material compatibility with hydrogen and natural gas mixtures is uncertain. Inside the End-Use Systems sensitive devices are included:

- Underground storage: gas storage is a key component in the natural gas chain. Although it is very difficult to identify and quantify all the relevant processes related to underground storage phenomena, approximately twenty reservoir phenomena which could impact reservoir exploitation have been identified [29]. The most serious issue identified in aquifers and oil/gas depleted fields is the potential for bacterial growth. Other issues are loss of gas, potential for damage to the cavity and production of H_2S. In case of salt cavern storage, it was not detected any problem [29]. However, it is important to point out that it is not possible at the moment to define a limit value for the maximum acceptable hydrogen admixture for natural gas stored underground.
- CNG steel tanks, metallic and elastomer seals: the expressed limit of 2% is the maximum amount of hydrogen for CNG vehicles [29]. This limit is reported in ISO 11439 and DIN 51624 [29] and it has been determined to avoid accelerated crack propagation in steel because of hydrogen embrittlement. All gas carrying components inside the vehicle (for example, metallic or polymeric seals) are currently designed and tested for a maximum 2% H_2 [29].
- Gas engines: as described above, the admixture of hydrogen and natural gas modifies flame speed and reactivity making them greater as hydrogen concentration arises. Moreover, even low fractions of hydrogen

can cause engine knock. Recommendations are about 2-5% of hydrogen depending on the source of the gas [29].

- Gas turbines: current fuel specifications for many gas turbines place a limit on hydrogen volume fraction in natural gas below 5%. Exceptions are syngas turbines (that can accept hydrogen fractions higher than 50%) and other specific gas turbines which can burn natural gas containing 10% of hydrogen and even more [29].
- Specific gas burners in the domestic sector: the addition of hydrogen leads to an increasing flame speed and reduction in Wobbe Index. Although long term impacts are not known, the injection of 10% of H_2 in natural gas grid seems to be reasonable for the domestic and commercial appliances such as boilers, cookers and oven, water heater, space heaters and so on [29].

2.5.4. Other possible issues

- Impact of hydrogen on the durability of gas meters

Some studies were conducted about the durability of gas meters in presence of a hydrogen injection (such as [30], [31]), showing that there are no particular issues when the gas mixture contains less than 50% of hydrogen.

- Odorants

The odorants are used in gas grids to allow to quickly identify a gas leak. THT is the most used odorant within European gas networks, while NB is the primary odorant used by UK networks [32]. A series of tests was conducted by the Hy4Heat project (published in 2020, [32]) in order to understand if these odorants are compatible with the presence of hydrogen in the grid. Based on the testing, the conclusion is that for a 100% hydrogen gas grid used for heating (similar to the current natural gas grid), the currents odorants (THT and NB) would remain suitable, providing the characteristic gas leak smell and without indications of additional risk or damage to pipelines, appliances or residences. Further expensive tests would need to be carried out before it could be provided that any of the odorants would not damage a fuel cell.

In conclusion, in table 2.2 a study published by the Fraunhofer Institute [28] in 2022 about the maximum hydrogen blending rate accepted for some selected components is shown.

Table 2.2: Limitation for H_2 blending rates of components of gas infrastructure and utilization options (TS: Transmission system, DS: Distribution System, U: Utilization) [28]

		% H2	1	2	5	10	20	25	30	40	50	60	70	80	90	100
TS	Pipeline (steel, >16 bar)	10%														
TS	Compressors	5%														
ST	Storage (salt caverns)	100%														
TS/DS	Valves	10%														
TS/DS	Volume converters	10%														
TS/DS	Volume measurement	10%														
DS	Pipeline (plastics, <16 bar)	100%														
DS	Pipeline (steel, <16 bar)	25%														
DS	House installation	30%														
U	Gas engines	10%														
U	Gas cooker	10%														
U	Atmospheric gas burner	10%														
U	Condensing boiler	10%														
U	CNG-vehicles	2%														
U	Gas turbines	1%														

	No adjustments needed		Further R&D is required
	Modifications may be needed		Insufficient information, R&D demand

2.5.5. Hydrogen separation

Next to the importance of developing the appropriate technology to inject hydrogen from the gas grids, it is fundamental to focus on technologies for extracting hydrogen from the network to obtain high purity hydrogen. The current technologies for separation of hydrogen are reported in this section, followed by a table that summarises the advantages and disadvantages of each technology (table 2.3).

- Pressure Swing Adsorption (PSA) is the mature technology used in refineries to produce high-purity hydrogen: hydrogen is delivered at high pressure and the non-hydrogen materials are released at low pressure. PSA works highly efficiently for streams with high hydrogen concentrations.

- Hydrogen separation can also be done by means of cryogenic separation. Although liquefying hydrogen through cryogenic processes remove all impurities present in hydrogen, the energy needed to cool hydrogen down to -253 °C is about 30% of stored energy [29].
- Membrane technology is another industry-practiced technology for hydrogen extraction and purification. Membrane technologies work very efficiently with relatively high hydrogen concentrations. The purity of product gas can be high at very low fractional recovery but monotonically decreases as recovery increases, as the relative slower co-permeation of impurities proceed to a greater degree. Most applications using membrane technology industrially recover the bulk hydrogen at 95-99% purity [29].
- Electrochemical hydrogen separation (hydrogen pumping) can be used to selectively extract and compress hydrogen from gas mixtures. It operates on principles in common with fuel cell systems, using fuel cell stacks and passing the process gas across one side of the stack. By applying a current across the stack, hydrogen is atomically dissociated from the process gas and is re-associated into hydrogen on the product side.

Table 2.3: Advantages and drawbacks of the technologies for H_2 separation

Technology	Advantages	Disadvantages
PSA	High H_2 separation capacity	Not economically attractive for H_2/NG < 10%
	High H_2 purity (but offgas released at low pressure)	High energy cost due to compression
		Low H_2 recovery
Cryogenic distillation	Low purity H_2 streams can be treated (>10%)	Extremely high energy cost for cooling
		Not feasible for H2/NG <10%
Polymeric membranes	Low energy cost	Relatively low H_2 permeance and selectivity
	Modular	Degradation at high temperatures (>200°C)
		Not feasible for H_2/NG <10%
Pd-based membrane using metallic/ ceramic supports	Low energy cost	Degradation at low temperatures (<200°C)
	Modular	Degradation in presence of H_2S
	Very good H_2 permeance	Low recoveries for <10% H_2/NG streams
Ultra-thin Pd-based membranes using ceramic porous supports	Low energy cost	Degradation at low temperatures (<200°C)
	Modular	
	The highest H_2 permeance for supported membranes	Degradation in presence of H_2S
Electrochemical hydrogen purification	High H_2 separation capacity	Low recoveries for <10% H_2/NG streams
	High H_2 purity	High energy cost if used independently

2.6. Hydrogen final uses

Global hydrogen demand reached more than 94 million tonnes (Mt) in 2021, a 5% increase from the previous year and compared to 91 Mt in 2019 (pre-pandemic level). Most of the increase was for the use of hydrogen in traditional applications, particularly in chemicals and in refining [33]. Demand for hydrogen in new applications, such as in heavy industry, transport, power generation and the building sectors or the production of hydrogen-derived fuels, was very low in 2021, at around 40 kilotonnes H_2 (about 0,04% of global hydrogen demand) [33].

The IEA Stated Policies Scenario (STEPS) suggests, based on the current and announced policies, that hydrogen demand could reach 115 Mt by 2030 [33]. The rest of this chapter examines the state of art of hydrogen demand in the refining, industry, transport, buildings and power generation sectors.

2.6.1. Refining

Refineries use hydrogen to remove impurities, especially sulphur, and to upgrade heavy oil fractions into lighter products. Oil refining was the single largest consumer of hydrogen in 2021 (close to 40 Mt H_2). Nearly half of global hydrogen demand for refining in 2021 was in two regions: North America at almost 10 Mt and China at more than 9 Mt [33].

Almost all hydrogen used in refineries is produced from unabated fossil fuels, resulting in more than 200 Mt CO_2 emitted in 2021 [33]. In 2021, there were only eleven plants to produce low-emission hydrogen (seven plants retrofitted with CO_2 capture and four using electrolysers), producing it for an amount of around 260 kt (around 0,7% of hydrogen demand in refining) [33]. Projects under development to replace unabated fossil-fuel based hydrogen with low-emission hydrogen in refining are limited in number and size.

Table 2.4: Selected projects operative and under development to decarbonize hydrogen production in refining [33]

Project/location	Status	Start-up date	Technology	Size
Port Arthur (US)	Operational	2013	Natural gas + CCUS	900 kt CO_2 year 118 kt H_2/year
REFHYNE (Germany)	Operational	2021	Electrolyser	10 MW
Gela biorefinery (Italy)	Feasibility studies	2023	Electrolyser	20 MW
HySynergy (Denmark)	Under development	2022	Electrolyser	20 MW by 2022 300 MW by 2025 1 GW by 2030

2.6.2. Industry

Today the main uses of hydrogen in the industry sector are to produce ammonia (34 Mt of hydrogen demand), methanol (15 Mt) and DRI (direct reduced iron) in the steel industry (5 Mt) [33].

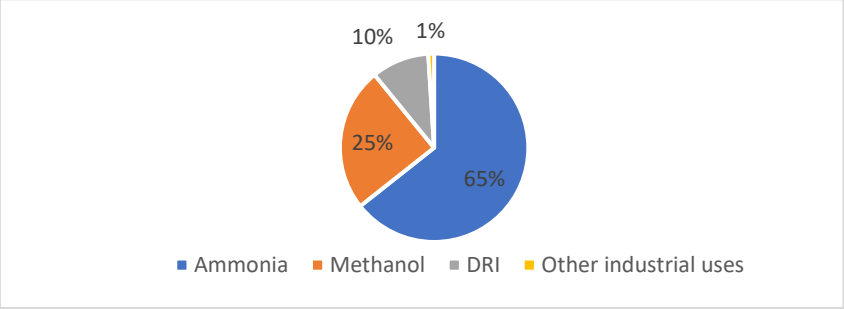

Figure 2.11: Hydrogen demand in industry, 2020 [34]

Virtually, all hydrogen used in the industry sector today is produced from unabated natural gas or coal, leading to 630 Mt of direct CO_2 emissions on a net basis, or 7% of industrial CO_2 emissions in 2021 [33]. New hydrogen applications in industry have the potential to curb growth in greenhouse gas emissions to 2030, with many technologies currently under development. These include new low-emission processes for conventional industrial outputs, such as electrolytic and CCUS-equipped ammonia, methanol and steel production, as well as hydrogen use for industrial heat demand, among other applications.

- Ammonia is the starting point for all nitrogen fertilisers, which account for around 70% of global ammonia demand (the remaining 30% is for a wide range of industrial applications). Producing one tonne of ammonia requires around 180 kg of hydrogen: total production of ammonia was around 190 Mt in 2021, representing approximately 34 Mt of demand for hydrogen, or around two-thirds of hydrogen demand in the industry sector [33].
  One tonne of ammonia production results in around 2,2 tonnes of CO_2 emissions on average.
- Methanol is used mainly as an intermediate product to produce other chemicals (formaldehyde is its largest-volume derivative).
  Around 130 kg of hydrogen is required as feedstock per tonne of methanol. The 113 Mt produced in 2021 globally led to around 15 Mt of hydrogen demand, and virtually 100% of this production was from fossil fuels [33]. One tonne [33]. One tonne of methanol production generates 2,2 tonnes CO_2 on average with coal-based production, which is dominant in China, significantly more emissions-intensive than the natural gas-based production.
- The production of DRI in the steel industry is an avenue for hydrogen applications using both existing and new process technology. Conventional DRI technology uses a mixture of carbon monoxide and hydrogen, all generated from fossil fuels, to chemically reduce iron for steel making.
  Accounting for around 5 Mt of industrial hydrogen demand in 2021 [33], DRI already constitutes a significant opportunity to reduce emissions associated with existing industrial applications.

Two key technology families can achieve substantial emissions intensity reductions for the industrial sector: electrolysis and CCUS.

Table 2.5: Selected projects investigating the use of low-carbon hydrogen in chemical sector [33]

Project/location	Status	Start-up date	Technology	Size
Coffeyville fertiliser (US)	Operational	2013	CO_2 capture from oil-based ammonia production	1 Mt CO_2/year
Green Wolverine (Sweden)	Under development	2030	Electrolytic ammonia production	100 kt H_2
Commercial Plant Svartsengi (Iceland)	Operational	2011	Electrolytic methanol production from dedicated renewables	6 MW
North-C-Methanol (Belgium)	Under development	2028	Electrolytic methanol production from dedicated renewables	Up to 300 MW
HYBRIT (Sweden)	Operational	2021	Hydrogen production for DRI	1,8 Mt H_2 by 2030
SALCOS (Germany)	Under development	2025	Blending of hydrogen into natural gas based DRI	136 kt hydrogen capacity

2.6.3. Electricity generation

Hydrogen plays only a negligible role as a fuel in the power sector today. It accounts for less than 0,2% of global electricity generation [33] and it can be used as fuel in reciprocating gas engines and gas turbines. Today's reciprocating gas engines can handle gases with a hydrogen content of up to 70% (on a volumetric basis) and various manufacturers have demonstrated engines using 100% hydrogen that should be commercially available in upcoming years. Gas turbines can also operate on hydrogen-rich gases (in Korea, a 45 MW gas turbine at a refinery has been operating on gases of up to 95% hydrogen for 25 years [33]).

Fuel cells can convert hydrogen into electricity and heat, producing water but no direct emissions. These systems can achieve high electrical efficiencies (over 60%) and maintain high efficiency even at part load. The main fuel cells technologies for electricity and heat generation are:

- Polymer electrolyte membrane fuel cells (PEMFCs), which operate at low temperatures and can be used for powering automobiles and for stationary power production.
- Phosphoric acid fuel cells (PAFCs), used as stationary power generators with outputs in the range of 100-400 kW.

- Molten carbonate fuel cells (MCFCs) and solid oxide fuel cells (SOFCs), which operate at higher temperatures (600°C and 800-1000°C, respectively) and can be used for heating and cooling in buildings and industry and for cogeneration.
- Alkaline fuel cells (AFCs), which operate at low temperatures and can be used in stationary applications. It is the oldest technology, now surpassed.

Despite the low deployment levels of hydrogen in the power sector so far, interest in the use of hydrogen and ammonia is increasing. Co-firing with hydrogen or ammonia can reduce emissions in existing gas and coal fired power plants in the near term. In the longer term, hydrogen and ammonia-fired power plants can support the integration of variable renewables by providing flexibility or large-scale, seasonal storage to electricity systems. Several projects have been announced or are under development that could represent around 3500 MW of hydrogen and ammonia-fired power plant capacity worldwide by 2030 [33]. Around 85% of these projects focus on the use of hydrogen in combined-cycle or open-cycle gas turbines and the rest in fuel cells.

Table 2.6: Electricity sector hydrogen projects under developments [33]

Project/location	Status	Start-up date	Technology	Size
Daesan Green Energy (Korea)	Operational	2020	PAFCs fuelled by by-product hydrogen from petrochemical industry	50 MW
Long-Ridge Energy Terminal (US)	Operational	2022	5% co-firing of H2 with natural gas	485 MW
Saltend CHP (UK)	Under development	2028	30% co-firing of H2 in a CCGT	1,4 GW

2.6.4. Buildings

The heating sector is difficult to decarbonise, with existing (old) multi-family buildings and very cold climates being particularly challenging because integrating efficient low-temperature solutions depends on space availability, energy system layout and overall building performance, in addition to logistical and economic costs for building occupants. Nevertheless, since hydrogen equipment can be compatible with existing buildings' energy systems, hydrogen applications can support decarbonisation.

Four main groups of technologies can operate on hydrogen at the building level:

- Hydrogen boilers can be practical where gas networks exist because consumers will be familiar with the basic technology and its upfront capital costs (typical size of 30 kW_{th}).
- Fuel cells that co-generate heat and electricity include SOFCs and PEMFCs (size between 1 and 5 kW_e). SOFCs require a high temperature but also provide high electrical efficiency and a more stable load compared with PEM cells, which work at lower temperature (60-80 °C) on intermittent load schedules but offer lower electrical efficiency.
- Hybrid heat pumps combine a boiler and an electric heat pump. The boiler operates only when the heat pump cannot meet heating demand. They are an interesting option in cold climates where hydrogen can be used to cover peak demand during very cold periods, but they have additional costs and require both electricity and hydrogen connections.
- Gas-driven heat pumps have a gas engine that produces electricity to run a heat pump.

Today, more than 90% of heat district networks rely on the use of fossil fuels. Their decarbonisation will be fundamental to deliver low-emission heat in dense urban areas in particular.

Table 2.7: Selected key projects for deploying hydrogen, 2020 [33]

Project/location	Start-up date	Description
Stad Aan'T Haringvliet (Netherlands)	2022	A demonstration house has been heated using hydrogen boiler
Murcia (Spain)	2022	Pure hydrogen boiler in a hospital
UK	2022	Several hybrid heat pumps succesfully tested

2.6.5. Transport

Hydrogen demand in transport totalled over 30 kt in 2021, more than 60% higher than the previous year [33]. As a share of total hydrogen demand, however, transport represents only 0,03%, and as a share of total transport energy, hydrogen represents only 0,003% [33].

Road vehicles, by far, are the major source of hydrogen demand in transport. Most of this is consumed in trucks and buses due to their high annual mileage and heavy weight relative to the larger stock of fuel cell electric cars.

Hydrogen tanks' capacity vary from 5 kg car tanks to 30-35 kg bus and truck tanks, allowing an autonomy that can reach 800 km [33].

Given that most of the FCEVs are cars, the majority of refuelling stations are configured to dispense hydrogen at 700 bar for passenger light-duty vehicles. Buses store hydrogen at lower pressures, so some stations are dual pressure, able to dispense at 700 (for cars) or 350 bar (for buses), while other stations only dispense at 350 bar (for buses and other commercial vehicles) [33].

Table 2.8: Transport industry announcement for FCEVs [33]

Company	Target	Target year	Vehicle category
BMW	Limited-series fuel cell SUV release	2022	Passenger vehicle
Toyota Motor Corp	Deployment of 600 FCEV taxis in greater Paris region	End of 2024	Passenger vehicle
Riversimple	Light goods vehicle model release	2023	Light commercial vehicle
H2Bus Consortium	Deployment of 600 fuel cell buses	2023	Bus
Nikola	Purchase order of up to 800 fuel cell trucks to US Anheasuer-Busch	2023	Truck
MAN	Deployment of hydrogen fuel cell demonstration fleet	2024	Truck
Industry Coalition	Deployment of 100000 heavy-duty fuel cell trucks in Europe	From 2030	Truck

3 Fluid-dynamic model

This chapter has the objective to describe the fluid-dynamic model adopted in this work and the reason behind certain assumptions in order to solve a gas distribution network (i.e., to find the proper flow-pressure working points).

3.1. Compressible flow in pipelines

In this work, the general pipeline flow problem is developed under these assumptions [35]:

- Constant pipeline section.
- One-dimensional flow.
- Single phase flow.
- Newtonian fluid.
- Compressible fluid.

3.1.1. Unsteady state

Unsteady state is typical of a gas distribution network. In general, the operating conditions of the flow are fully defined when its temperature and pressure (p, T) and the mass flow rate q are known. The conservation equations to set the problem are the continuity equation (3.1), the momentum equation (3.2), the energy equation (3.3).

$$\frac{\partial \rho}{\partial t} + \frac{\partial (\rho u)}{\partial x} = 0 \tag{3.1}$$

$$\frac{\partial (\rho u)}{\partial t} + \frac{\partial (\rho u^2)}{\partial x} = -\frac{\partial p}{\partial x} - \frac{f}{2D}\rho u^2 - \rho g \sin\theta \tag{3.2}$$

$$\frac{\partial (\rho e)}{\partial t} + \frac{\partial (\rho u e)}{\partial x} + \frac{\partial (u p)}{\partial x} - q\frac{P}{A} - k\frac{\partial^2 T}{\partial x^2} - \frac{f}{2D}\rho u^3 = 0 \tag{3.3}$$

In the equations above, ρ is the density of the gas [kg/m^3], u is the axial velocity [m/s], e is the specific energy [J/kg], f is the friction factor, k is the thermal conductivity, P is the perimeter [m] and A is the area [m^2] of the section.

Moreover, in order to close the problem, the 4th unknown present in this equation set (the gas density ρ) has to be related to the thermodynamic p – T coordinates of the system. The real gas equation of state (3.4) accounts for the non-ideality of the gas by means of the compressibility factor z:

$$\frac{p}{\rho} = \frac{z\,R\,T}{MM} \tag{3.4}$$

where R is the universal gas constant (equal to 8314 J/mol/K) and MM is the gas molecular weight (in [kg/kmol]).

The continuity equation (3.1) acquires a certain importance in this problem as we are dealing with the assumption of compressible flow (i.e., the density ρ is not constant), so the volumetric gas flow rate is not conserved. It is conventional for the natural gas network to refer to the standard volumetric flow rate F (as a conserved quantity) rather than to the mass flow rate q. Standard conditions are defined at pressure p_0 = 1 atm and temperature T_0 = 15 °C.

In the momentum equation (3.2), the momentum material derivative equals the sum of the forces acting on the flow. Three different contributes appear on the right-hand side of the balance:

- A pressure gradient term;
- A frictional loss term;
- A gravitational loss term.

In most engineering applications, both the convective terms are dropped. Above all, it is possible to demonstrate that the second term (in absolute terms) is much lower than the pressure force contribute:

$$\left|u^2 \frac{\partial \rho}{\partial x}\right| \ll \left|\frac{\partial \rho}{\partial x}\right| \tag{3.5}$$

In the energy equation (3.3), the energy material derivative is associated to four different contributes, appearing on the right-hand side of the balance (neither compression nor expansion work is assumed to be done on/by the fluid):

- A pressure work rate term;
- A heat addition (due to convection) rate term;

- A heat addition (due to conduction) rate term;
- A frictional source term.

In literature, two extreme approaches are described relatively to the energy balance [36]. The adiabatic flow model is associated to fast dynamic changes, which allow no time for heat transfer to take place between the gas duct and its surroundings. The isothermal model, instead, is associated to slow dynamic changes, where temperature variations within the gas are sufficiently slow to be cancelled out by heat exchange process. In this last case, the energy equation becomes redundant and it is decoupled from the momentum balance, resulting in an important simplification for the problem.

At the distribution level, isothermal flow assumption can be made, since the temperature increase due to frictional effect is not meaningful at this stage. As the ground is in thermal equilibrium with the ambient (at its surface), the value of the temperature parameter is taken as equal to the standard ambient temperature, that is T_0 = 15 °C.

3.1.2. Steady state

A subcategory of pipeline models is characterized by the simplifying assumption of working in steady state conditions. Such a condition is unlikely to be encountered in real life operations, where time dependent withdrawal profiles are to be satisfied. On the other hand, it may be a simple and efficient tool for design concerns, in order to derive an optimal network configuration. The steady formulation of the governing equations is: continuity equation (3.6); momentum equation (3.7); energy equation (3.8).

$$\frac{\partial (\rho u)}{\partial x} = 0 \tag{3.6}$$

$$\frac{\partial p}{\partial x} + \frac{f}{2D}\,\rho u^2 + \frac{p\,MM}{Z\,R\,T} g \sin\theta = 0 \tag{3.7}$$

$$\frac{\partial}{\partial x}\left(\rho u \left(e + \frac{p}{\rho}\right)\right) - q\frac{P}{A} - k\frac{\partial^2 T}{\partial x^2} - \frac{f}{2D}\,\rho u^3 = 0 \tag{3.8}$$

Pipeline flow equations are meant to relate the gas flow rate to the properties of both the pipe (diameter D, roughness ε, length L) and the fluid (molecular weight MM, dynamic viscosity μ) and the p - T operating conditions. Its general form can be obtained by integrating the momentum equation (multiplied by p) term-by-term.

In this operation, a commonly adopted approach is to consider the pressure at the gravitational force term as an average value, rather than an unknown. The compressibility factor is also considered as an average value for the pipe, while the average temperature is equal to the temperature itself (under the isothermal flow assumption).

By integrating the pressure force term, we obtain:

$$\int_1^2 p\, dp = \frac{p_2^2 - p_1^2}{2} \tag{3.9}$$

By integrating the frictional loss term, we obtain:

$$\frac{f}{2D}\frac{(\rho_0 F)^2}{A^2}\int_1^2 \frac{Z\,R\,T}{MM}\, dx = -\frac{f}{2D}\frac{(\rho_0 F)^2}{A^2}\frac{Z_{av}\,R\,T}{MM}\, L \tag{3.10}$$

By integrating the gravitational force term, we obtain:

$$-\int_1^2 \frac{p^2\, MM}{Z\,R\,T} g \sin\theta\, dx = -\frac{p_{av}^2 MM}{Z_{av} RT}\, g\Delta h \tag{3.11}$$

The integration results are then rearranged to give the general flow equation, as expressed in (3.12):

$$F = \frac{\pi}{4}\sqrt{R}\,\frac{Z_0 T_0}{p_0}\,\frac{D^{5/2}}{\sqrt{f}}\left(\frac{p_1^2 - p_2^2 - \frac{2\,MM}{Z_{av}\,RT}\; p_{av}^2\, g\Delta h}{L\, Z_{av}\; T\; MM}\right)^{\frac{1}{2}} \tag{3.12}$$

The proper average pressure to be applied in the gravitational term is analytically found in the simplifying case of horizontal pipe, and then extended (allowing a certain error) also for possible applications. If the hydrostatic pressure term is null, the pressure gradient is inversely proportional to ρ (and hence to p).

$$p_{av} = \frac{\int_1^2 p\, dx}{\int_1^2 dx} = \frac{\int_1^2 p^2\, dp}{\int_1^2 p\, dp} = \frac{2}{3}\left(p_1 + p_2 - \frac{p_1\, p_2}{p_1 + p_2}\right) \tag{3.13}$$

The difference among the several reported models is not in their formal aspect, but in the compressibility factor z correlation and friction factor f definition.

3.2. Compressibility factor

The compressibility factor z is the parameter accounting for the non-ideality of the gas.

$$p = \rho z \hat{R} T \tag{3.14}$$

As shown in (3.14), composition influences both the specific mass gas constant $\hat{R}$ and the compressibility factor z, pressure and temperature dependence of the latter must be included, too.

Several models, either empirical correlations or equations of state, exist in literature to describe the volumetric behaviour of gas mixtures with different accuracy. Among them, two suitable models are the Papay ((3.15), [37]) and the AGA (American Gas Association) ((3.16), [37]).

$$z_{Papay}(p,T) = 1 - 3{,}52\, p_r\, e^{-2{,}260 T_r} + + 0{,}274\, p_r^2\, e^{-1{,}87\, T_r} \tag{3.15}$$

$$z_{AGA}(p,T) = 1 + 0{,}257\, \frac{p}{p_{pc}} - 0{,}533\, \frac{p}{p_{pc}}\, \frac{T_{pc}}{T} \tag{3.16}$$

In both the equations, the composition-dependence is expressed by means of the pseudo-critical pressure (p_{pc}) and temperature (T_{pc}), which are defined as the molar weighted averages of the components critical pressures (p_c) and temperatures (T_c).

$$p_{pc} = \sum_{i=1}^{N} X_i\, p_{c,i} \tag{3.17}$$

$$T_{pc} = \sum_{i=1}^{N} X_i\, T_{c,i} \tag{3.18}$$

Pseudo-reduced quantities are defined as the ratio between the state pressure and temperature and their pseudo-critical values.

$$p_{pr} = \frac{p}{p_{pc}} \tag{3.19}$$

$$T_{pr} = \frac{T}{T_{pc}} \tag{3.20}$$

Another way to evaluate the compressibility factor of a gas mixture is through the use of the computer program "Refprop" (by NIST, [38]).

In this chapter, the compressibility factor of different gas compositions is calculated using the Papay and the AGA equations and the Refprop program: five different

gas mixtures are considered, starting from natural gas only and adding, gradually, different percentages of hydrogen. In table 3.1, the five mixtures are reported:

Table 3.1: Molar compositions of the five gas mixtures considered

	Gas 01	Gas 02	Gas 03	Gas 04	Gas 05
Methane	0,97	0,873	0,776	0,485	0
Ethane	0,02	0,018	0,016	0,01	0
Propane	0	0	0	0	0
Carbon dioxide	0,005	0,0045	0,004	0,0025	0
Nitrogen	0,005	0,0045	0,004	0,0025	0
Hydrogen	0	0,1	0,2	0,5	1

The thermo-physical properties of each species are reported in table 3.2:

Table 3.2: Thermo-physical properties of gas species

	MM [kg/kmol]	Tc [K]	p_c [bar]
Methane	16,04	190,56	45,99
Ethane	30,07	305,83	48,8
Propane	44,1	369,82	42,5
Carbon dioxide	44,01	304,2	73,86
Nitrogen	28,01	126,2	33,9
Hydrogen	2,02	33,2	12,97

The three models adopted need to be compared with the ISO-12213 reference formulation [39], which is an implicit z-equation:

$$z = 1 + B\rho_m - \rho_r \sum_{n=13}^{18} C_n^* + \sum_{n=13}^{58} C_n^* \left(b_n - c_n k_n {\rho_r}^{k_n}\right) \rho_r \exp\left(-c_n {\rho_r}^{k_n}\right) \quad (3.21)$$

b_n, c_n, k_n are constants and B, K, C_n^* are coefficients which are function of temperature and composition. The standard procedure is based on an iterative algorithm, as the molar density ρ_m is function of Z. The reduced density ρ_r is also related to the molar density by means of a mixture size parameter K:

$$\rho_r = K^3 \rho_m \quad (3.22)$$

The comparison between the three z-models is carried out with the objective of understanding if they are suitable to describe the non-ideality of the flow at different concentrations of hydrogen in the gas and at a wide range of pressures (in particular the gas distribution pressure range, below 5 bar).

To evaluate the accuracy of the models, maximum absolute relative deviations (ARD), with respect to the ISO reference formulation, has been calculated as reported in (3.23):

$$ARD\ (p) = \frac{|Z_{ISO}(p) - Z_i(p)|}{Z_{ISO}(p)};\ \mathrm{i} = \{AGA, Papay, Refprop\} \tag{3.23}$$

The following figures show the difference between the three z-models and the comparison with the ISO reference formulation, varying the pressure between 0 and 100 bar.

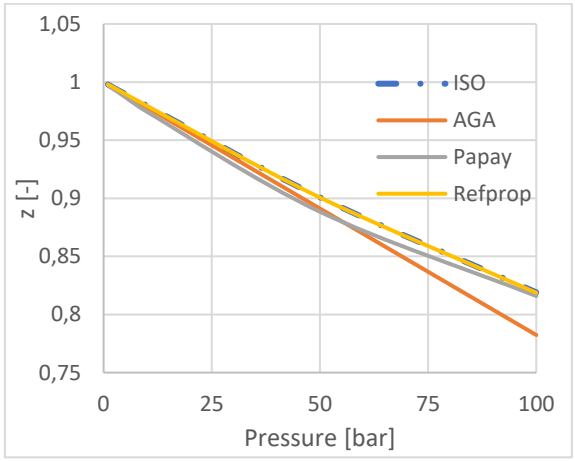

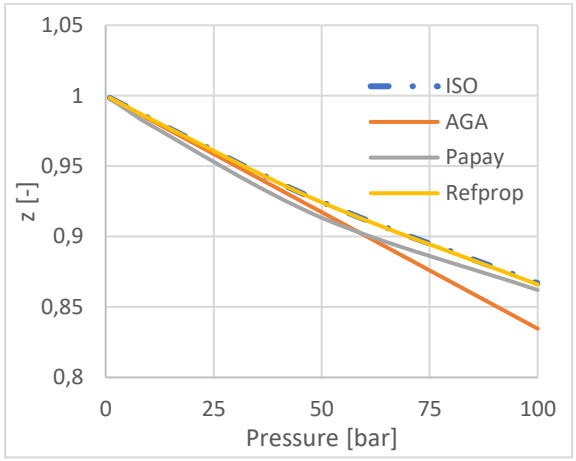

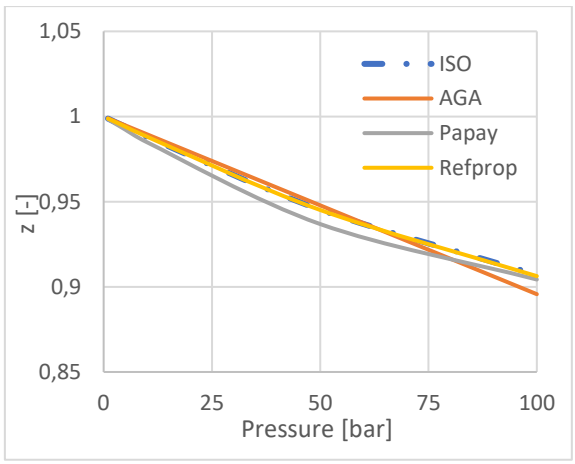

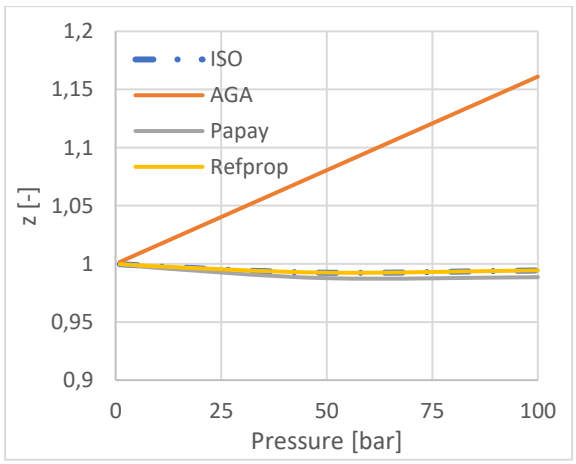

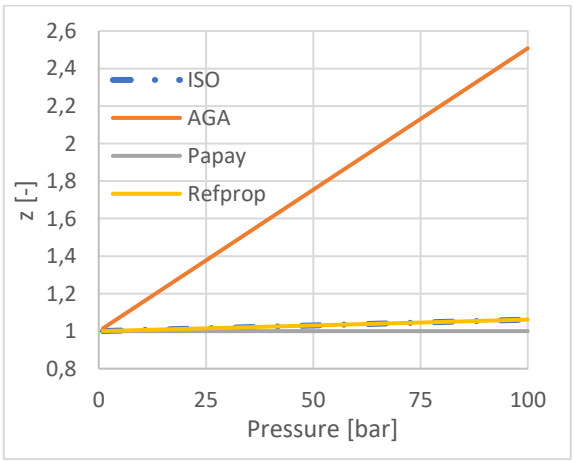

Figure 3.1: Z(p) profile of: Gas 01, 0% H_2 (top-left); Gas 02, 10% H_2 (top-right); Gas 03, 20% H_2 (middle-left); Gas 04, 50% H_2 (middle-right); Gas 05, 100% H_2 (bottom)

Table 3.3: Maximum ARD of z compared to ISO (p < 5 bar)

	Gas 01 (0% H_2)	Gas 02 (10% H_2)	Gas 03 (20% H_2)	Gas 04 (50% H_2)	Gas 05 (100% H_2)
AGA	0,07%	0,03%	0,08%	0,92%	7,22%
Papay	0,28%	0,23%	0,17%	0,06%	0,30%
Refprop	0,02%	0,0003%	0,003%	0,01%	0,01%

Table 3.4: Maximum ARD of z compared to ISO (p > 5 bar)

	Gas 01 (0% H_2)	Gas 02 (10% H_2)	Gas 03 (20% H_2)	Gas 04 (50% H_2)	Gas 05 (100% H_2)
AGA	4,48%	3,72%	1,26%	16,77%	136,25%
Papay	1,38%	1,21%	0,90%	0,58%	5,79%
Refprop	0,04%	0,10%	0,09%	0,01%	0,01%

The compressibility factor analysis shows that the AGA correlation cannot be adopted to represent the non-ideality of gases with high fractions of hydrogen, both at high and low pressures. On the contrary, the Papay correlation has a good agreement with the ISO-12213 for all the gas compositions, in particular at the gas distribution pressure range, that is below 5 bar, as well as the values calculated through Refprop.

3.3. Friction factor

Several approaches are available to relate the friction factor to fluid dynamics and geometries, summarized by non-dimensional parameters like Reynolds number Re and relative surface roughness ε/D.

For a laminar flow (Re < 2300), the Hagen-Poisseuille formula ((3.24), [40]) is used to approximate the friction factor:

$$f = \frac{64}{Re} \tag{3.24}$$

In the turbulent region (Re > 2300), the implicit Colebrook-White is the most complete and accurate ((3.25), [40]), but it requires a dedicated solution step integrated in the global fluid dynamics solver:

$$\frac{1}{\sqrt{f}} = -2\log\left(\frac{1}{3{,}71}\,\frac{\varepsilon}{D} + \frac{2{,}51}{Re\sqrt{f}}\right) \tag{3.25}$$

In this work, two explicit correlations are taken in consideration to approximate the friction factor in the turbulent region: the Hofer ((3.26), [40]) and the Chodanovic-Odischarija ((3.27), [40]) approximations:

$$f_{Hofer} = \frac{1}{2\,\log_{10}\left(\frac{4{,}518}{Re}\log_{10}\left(\frac{Re}{7}\right)+\frac{K}{3{,}71D}\right)^2} \tag{3.26}$$

$$f_{C-O} = 0{,}067\left(\frac{0{,}067}{\frac{158}{Re}+2\,\frac{k}{D}}\right)^{0{,}2} \tag{3.27}$$

The relative roughness is a meaningful parameter in determining the fluid-dynamics of the system. Pipeline diameters are of the order of 100 mm at distribution level, as reported by UNI 9165:2004 [41], and the roughness of the steel is of the order of few μm (a value of 48 μm is used in this work).

UNI 9165:2004 also specifies the maximum gas velocity in the pipes in order to avoid both noise and mechanical issues. The allowed value is equal to 20/25 m/s at pressures between 0,5 and 5 bar. By the way, lower velocities (around 10 m/s) are taken in literature as general design conditions.

It has been verified that the gas distribution network works under design conditions with fully turbulent flows even at low velocities. The aim of this analysis is to compare the two approximating formulas mentioned above with the implicit Colebrook-White equation for the five mixtures at different velocities (between 5 m/s and 25 m/s) to understand if they are suitable to describe the friction factor. To evaluate the accuracy of the models, the maximum ARD of the two correlations with respect to the Colebrook-White formulation has been calculated as reported in (3.28):

$$ARD\ (Re) = \frac{|f_i\,(Re) - f_{Colebrook}\,(Re)\,|}{f_i\,(Re)};\ \mathrm{i} = \{Hofer,\ Chodanovic\} \tag{3.28}$$

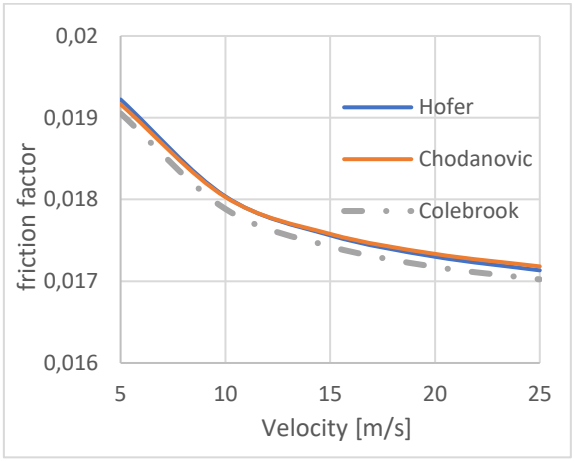

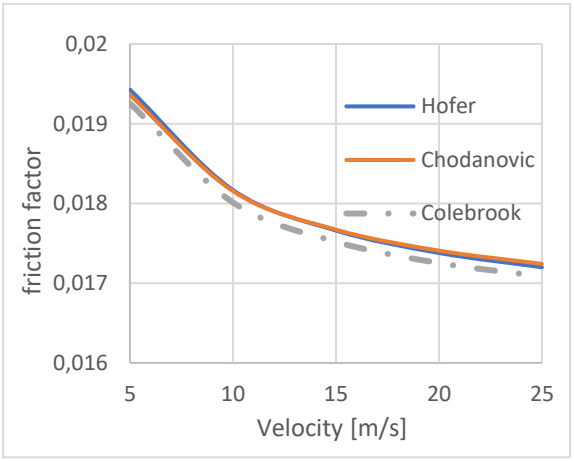

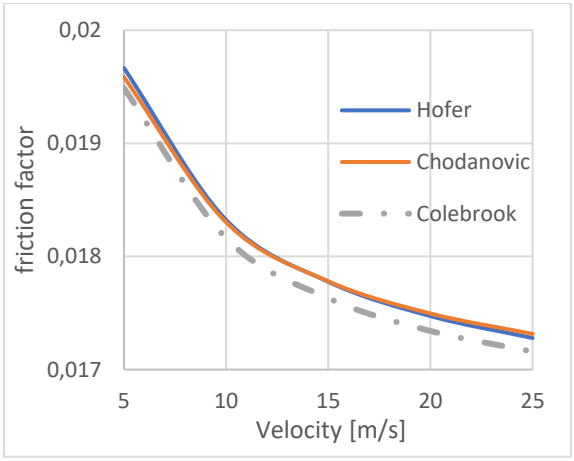

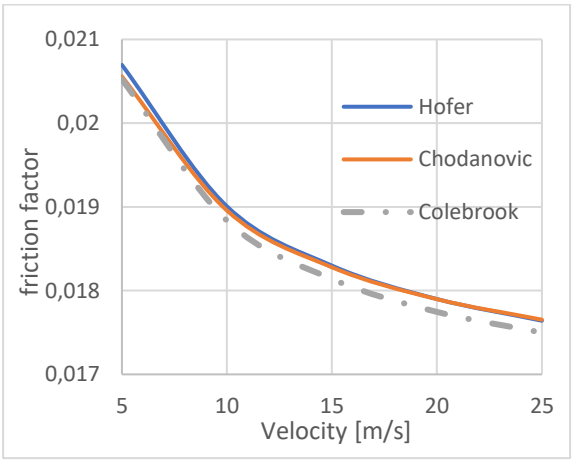

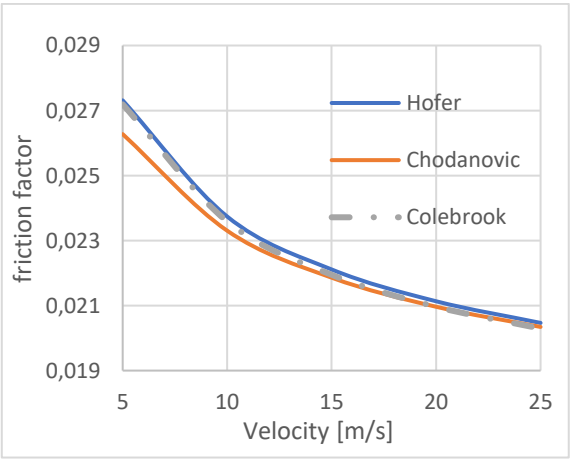

Figure 3.2: f(v) profile of: Gas 01, 0% H_2 (top-left); Gas 02, 10% H_2 (top-right); Gas 03, 20% H_2 (middle-left); Gas 04, 50% H_2 (middle-right); Gas 05, 100% H_2 (bottom)

Table 3.5: Maximum ARD compared to Colebrook formulation

	Gas 01 (0% H_2)	Gas 02 (10% H_2)	Gas 03 (20% H_2)	Gas 04 (50% H_2)	Gas 05 (100% H_2)
Hofer	0,89%	0,89%	0,90%	0,89%	0,85%
Chodanovic	0,93%	0,91%	0,90%	0,88%	3,35%

The friction factor analysis shows that both the correlations are suitable to approximate the Colebrook-White formulation, but the Hofer approximation is better at very high levels of hydrogen, since deviations above 3% have been found for a gas with 100% H_2 using the Chodanovic correlation.

4 Case study

In this chapter, a gas distribution network is studied, considering the medium pressure level (pipes of species IV) in steady state conditions. Firstly, the network is studied in the base case, considering a 100% natural gas grid and evaluating pressures at the demand nodes, velocities in the pipes and gas flow processed by the reducing stations (REMI). Secondly, an injection of biomethane is added to the grid to analyze its impact on the network parameters. Different biomethane flows and different positions of injection are considered; moreover, a parameter that can estimate what is the optimal position to inject the biomethane source is introduced. Lastly, the effect of hydrogen presence in the grid is studied. The base case is compared with a 100% H_2 grid (in winter and summer) and with different mixtures having increasing fraction of hydrogen. Then, the addition of a hydrogen source in different positions of the natural gas grid is studied, introducing the concept of gas quality tracking and evaluating the thermal input introduced in the grid. Finally, the case in which one of the two natural gas station is substituted by hydrogen is simulated.

The simulations are performed using a program developed in Matlab. In the next section (4.1) the explanation of how the program works is present.

In table 4.1, a list of all the cases considered in this chapter is reported.

Table 4.1: List of the case studies

Case 1	Base case (100% NG grid)
Case 2	Biomethane injection (same flow rate)
Case 3	Biomethane injection (sensitivity analysis)
Case 4	100% H_2 grid (winter and summer)
Case 5	Increasing fractions of H_2 in the gas
Case 6	H_2 injection (same flow rate)
Case 7	H_2 injection (sensitivity analysis)
Case 8	One NG supply and one H_2 supply

4.1. Description of the simulation model

The graphical representation of the network examined (figure 4.1) is given in terms of directed graphs. Each trough is associated with a direction, which is represented by an arrow. From the model point of view, it means for each pipeline to define an upstream and a downstream node. The model is able to handle with algebraic quantities, regardless of the sign, so that negative flows are simply associated to a conventional direction; however, identifying the convention with the physical direction of the flow, when possible, is really helpful in post-analysing the simulation results.

Other than direction, grid troughs are characterized by a geometrical volume and by terminal nodes. Pipe volume is graphically represented by troughs whose width is proportional to its own diameter. Two kinds of nodes can be distinguished in this model:

- Source nodes are the ones connecting the distribution network with the upstream transmission level. Physically they represent the reducing and metering stations (REMI), imposing the inlet pressure for the gas flow (the solution of the network requires the definition of a pressure level at least at one point). This node is represented by a red upwards triangle in the following graphical representations.
- Sink nodes are the multiple withdrawal points in the grid. In these points the flow withdrawn from the network is imposed as a boundary condition. This kind of node is represented by a blue circle in the following graphical representations.

In the following simulations, the assumption (debated in section 3.1) of isothermal flow is applied, with an adopted valued T_0 = 15°C, so that the energy equation becomes redundant in the model.

The gas distribution network analyzed is a medium-pressure network that resembles a medium-sized city. The natural gas is injected at a pressure of 5 bars by two city-gate stations, placed in the right (REMI A) and in the left (REMI B) areas of the grid. The network supplies gas to three industrial users and eleven domestic withdrawal nodes. The residential users, then, receive the gas through the pipes of different low-pressure subnetworks, located in the urban areas. The total demand of natural gas is 11300 Sm^3/h in the winter case (standard conditions: 1 bar and 15°C).

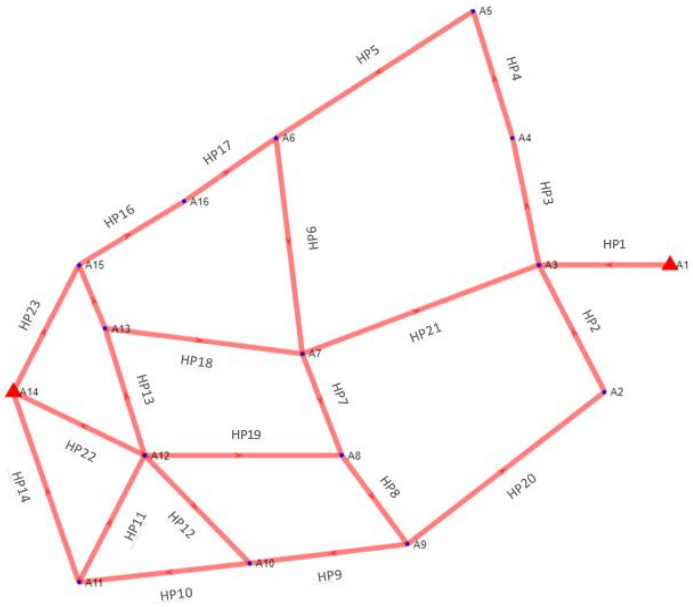

Figure 4.1: Gas distribution network simulated

Table 4.2 reports the length of the pipes; table 4.3 reports the flow rate demand of each withdrawal node. All the pipes are assumed to have a diameter of 108 mm.

Table 4.2: Pipes length

Pipe	Length [m]	Pipe	Length [m]
HP1	700	**HP13**	1000
HP2	600	**HP14**	500
HP3	500	**HP15**	600
HP4	500	**HP16**	500
HP5	800	**HP17**	600
HP6	800	**HP18**	1000
HP7	500	**HP19**	800
HP8	1000	**HP20**	900
HP9	800	**HP21**	1000
HP10	500	**HP22**	800
HP11	700	**HP23**	800
HP12	700		

Table 4.3: Withdrawal nodes demand

Node	Type	Demand [Sm³/h]
A2	Industrial	1500
A3	Domestic	700
A4	Domestic	600
A5	Industrial	1200
A6	Domestic	800
A7	Domestic	700
A8	Domestic	600
A9	Domestic	800
A10	Domestic	800
A11	Industrial	1100
A12	Domestic	700
A13	Domestic	600
A15	Domestic	500
A16	Domestic	600

The simulation model evaluates gas pressure at demand nodes; velocity and pressure drop in each pipe. These values must be checked to satisfy the gas demand by users and respect gas standards (in terms of maximum/minimum pressure and maximum velocity). It is also important to evaluate the flow elaborated by the reducing stations in order to guarantee the correct operation of the network. Moreover, the gas quality tracking is implemented in this work in order to evaluate the thermal input supplied to the network in the case of a mixing between natural gas and hydrogen, since every demand node receives a gas with a different composition (so a different lower heating value).

4.2. Base case

The base case ("case 1") is the case in which the two reducing stations supply natural gas to the network. Table 4.4 shows the molar composition of the natural gas used for modelling and simulating the network studied. The gas is composed of a high percentage of methane (CH_4) and a low percentage of ethane (C_2H_6), nitrogen (N_2) and carbon dioxide (CO_2). Main parameters which characterize the gas mixture are shown in table 4.5.

Table 4.4: Composition of the gas supplied by the city gate stations

Species	x
CH_4	0,97
C_2H_6	0,02
C_3H_8	0
CO_2	0,005
N_2	0,005
H_2	0

Table 4.5: Properties of the gas supplied by the city gate stations

	MM [kg/kmol]	LHV [MJ/kg]	ρ [kg/Sm³]	LHV [MJ/Sm³]
Natural gas	16,52	48,5	0,691	33,51

The pressure at the demand nodes and the velocity of the gas through the pipes are represented in figures 4.2.

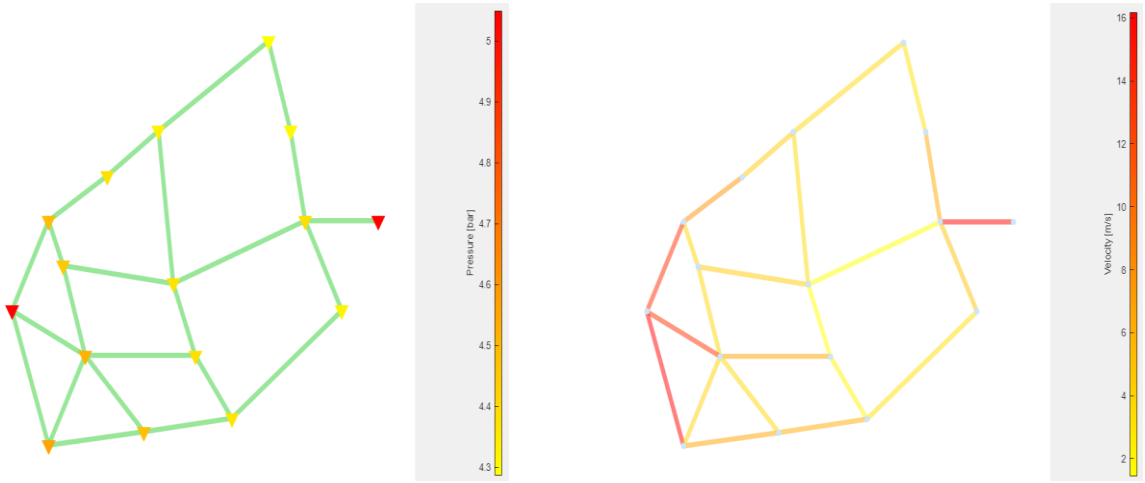

Figure 4.2: Case 1: gas pressure at the demand nodes (left); gas velocity through the pipes (right)

The main results of the simulation of case 1, in terms of pressures, velocities, flows and thermal power supplied, are reported in table 4.6. All the following simulations will provide results that will be compared to this one.

Table 4.6: Main results of the simulation (case 1)

	Case 1	
Max P loss (pipes) [bar]	0,586	HP1
Max P loss (pipes) [mbar/m]	0,858	HP14
Max F (pipes) [Sm^3/h]	3102	HP14
Min F (pipes) [Sm^3/h]	261	HP7
Max velocity (pipes) [m/s]	16,02	HP14
Max P (nodes) [bar]	5	A1, A14
Min P (nodes) [bar]	4,329	A5
F in REMI A [Sm^3/h]	3036	A1
F in REMI B [Sm^3/h]	8264	A14
Thermal input [MW]	105,2	

The first consideration coming out from the steady analysis is that most of the flow is injected in the reducing station in the left area of the grid (REMI B) because it has

a larger concentration of demand nodes (high loaded branch). In particular, the 73% of the total natural gas demand is supplied by the station in the left side of the network. Therefore, the higher pressure drops per unit of length are in the pipes connected to this station (because of the higher volumetric flow), in particular in HP14 because the gas is supplied to an industrial node (A11). The pressure drop is large also in the pipe connected to the right reducing station (REMI A), that is HP1, because all the injected gas flows through this pipe, while the gas supplied from REMI B is distributed through three pipes. The maximum pressure loss is reached in HP1 (11,7%) not only for this reason but also because this pipe is longer than the ones connected to REMI B.

Overall, the demand nodes in the left branch receive gas at a higher pressure than those in the right branch, mainly because they are closer to a city-gate station (REMI B), so the pressure losses through the pipes are lower.

A similar discussion can be made about the gas velocities. The velocities are higher where the flow is larger, as explained by (4.1).

$$v = \frac{F}{A} = \frac{\rho\, \dot{m}}{\pi\, \frac{D^2}{4}} \tag{4.1}$$

Since all the pipes have an equal diameter and the same gas is supplied to the network, so the density is the same, the velocity is higher where a larger amount of gas flows.

However, the velocity is largely below the upper limit (25 m/s) in all the pipes of the network. The maximum velocity (16 m/s) is reached where the maximum quantity of gas flows, so HP14.

As expected, the central area has the lower pressures and velocities because the nodes are not close to the reducing stations, with a consequent low utilization of some pipes, such as HP4. Anyway, all the values are acceptable, with a minimum pressure of 4,3 bar in A5, that is an industrial node and therefore has a higher demand.

The total thermal power needed by the grid has been calculated as in (4.2):

$$\dot{Q}\ [\mathrm{MW}] = \sum_{i=1}^{N_d} \frac{F_i \left[\frac{Sm^3}{h}\right] * \rho_i \left[\frac{kg}{Sm^3}\right] * LHV_i \left[\frac{MJ}{kg}\right]}{3600} \tag{4.2}$$

When only natural gas is injected, like in this case, the density and the lower heating value are the same in all the points of the grid, so only the flow withdrawn by each demand node changes.

The injection of biomethane, in cases 2 and 3, does not influence the thermal power because its properties are assumed to be the same as those of natural gas. So, it is not needed to evaluate it again.

On the contrary, a hydrogen injection (cases 4, 5, 6, 7, 8) changes the properties of the gas that flows in the grid, so the thermal power supplied to each withdrawal node needs to be calculated again whenever hydrogen is present in the network.

4.3. Influence of the position of a decentralized injection

Biomethane and hydrogen injections can be modelled as decentralized injections with constant flow profiles, meaning a gas flow rate which is set into the grid independently of its working conditions.

The problem of a decentralized source is that it may lead to an issue concerning the system pressure. If the amount of injected flow is exceeding the demand on its branch, part of the flow would travel towards the remaining part of the network, which means for the injection point to work at a higher pressure than the reducing stations. This solution is physically not sustainable, as the whole network is designed to resist at a maximum pressure level that is the one imposed at the connection with the transmission lines. The solution to avoid this problem is an action of the DSO (Distribution System Operator) in downgrading the imposed pressure at the REMI stations, so that the maximum pressure at the decentralized injection is lower than 5 bar.

The objective of this section is to propose some parameters that can establish what is the optimal position of the grid to place a decentralized injection, so that there is no need of an intervention of the DSO on the parameters of the network. In fact, in a real network there are thousands of nodes, so it would be important to find some parameters that allow to do a priori evaluation on which positions of the grid are more convenient to place a decentralized injection.

The factors considered in this work that can influence the injection are its distance from the demand nodes and from the city-gate stations and the flow rate withdrawn by each node. So, some parameter that take into account these factors have to be

considered, with the goal of establishing a ranking of the demand nodes in order to understand if it is convenient to place the decentralized injection next to them. Other factors that can influence the injection are not included in the index at the moment, as, for example, the mesh of the grid (each node is connected to a different number of pipes) and the fact that the demand profile is not constant in the real situations.

The first parameter proposed (η) classifies every node j considering the ratio between the flow rate withdrawn by the node and its distance from the others:

$$\eta_j = \sum_{i=1}^{N_d} \frac{F_i}{dist\ (i,\ j)} \left[\frac{Sm^3}{h*m}\right] \tag{4.3}$$

This number should be the higher possible, since the decentralized injection is expected to be more convenient near a high demand node, even if this parameter is also influenced by the position of the node in the network.

The second parameter (σ) considers the effect of the presence of the reducing and metering stations (REMI), taking into account, for each node, the ratio between the flow rate injected in each REMI and the distance of the node from that REMI.

$$\sigma_j = \sum_{i=1}^{N_{REMI}} \frac{F_{REMI,\,i}}{dist\ (i,\ j)} \left[\frac{Sm^3}{h*m}\right] \tag{4.4}$$

This number should be the lower possible, since the decentralized injection is expected to be more convenient far from a big REMI station, in order to reach the demand nodes that are not close to a natural gas injection point.

The ranking of the nodes established by these two parameters is shown in table 4.7.

Table 4.7: Ranking of the demand nodes according to η and σ

Node j	η [$Sm^3/h/m$]	Node j	σ [$Sm^3/h/m$]
A3	8,44	**A5**	4,88
A8	8,23	**A4**	5,15
A4	8,22	**A2**	5,43
A7	8,18	**A6**	5,69
A12	7,41	**A7**	5,86
A10	7,23	**A9**	6,13
A6	7,17	**A8**	6,63
A13	7,01	**A3**	7,07
A16	6,84	**A13**	7,09
A15	6,74	**A16**	7,42
A11	6,39	**A10**	9,37
A9	6,22	**A15**	11,29
A5	6,07	**A12**	11,39
A2	5,74	**A11**	17,46

Table 4.7 shows that the industrial nodes have lower values of η, despite the high flow demand, because of their position in the network (high distance from the other nodes of the grid). The parameter σ has lower values for the nodes in the right side of the network, where a smaller amount of gas is injected.

Furthermore, a parameter (μ) that takes in account both the effects described by summing them is searched. Two ways to link η and σ are considered:

- μ_1 sums the two effects, resulting in a dimensional parameter.

$$\mu_{j,1} = \eta_j + \sigma_j \left[\frac{Sm^3}{h*m}\right] \tag{4.5}$$

  Since η has to be maximized and σ has to be minimized, it is not immediately clear if the higher or lower values of μ_1 should be considered more convenient for the injection.

Table 4.8: Influence of η and σ on μ_1

Node j	μ_1 [$Sm^3/h/m$]	% η	% σ
A5	10,95	55%	45%
A2	11,17	51%	49%
A9	12,36	50%	50%
A6	12,86	56%	44%
A4	13,38	61%	39%
A7	14,04	58%	42%
A13	14,10	50%	50%
A16	14,27	48%	52%
A8	14,86	55%	45%
A3	15,52	54%	46%
A10	16,60	44%	56%
A15	18,04	37%	63%
A12	18,81	39%	61%
A11	23,85	27%	73%

In table 4.8, it is shown how the nodes more influenced by σ have got higher values of μ_1 and the ones more influenced by η have got lower values of μ_1. Therefore, the nodes better ranked are considered to be the ones with lower values of $\mu_1$in order to maximize η and minimize σ.

- μ_2 considers the ratio between η, that has to be maximized, and σ, that has to be minimized, resulting in a dimensionless number that should be maximized.

$$\mu_{j,2} = \frac{\eta_j}{\sigma_j} [-] \tag{4.6}$$

Table 4.9 reports the ranking of the nodes according to the two ways to calculate the parameter μ.

Table 4.9: Ranking of the demand nodes according to μ

Node j	μ_1 [$Sm^3/h/m$]	Node j	μ_2 [-]
A5	10,95	**A4**	1,6
A2	11,17	**A7**	1,39
A9	12,36	**A6**	1,26
A6	12,86	**A5**	1,25
A4	13,38	**A8**	1,24
A7	14,04	**A3**	1,19
A13	14,10	**A2**	1,06
A16	14,27	**A9**	1,01
A8	14,86	**A13**	0,99
A3	15,52	**A16**	0,92
A10	16,60	**A10**	0,77
A15	18,04	**A12**	0,65
A12	18,81	**A15**	0,6
A11	23,85	**A11**	0,37

The two rankings are very similar: for example, the last four nodes of the two sequences are the same; just some nodes, such as A2, A9, A4, change position. One of the goals of the chapters 4.4 and 4.8 is to understand if the parameters used are suitable to decide what are the best positions to place a decentralized injection (biomethane or hydrogen) and which parameter is better among μ_1 and μ_2, in particular evaluating the nodes that show a change of position in the two sequences determined by μ_1 and μ_2.

4.4. Biomethane decentralized injection

The choice of introducing a biomethane decentralized injection deals with the characteristics of biomethane production, which occurs at an almost constant rate and generally without a storage capacity. Moreover, as biomethane composition is similar to the one of natural gas, quality tracking is not required.

In the following simulations (cases 2 and 3), the base scenario (case 1) is compared with the injection of biomethane in five different positions of the grid (positions A, B, C, D, E), basing on the ranking of the nodes established by the parameter μ. The positions chosen for the injection are different in terms of closeness to the natural gas stations and in terms of branch load. The goal is to establish if the results obtained agree with the nodes ranking, in order to establish if the parameter μ can

be assumed to be a good way to understand what the best position of biomethane injection in a network is from the point of view of the DSO.

- Pos. A: near to the node A2, an industrial node in a lowly loaded branch, close to REMI A.

- Pos. B: near to the node A6, a domestic node in a lowly loaded branch.

- Pos. C: near to the node A11, an industrial node in a highly loaded branch, close to REMI B.

- Pos. D: near to the node A15, a domestic node in a highly loaded branch, close to REMI B.

- Pos. E: near to the node A4, a domestic node in a lowly loaded branch, close to REMI A.

Table 4.10: Positions of biomethane injection (cases 2 and 3)

Position of injection	Nearest node	$\eta \left[\frac{Sm^3}{h\,m}\right]$	$\sigma \left[\frac{Sm^3}{h\,m}\right]$	$\mu_1 \left[\frac{Sm^3}{h\,m}\right]$	$\mu_2\,[-]$
Pos. A	A2	5,74	5,43	11,17	1,06
Pos. B	A6	7,17	5,69	12,86	1,26
Pos. C	A11	6,39	17,46	23,85	0,37
Pos. D	A15	6,74	11,29	18,04	0,6
Pos. E	A4	8,22	5,15	13,38	1,6

In all the five cases, the pipe (HP24) connecting the biomethane injection (REMI C) to the nearest node has a length of 500 m. The node in which the biomethane is injected is an additional node, named A17.

At first, the comparison is made at a fixed quantity (3000 Sm^3/h, case 2) of biomethane injected (the total withdrawn gas is 11300 Sm^3/h); then, a sensitivity analysis is made varying the flow rate (between 500 and 3500 Sm^3/h, case 3) to observe its effect on the physical properties of the gas flowing in the grid.

4.4.1. Comparison at the same flow rate

In case 2, an injection of 3000 Sm^3/h of biomethane is applied to the positions A, B, C, D, E of the grid, in order to study the effects of an injection of the same amount of biomethane in different positions of the network.

In terms of gas velocity through the pipes, the situation is very similar to the base case in all the five scenarios because the biomethane has got the same properties of natural gas, therefore it does not significantly affect the velocity of the gas through the network. The pipe in which the higher amount of gas flows is now HP24, connected to the biomethane injection node, so the maximum velocity is now reached in this pipe.

The main differences among the simulations are in terms of gas pressure at the demand nodes. The maximum pressure drop is always in the pipe in which the biomethane is injected, since here the larger amount of gas flows and the higher velocity is reached. In order to keep the pressure of the biomethane injection below 5 bars, the nominal pressure in the natural gas REMI stations (REMI A and B) has to be decreased from 5 to 4,8 bars in positions A and B (lowly loaded branches) and to 4,7 bars in positions C and D (highly loaded branches); in the case 4E, it is decreased to 4,75 bars, so it is an intermediate case between the others. Therefore, the pressure of the gas that flows in the network is lower than in the grid with no biomethane injection. This effect is larger in cases 2C and 2D because of the higher downgrade of the natural gas injection pressure. As a consequence, the minimum pressure of the gas at the demand nodes is lower than in the other cases and the lowest value is reached in case 2C (4,15 bars in A5). Moreover, the cases 2B and 2E are the only ones in which the node A5 is not the point of minimum gas pressure (it is in node A2): the reason is that it is close both to the biomethane injection point and to the city-gate station.

The pressure at the demand nodes in the five cases is shown in the next figures (figure 4.3).

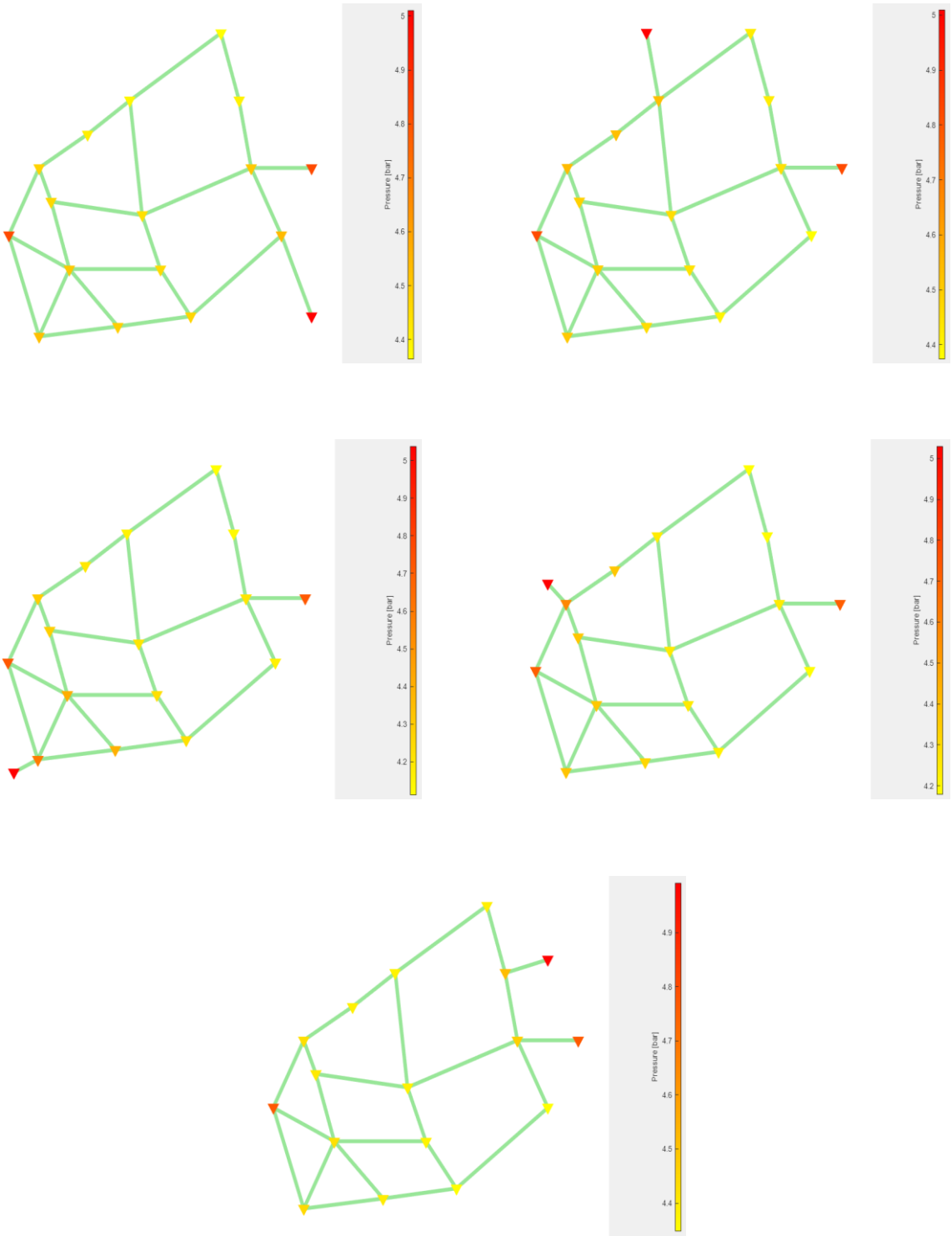

Figure 4.3: Gas pressure at the demand nodes (case 2A: top-left; case 2B: top-right; case 2C: middle-left; case 2D: middle-right; case 2E: bottom)

Table 4.11: Main results of the simulations (case 2)

	Case 1	Case 2A	Case 2B	Case 2C	Case 2D	Case 2E
Closest demand node to the injection	-	A2	A6	A11	A15	A4
η $\left[\frac{Sm^3}{h*m}\right]$	-	5,74	7,17	6,39	6,74	8,22
σ $\left[\frac{Sm^3}{h*m}\right]$	-	5,43	5,69	17,46	11,29	5,15
μ_1 $\left[\frac{Sm^3}{h*m}\right]$	-	11,17	12,86	23,85	18,04	13,38
μ_2 $[-]$	-	1,06	1,26	0,37	0,6	1,6
Max P loss (pipes) [bar]	0,586 (HP1)	0,404 (HP24)	0,404 (HP24)	0,461 (HP24)	0,418 (HP1)	0,405 (HP24)
Max P loss (pipes) [mbar/m]	0,858 (HP14)	0,807 (HP24)	0,807 (HP24)	0,803 (HP24)	0,804 (HP24)	0,81 (HP24)
Max F (pipes) [Sm^3/h]	3102 (HP14)	3000 (HP24)	3000 (HP24)	3000 (HP24)	3000 (HP24)	3000 (HP24)
Min F (pipes) [Sm^3/h]	261 (HP7)	311 (HP8)	92 (HP4)	12 (HP21)	51 (HP7)	186 (HP20)
Max velocity [m/s]	16,02 (HP14)	15,57 (HP24)	15,57 (HP24)	15,49 (HP24)	15,51 (HP24)	15,53 (HP24)
P in REMI A and B (A1, A14) [bar]	5	4,8	4,8	4,7	4,7	4,75
P in REMI C (A17) [bar]	-	4,96	4,96	4,99	4,98	4,94
Min P (nodes) [bar]	4,329 (A5)	4,41 (A5)	4,42 (A2)	4,15 (A5)	4,22 (A5)	4,392 (A2)
F in REMI A (A1) [Sm^3/h]	3036	2041	2198	2624	2501	1958
F in REMI B (A14) [Sm^3/h]	8264	6259	6102	5676	5799	6342
F in REMI C (A17) [Sm^3/h]	-	3000	3000	3000	3000	3000

4.4.2. Sensitivity analysis

In case 3, the quantity of biomethane injected in positions A, B, C, D, E is varied from 500 to 3500 Sm^3/h. The objective of this analysis is to understand how the pressure varies in the network when the amount of biomethane is increased in different points of the network. To do it, the trends of the natural gas injection pressure, the biomethane injection pressure and the minimum pressure at the demand nodes as a function of the quantity of biomethane injected are represented in the five positions.

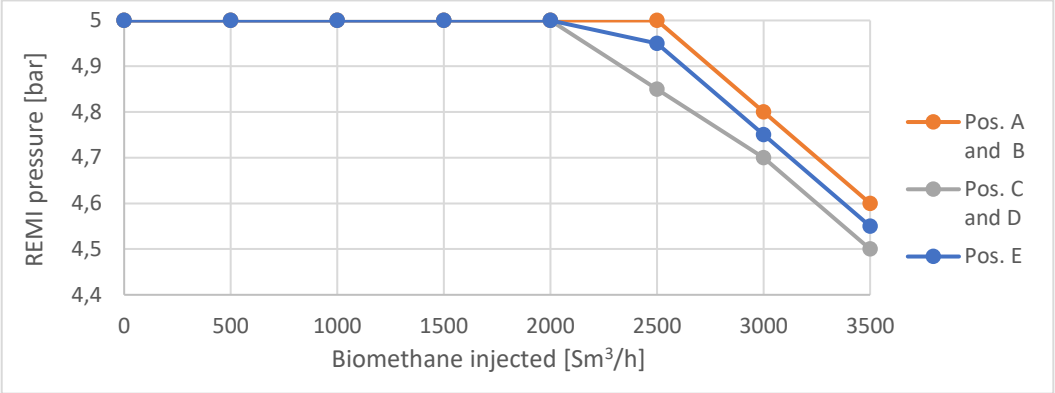

Figure 4.4: Natural gas REMI stations pressure as a function of biomethane injected

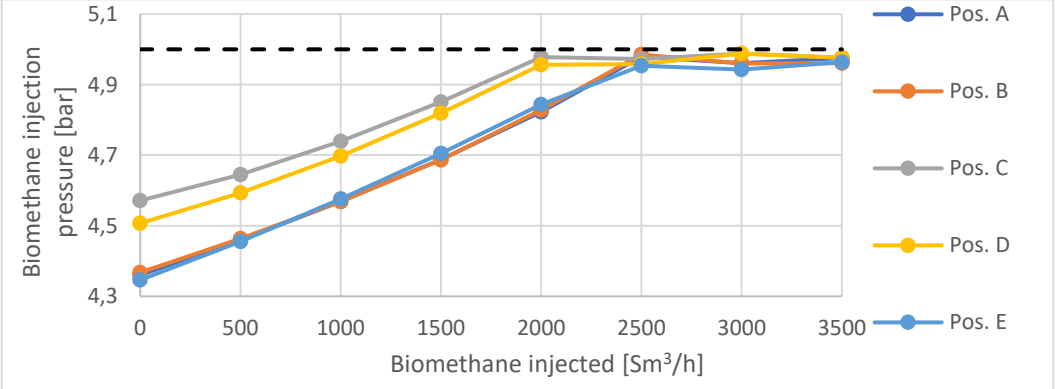

Figure 4.5: Biomethane injection pressure as a function of biomethane injected

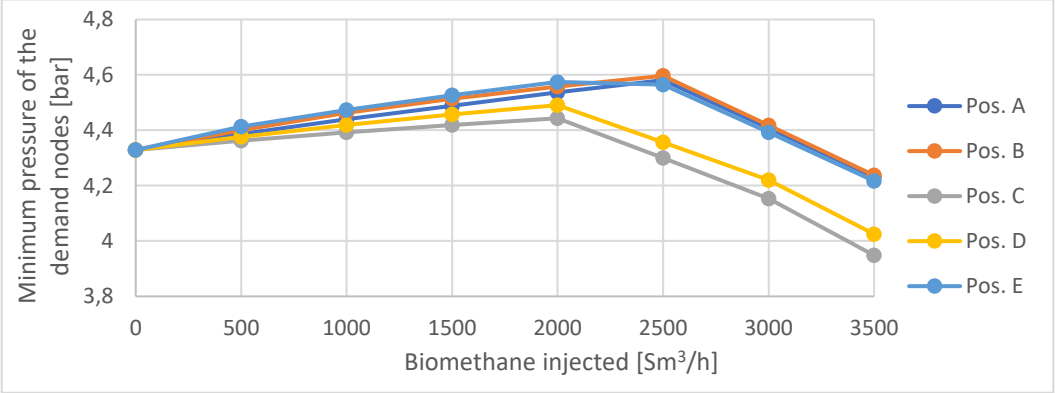

Figure 4.6: Minimum pressure at the demand nodes as a function of biomethane injected

The figures above show how there is no need of an intervention of the DSO to downgrade the pressure of the natural gas reducing and metering stations until the injection of 2500 Sm^3/h of biomethane in the cases 3A and 3B and 2000 Sm^3/h in the cases 3C, 3D and 3E, respectively about 22% and 18% of the total gas flow supplied to the network. Until this quantity, the injection pressure of the biomethane increases non-linearly (figure 4.5) and the minimum pressure in the grid increases linearly (figure 4.6). Supplying a larger amount of biomethane, its injection pressure would overcome the maximum pressure allowable (5 bars), causing the problems described at the beginning of this chapter. The solution is to decrease the natural gas pressure level, so that the pressure in the decentralized injection point is always kept below the upper limit. In the cases 3A and 3B, the natural gas REMI pressure is always higher, at the same volumetric flow, than in the cases 3C, 3D. The case 3E is an intermediate between the other cases.

The consequence of the increase of the quantity of biomethane injected is that the pressure level in the rest of the network is lower. At the same volumetric flow, the minimum pressure is lower in the cases 3C and 3D because of the lower injection pressure of the natural gas. In particular, the minimum pressure is below 4 bars when 3500 Sm^3/h of biomethane volumetric flow are injected in the position C.

These results imply that the positions in which a higher amount of biomethane can be injected, and so a lower quantity of natural gas is needed, are A and B, that are placed in the lowly loaded branch of the network. Here, a larger amount of biomethane flow can be injected before the intervention of the DSO to downgrade the pressure level is needed and, after that, a further quantity of biomethane can be supplied before the pressure level of the gas in the withdrawal nodes becomes too low.

The results observed both in case 2 (constant flow) and case 3 (variable flow) agree with the ranking of the nodes established by the parameter μ. In fact, the nodes A2 and A6 (related respectively to the positions A and B) are in the first positions of this ranking of both μ_1 and μ_2. A2, that is an industrial node, is closer to a natural gas distribution and metering station (REMI A) than A6, that is a domestic node, but they are both in a lowly loaded branch (so σ is low). On the other hand, A11 and A15 (related respectively to the positions C and D) are in the last positions of the ranking; in particular, A11, an industrial node in a highly loaded branch, is the worst node from the point of view of this ranking because σ is very high. A15 is in a highly loaded branch and is close to REMI B like A11, but it is in a better place of the grid, from the point of view of the distance by the other nodes, so σ is lower. The node A4, related to position E, has the highest value of η and it is the first node in the ranking established by μ_2, but the results show that an intervention on the grid would be needed at a lower amount of biomethane injected with respect to the cases A and B. So, from this point of view, the parameter μ_1 is better to classify the nodes.

4.5. 100% H_2 grid

In this section, the distribution grid is simulated substituting the natural gas of the base case with hydrogen supplied by the same two city gate stations. This analysis aims to evaluate the impact of the presence of the hydrogen on the network behaviour, comparing it with a 100% natural gas grid in terms of pressures, velocities and thermal power supplied to the withdrawal nodes.

The importance of this analysis is due to the different physical properties between natural gas (table 4.5) and hydrogen (table 4.12).

Table 4.12: Properties of hydrogen injected into the grid

	MM [kg/kmol]	LHV [MJ/kg]	ρ [kg/Sm3]	LHV [MJ/Sm³]
Hydrogen	2	120	0,084	10,08

Compared to natural gas, hydrogen is a fuel gas with very low mass density and specific energy, that is about one-third (as seen in chapter 2, figure 2.7). These important differences mean that the volumetric flow needed in a hydrogen grid is more than three times larger than in a natural gas grid, if the energy content is kept constant.

In this chapter, both the case in which volumetric flow remains the same and the case in which it is increased to supply the same thermal power as the base case are analyzed.

4.5.1. Constant volumetric flow

In this simulation (case 4a), the volumetric flow supplied to the withdrawal nodes is the same as in the base case. As explained before, hydrogen is a low mass density fuel, so the thermal input supplied is reduced to one-third of the energy needed.

The velocity of the gas through the pipes is very similar to the base case because both the volumetric flow and the pipes area are the same. It is not exactly the same because of the difference between natural gas and hydrogen in terms of compressibility factor and friction factor, as seen in chapter 3.

The main difference with respect to the natural gas network is that the pressure drops are largely reduced. This is caused by the much lower density of hydrogen than the one of natural gas (the hydrogen specific density is about the 10% of the natural gas one): this property makes hydrogen flow through the pipes producing lower pressure drops. The maximum pressure drop is 0,084 bar (around 1,7%, while it is 11,7% in case 1), whereas the pressure of the gas at the demand nodes is increase by around 10% with respect to case 1.

Figures 4.7 show the gas pressure at the demand nodes and the gas velocity in the pipes obtained in this simulation.

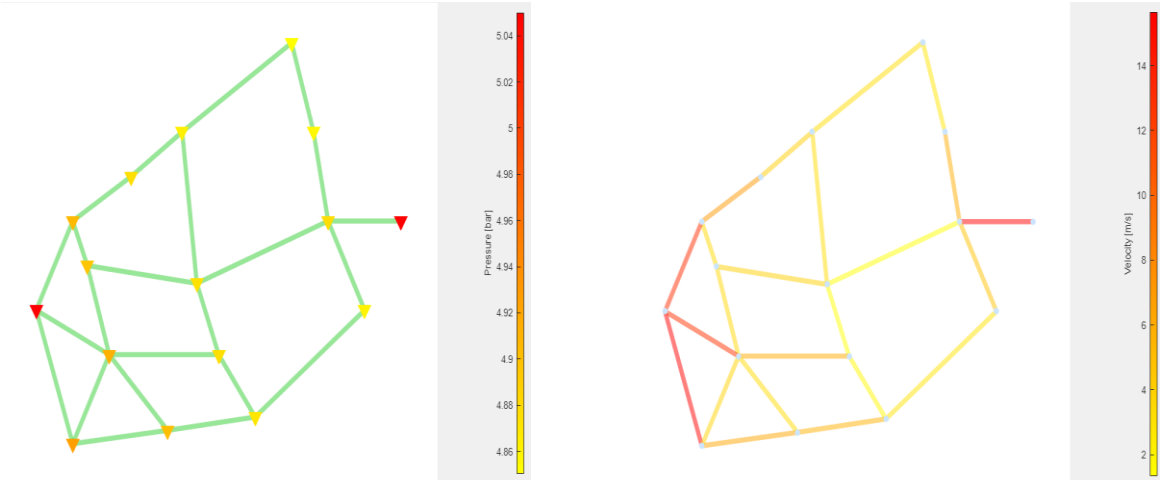

Figure 4.7: Case 4a: gas pressure at the demand nodes (left); gas velocity through the pipes (right)

4.5.2. Constant thermal power

In this simulation (case 4b), the volumetric flow supplied to the network is increased to 38430 Sm^3/h in order to maintain the same thermal input of the natural gas grid. The total volumetric flow needed by the network has been calculated by equation (4.2), knowing the thermal power that has to be introduced in the grid and the physical properties of hydrogen (density and lower heating value). This value is about 3,4 times higher than in the natural gas case due the smaller density of the hydrogen, even if its lower calorific value is higher.

As in the previous cases, the gas pressure at the demand nodes and the gas velocity in the pipes are represented in this case (figure 4.8) to compare them to the base scenario and to the case 4a.

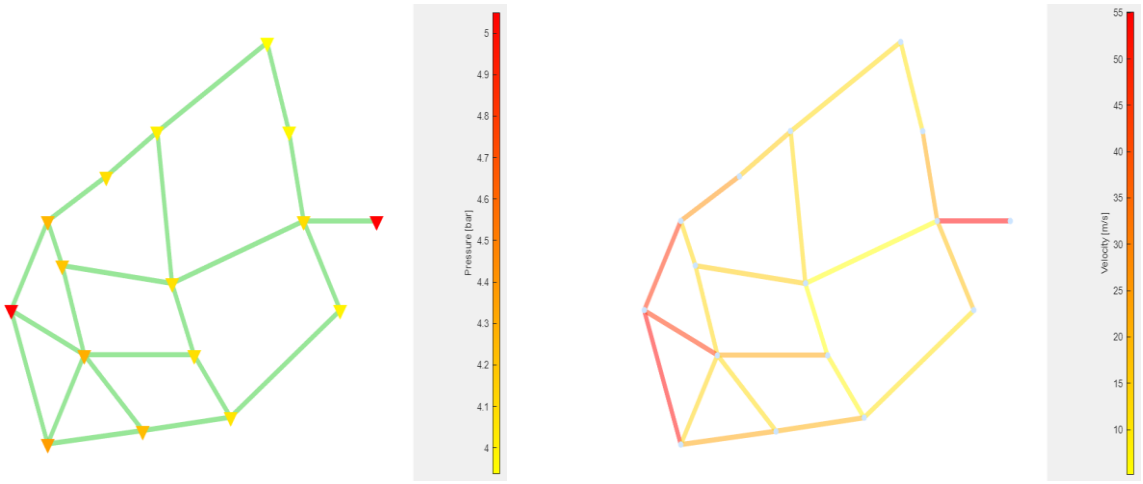

Figure 4.8: Case 4b: gas pressure at the demand nodes (left); gas velocity through the pipes (right)

The large increase of the volumetric flow causes a reduction of the pressure not only compared to the case 4a but also to case 1, despite the effect of the lower gas density that reduces the decrease of the pressure.

The pressure of the gas at the demand nodes is reduced to the 92-93% of case 1 and to 85% of the case 4a. The maximum pressure drop is 0,885 bar (around 17,7%) in HP1, the same pipe as in the base case. Also the pipes in which there are the maximum and the minimum amount of gas are the same as in case 1 (respectively

HP14 and HP7), as well as the pipe in which the maximum pressure drop per unit of length occur (HP14).

The main problem of this simulation regards the velocity of the gas through the pipes. The velocity, keeping constant the diameter of the pipes, depends on density and volumetric flow (equation (4.1)): the density reduction (by 90%) does not compensate the increase of the volumetric flow (by 3,4 times). As a result, an increase of the gas velocity by more than three times is obtained with respect to case 1. There are four pipes in which the gas velocity overcomes the upper limit of 25 m/s: HP1, HP14, HP22 and HP23, that are the pipes connecting to the gas distribution and metering stations (REMI A and B), reaching a maximum velocity of 54,55 m/s in HP1.

The solution comes from equation (4.1): increasing the flow section by adding a tube in parallel to the ones already existent in the pipes where the velocity is too high.

So, a new case (case 4c) is simulated, increasing the diameter of HP1 to 216 mm (the double of the base case, so the flow section increases by four times) and the diameter of HP14, HP22, HP23 to 150 mm (30% increase, the flow section almost doubles). The gas pressure at the demand nodes and the gas velocity in the pipes are represented in figure 4.9.

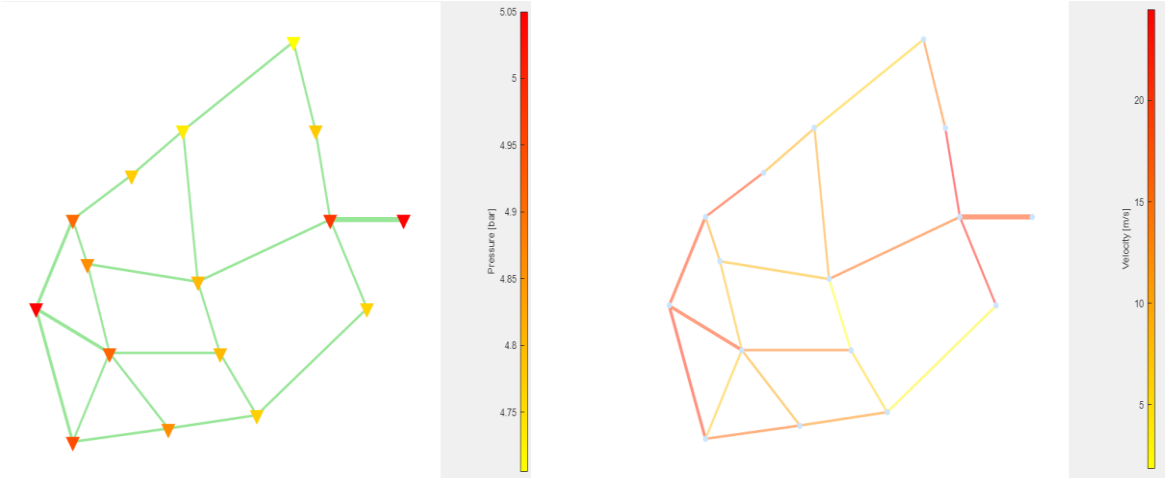

Figure 4.9: Case 4b: gas pressure at the demand nodes (left); gas velocity through the pipes (right)

The velocity is kept below the maximum limit in all the pipes, with the highest speed now reached in HP3 (24,24 m/s), that has maintained the same diameter as in the previous cases.

The velocity is kept below the maximum limit in all the pipes, with the highest speed now reached in HP3 (24,24 m/s), that has maintained the same diameter as in the previous cases.

The largest amount of gas now flows through HP1 because of the doubling of its diameter. However, it is not the pipe in which the highest value of pressure drop occurs because the flow passage area is larger. The effect of the diameter increase is that the pressure drops are lower, with an increase of the demand nodes pressure by around 15% compared to case 4b (and an increase by around 10% with respect to the base case). The maximum pressure drop is 0,154 bar (3,04%) in HP2, while the largest pressure loss per unit of length is in HP3, because of the highest velocity of the gas in this pipe.

The distribution of the flow in the two injection points is different with respect to case 1: REMI A supplies 27% of the total gas demand in the natural gas case and 40% in the hydrogen case. This is mainly due to the larger diameter increase in HP1.

The main results of the simulations of the cases 4a, 4b and 4c are reported and compared to case 1 in table 4.13.

Table 4.13: Main results of the simulations (case 4)

	Case 1	Case 4a	Case 4b	Case 4c
Max P loss (pipes) [bar]	0,586 (HP1)	0,087 (HP1)	0,885 (HP1)	0,154 (HP2)
Max P loss (pipes) [mbar/m]	0,858 (HP14)	0,126 (HP14)	1,27 (HP14)	0,286 (HP3)
Max F (pipes) [Sm^3/h]	3102 (HP14)	3096 (HP14)	10304 (H14)	14655 (HP1)
Min F (pipes) [Sm^3/h]	261 (HP7)	267 (HP7)	878 (HP7)	361 (HP7)
Max velocity [m/s]	16,02 (HP14)	15,5 (HP14)	54,55 (HP1)	24,24 (HP3)
Max P (nodes) [bar]	5 (A1, A14)	5 (A1, A14)	5 (A1, A14)	5 (A1, A14)
Min P (nodes) [bar]	4,33 (A5)	4,90 (A5)	3,98 (A5)	4,75 (A5)
F in REMI A (A1) [Sm^3/h]	3036	3069	10136	14655
F in REMI B (A14) [Sm^3/h]	8264	8231	27433	22914
Thermal input [MW]	105,2	31,6	105,2	105,2

4.5.3. Differences between winter and summer scenario

All the cases presented until this point refer to a winter condition, in which the domestic demand is higher because of the need for house heating in some hours during the day. A summer scenario is studied in this section: under these circumstances all the gas demands but the industrial ones are likely to drop. The choice has been to use a 20% withdrawal of the winter one at every domestic node, while keeping constant the industrial load. The objective is to compare the behaviour of a natural gas grid (case 1) and a hydrogen grid (case 4c) when a significant decrease of the load happens.

The total volumetric flow demand is reduced to 5300 Sm^3/h in the natural gas grid and to 17620 Sm^3/h in the hydrogen grid, so less than half of the gas supplied to the network in the winter.

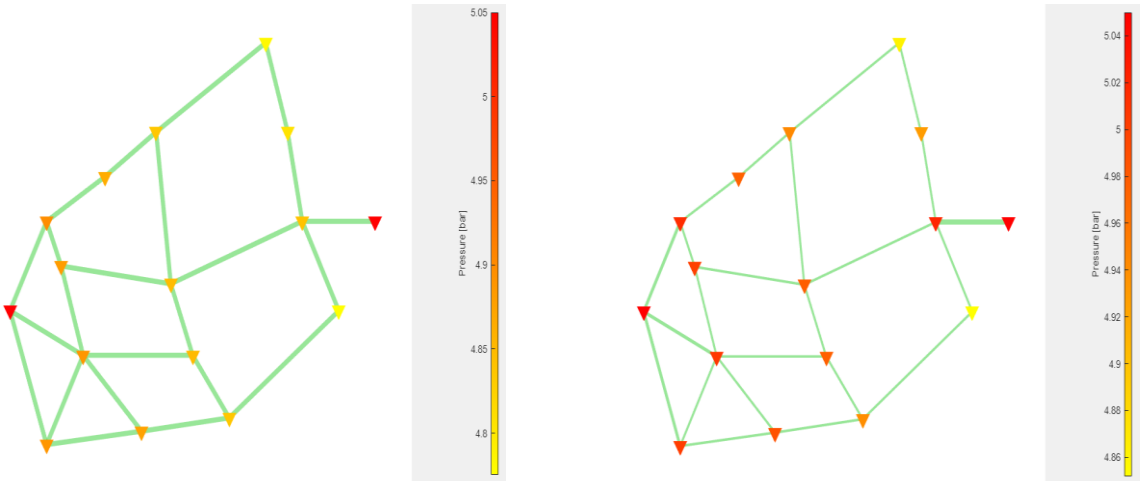

Figure 4.10: Gas pressure at the demand nodes in the summer case in case 1 (natural gas grid, left) and in case 4c (hydrogen grid, right)

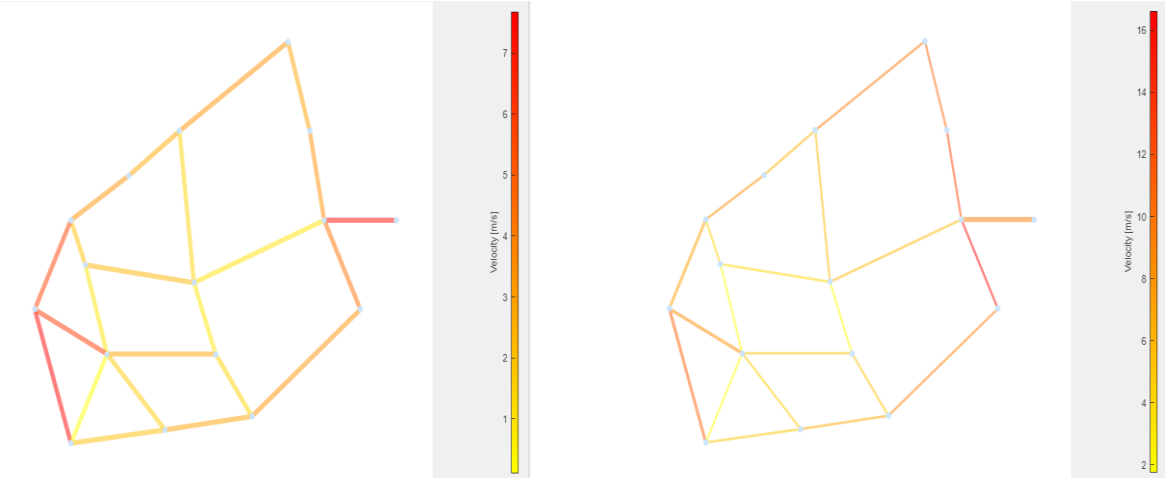

Figure 4.11: Gas velocity in the pipes in the summer case in case 1 (natural gas grid, left) and in case 4c (hydrogen grid, right)

The change of behaviour between summer and winter is similar for natural gas and hydrogen, with a decrease of the pressure drops and of the velocities due to the lower volumetric flow injected into the grid.

The maximum pressure drop occurs in the same pipe as in winter in both cases (HP1 in the natural gas grid, HP2 in the hydrogen grid), but it is reduced to 0,135 bars in

the case 1 and to 0,081 bars in case 4c (respectively 2,7% and 1,6%). The gas pressure at the demand nodes increases by 10-12% when natural gas is supplied to the grid and by 2-4% when hydrogen is injected, with the lower increases that happen in the industrial nodes, since the load remains constant.

The situation is more variable in terms of velocity: the gas is slower in most of the pipes due to the lower volumetric flow, but the decrease has a different rate in every pipe (up to 80% slower). There are also some pipes in which the gas is slightly faster than in the winter case (HP20 in both cases and HP5 in the hydrogen grid). This is mainly due to the different path of the gas through the network between winter and summer, since some nodes have the same demand in both seasons and some others have a demand reduced by 80%.

The results are shown in table 4.14.

Table 4.14: Main results of the simulations (cases 1 and 4c, winter and summer)

	Case 1	Case 1 - summer	Case 4c	Case 4c - summer
Max P loss (pipes) [bar]	0,586 (HP1)	0,135 (HP1)	0,154 (HP2)	0,081 (HP2)
Max P loss (pipes) [mbar/m]	0,858 (HP14)	0,208 (HP14)	0,286 (HP3)	0,135 (HP2)
Max F (pipes) [Sm^3/h]	3102 (HP14)	1514 (HP14)	14655 (HP1)	7342 (HP1)
Min F (pipes) [Sm^3/h]	261 (HP7)	21 (HP7)	361 (HP7)	344 (HP7)
Max velocity [m/s]	16,02 (HP14)	7,6 (HP14)	24,24 (HP3)	16,09 (HP2)
Max P (nodes) [bar]	5 (A1, A14)	5 (A1, A14)	5 (A1, A14)	5 (A1, A14)
Min P (nodes) [bar]	4,329 (A5)	4,823 (A2)	4,753 (A5)	4,90 (A2)
F in REMI A (A1) [Sm^3/h]	3036	1450	14655	7342
F in REMI B (A14) [Sm^3/h]	8264	3850	22914	10279
Thermal input [MW]	105,2	49,3	105,2	49,3

4.6. Effect of different fractions of H_2 in the gas

As observed in the section 4.4, the substitution of the natural gas with hydrogen in the network has strong effects on velocities, pressures and thermal power supplied to the withdrawal nodes. The goal of this section is to analyze how these properties behave gradually increasing the fraction of hydrogen in the natural gas, assuming that the blending between natural gas and hydrogen has already happened when they enter the grid analyzed. In particular, gases with a hydrogen molar fraction of 5%, 10%, 20%, 50% are considered (case 5).

The injection of hydrogen fractions into the gas changes the molar mass, the density and the lower heating value (LHV) of the mixture. As a consequence, the volumetric flow has to vary to keep the thermal input constant in the network.

The equations used to calculate the volumetric flow that has to be supplied to the grid given the molar fractions of every mixture are reported below:

$$MM\left[\frac{kg}{kmol}\right] = \sum_{i=1}^{N_s} MM_i * x_i \tag{4.7}$$

$$y_i = x_i * \frac{MM}{MM_i} \tag{4.8}$$

$$LHV\left[\frac{MJ}{kg}\right] = \sum_{i=1}^{N_s} LHV_i * y_i \tag{4.9}$$

$$LHV\left[\frac{MJ}{Sm^3}\right] = \rho\left[\frac{kg}{Sm^3}\right] * LHV \tag{4.10}$$

$$F\left[\frac{Sm^3}{h}\right] = \sum_{i=1}^{N_d} \frac{Thermal\ power\ needed_i\ [MW]}{Specific\ energy\left[\frac{MJ}{Sm^3}\right]} * 3600 \tag{4.11}$$

The results of these calculations are reported in table 4.15.

Table 4.15: Results of the calculations used to obtain the volumetric flow

H_2 molar fraction in the gas	0%	5%	10%	20%	50%	100%
Density of the gas [kg/Sm³]	0,691	0,661	0,63	0,569	0,387	0,084
LHV of the gas [MJ/kg]	48,5	48,9	49,5	50,6	56,3	120
Specific energy of the gas [MJ/Sm³]	33,5	32,4	31,2	28,8	21,8	10,1
Total volumetric flow [Sm³/h]	11300	11706	12154	13148	17384	37570

Increasing the molar fraction of hydrogen in the mixture, the density of the mixture decreases and its LHV goes up, but with a minor variation than the one of the density. As a result, the specific energy of the gas linearly decreases and the quantity of gas supplied to the network grows in a non-linear way (figure 4.12).

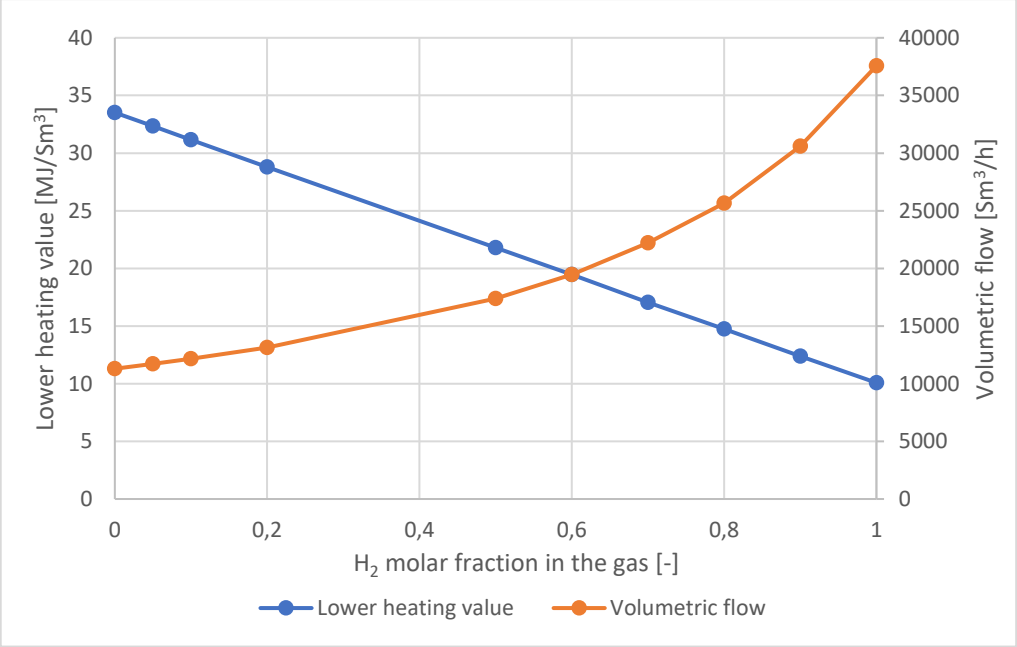

Figure 4.12: Lower heating value and volumetric flow as a function of the hydrogen fraction

The composition variation and the volumetric flow increase have a significant impact on the physical properties of the gas flowing in the network.

If the volumetric flow was kept constant, decreasing the thermal power supplied to the network, the pressure of the gas at the demand nodes would increase in an almost linear way when a higher fraction of hydrogen is present, given the decrease of the density of the mixture. In particular, the pressure of a gas with 50% H_2 molar fraction at the demand nodes is about 5% higher than the one of a gas with no hydrogen.

Increasing the volumetric flow in order to keep the thermal power constant, the pressure goes down with higher fractions of hydrogen despite the density reduction. Also in this case, the trend of the pressure is linear, with a (about) 5% pressure decrease for a gas with 50% H_2 molar fraction with respect to the natural gas without hydrogen.

In figure 4.13, the pressure of the gas at some of demand nodes in different parts of the network (A2 and A3 in the right side, A6 and A9 in the middle, A10 and A11 in the left side) is reported, showing that the nodes in the right side of the network withdraw the gas with the higher pressure and the ones in the middle of the grid receive the gas with the lower pressure.

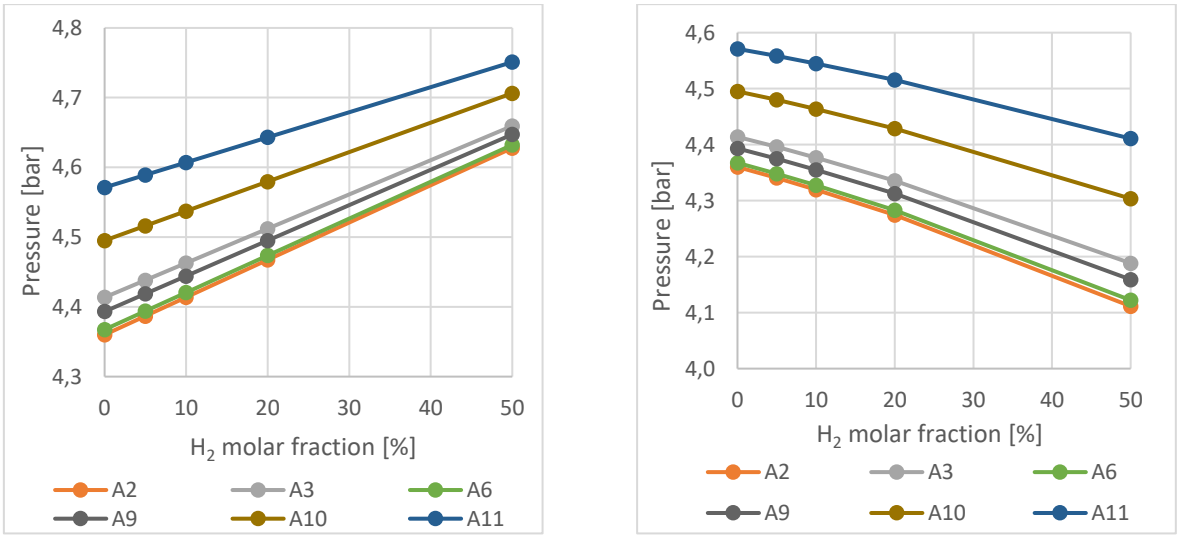

Figure 4.13: Gas pressure at the demand nodes in the constant volumetric flow case (left) and in the constant thermal power case (right)

In tables 4.16, the percentage variations of the pressure at the demand nodes with respect to the case without hydrogen are reported.

Table 4.16: Gas pressure variation at the demand nodes (constant flow, left; constant thermal power, right)

x H2	5%	10%	20%	50%
A2	+0,6%	+1,2%	+2,5%	+6,1%
A3	+0,6%	+1,1%	+2,2%	+5,6%
A4	+0,6%	+1,3%	+2,5%	+6,3%
A5	+0,7%	+1,3%	+2,6%	+6,5%
A6	+0,6%	+1,2%	+2,4%	+6,1%
A7	+0,6%	+1,1%	+2,3%	+5,7%
A8	+0,6%	+1,1%	+2,3%	+5,6%
A9	+0,6%	+1,2%	+2,3%	+5,8%
A10	+0,5%	+0,9%	+1,9%	+4,7%
A11	+0,4%	+0,8%	+1,6%	+3,9%
A12	+0,4%	+0,9%	+1,7%	+4,4%
A13	+0,5%	+1,0%	+2,0%	+4,9%
A15	+0,5%	+0,9%	+1,8%	+4,6%
A16	+0,6%	+1,1%	+2,3%	+5,6%

x H2	5%	10%	20%	50%
A2	-0,4%	-0,9%	-2,0%	-5,7%
A3	-0,4%	-0,8%	-1,8%	-5,1%
A4	-0,5%	-1,0%	-2,0%	-5,9%
A5	-0,5%	-1,0%	-2,1%	-6,0%
A6	-0,4%	-0,9%	-1,9%	-5,6%
A7	-0,4%	-0,9%	-1,8%	-5,2%
A8	-0,4%	-0,8%	-1,8%	-5,2%
A9	-0,4%	-0,9%	-1,8%	-5,3%
A10	-0,3%	-0,7%	-1,5%	-4,3%
A11	-0,3%	-0,6%	-1,2%	-3,5%
A12	-0,3%	-0,6%	-1,4%	-3,9%
A13	-0,4%	-0,7%	-1,5%	-4,5%
A15	-0,3%	-0,7%	-1,4%	-4,1%
A16	-0,4%	-0,8%	-1,8%	-5,2%

The velocity of the gas through the pipes also changes as the gas composition varies. If the volumetric flow supplied to the network was kept the same, the velocity would be reduced due to the lower density of the gas. However, the percentage variation is significantly different between the pipes. The pipes in which the gas is fast, like HP1 and HP22, are the ones that are less affected by the increase of the hydrogen fraction (here, the gas is 1,8% slower in a gas with 50% H_2 compared to 0% H_2), while the composition has a stronger influence on a slower gas (up to 5% slower in a gas blended with 50% H_2).

Increasing the volumetric flow, the gas velocity goes up with higher fractions of hydrogen, but it is now strongly influenced by the composition. The percentage increase of the velocity grows as the fraction of hydrogen in the gas is greater, up to 60% in some pipes in a 50% H_2 gas. This happens because velocity follows the trend of the volumetric flow. The maximum velocity is reached in HP1 and it is almost equal to 25 m/s, meaning that the pipe diameter has to increase for hydrogen fractions higher than 50%.

Figure 4.14 shows the velocity of the gas in the pipes in the two cases (constant flow rate and constant thermal power) in different places of the network (HP1 and HP2 in the right side, HP5 and HP7 in the middle, HP11 and HP23 in the left side).

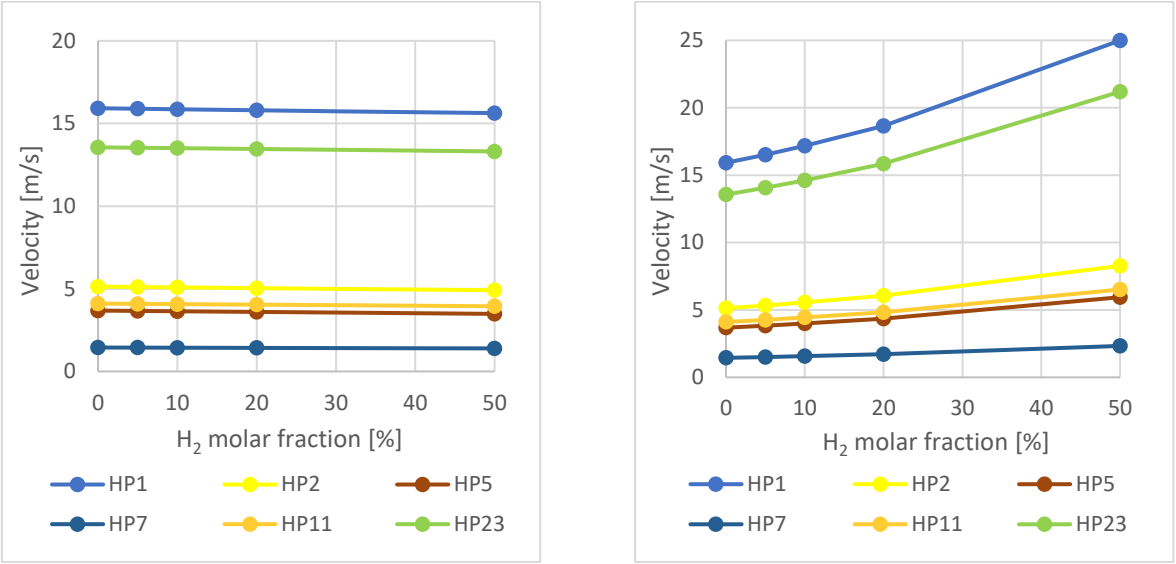

Figure 4.14: Gas velocity at the demand nodes in the constant volumetric flow case (left) and in the constant thermal power case (right)

Table 4.17 show the percentage variation of the velocity, with respect to the case without hydrogen, considering the different fractions of hydrogen in the gas.

Table 4.17: Gas velocity variation in the pipes (constant volumetric flow, left; constant thermal power, right)

x H2	5%	10%	20%	50%
HP1	-0,2%	-0,4%	-0,8%	-1,8%
HP2	-0,5%	-0,9%	-1,8%	-4,2%
HP3	-0,5%	-0,9%	-1,8%	-4,4%
HP4	-0,5%	-1,0%	-1,9%	-4,5%
HP5	-0,6%	-1,1%	-2,2%	-5,4%
HP6	-0,5%	-1,1%	-2,1%	-5,3%
HP7	-0,4%	-0,8%	-1,6%	-3,7%
HP8	-0,5%	-1,1%	-2,1%	-5,2%
HP9	-0,4%	-0,9%	-1,8%	-4,3%
HP10	-0,3%	-0,7%	-1,3%	-3,2%
HP11	-0,4%	-0,8%	-1,6%	-4,0%
HP12	-0,4%	-0,9%	-1,7%	-4,3%
HP13	-0,4%	-0,8%	-1,7%	-4,2%
HP14	-0,2%	-0,3%	-0,6%	-1,6%
HP15	-0,4%	-0,8%	-1,7%	-4,2%
HP16	-0,4%	-0,8%	-1,6%	-4,0%
HP17	-0,5%	-0,9%	-1,9%	-4,5%
HP18	-0,5%	-1,0%	-2,0%	-5,0%
HP19	-0,4%	-0,8%	-1,7%	-4,0%
HP20	-0,5%	-1,1%	-2,2%	-5,4%
HP21	-0,5%	-0,9%	-1,8%	-4,3%
HP22	-0,2%	-0,4%	-0,7%	-1,8%
HP23	-0,2%	-0,4%	-0,7%	-1,8%

x H2	5%	10%	20%	50%
HP1	+3,8%	+7,9%	+17,1%	+57,0%
HP2	+4,0%	+8,3%	+18,2%	+61,3%
HP3	+4,0%	+8,4%	+18,2%	+61,3%
HP4	+4,0%	+8,5%	+18,4%	+62,1%
HP5	+4,0%	+8,4%	+18,2%	+61,4%
HP6	+4,0%	+8,3%	+18,2%	+60,8%
HP7	+4,0%	+8,4%	+18,1%	+61,1%
HP8	+3,9%	+8,3%	+18,1%	+60,6%
HP9	+3,9%	+8,2%	+17,9%	+60,2%
HP10	+3,9%	+8,1%	+17,7%	+59,1%
HP11	+3,8%	+8,1%	+17,5%	+58,6%
HP12	+3,9%	+8,1%	+17,7%	+59,1%
HP13	+3,9%	+8,1%	+17,7%	+59,2%
HP14	+3,7%	+7,8%	+16,9%	+56,0%
HP15	+3,9%	+8,1%	+17,7%	+59,4%
HP16	+3,9%	+8,2%	+17,9%	+60,1%
HP17	+3,9%	+8,3%	+18,2%	+61,1%
HP18	+3,9%	+8,2%	+17,9%	+60,0%
HP19	+3,9%	+8,2%	+17,9%	+59,9%
HP20	+4,0%	+8,3%	+18,1%	+61,0%
HP21	+4,0%	+8,3%	+18,1%	+60,7%
HP22	+3,7%	+7,8%	+16,9%	+56,2%
HP23	+3,7%	+7,8%	+17,0%	+56,3%

4.7. Gas quality tracking

In the previous section (chapter 4.6), natural gas and hydrogen are assumed to be mixed before entering the distribution grid that is object of the study, so the composition of the gas supplied to the demand nodes is fixed. In the next sections, the two gases are injected in different positions of the grid, so they mix in some points of the network.

As discussed above, natural gas and hydrogen have different properties in terms of density and lower calorific value. The fact that they mix in the distribution grid means that every demand node withdraws a gas that can have a different composition with respect to the other ones, so different properties. In this context, knowing the composition of the gas in every point of the grid becomes crucial, so the concept of gas quality tracking is introduced in the model.

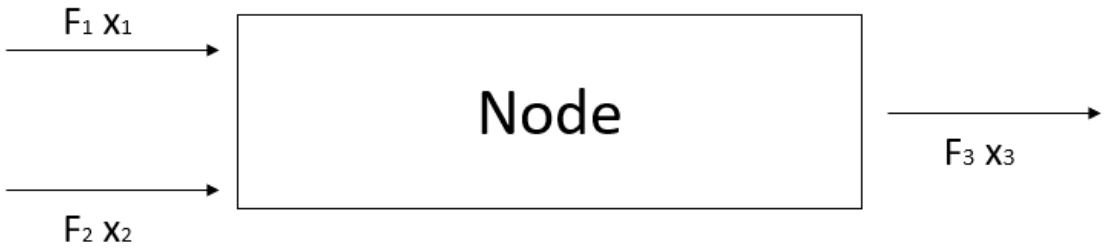

Figure 4.15: Example of a mixing between two flows in the grid

Figure 4.15 explains how the model has to work in order to track the composition of the gas flowing in the network. In every demand node, the flows coming from two or more pipes can arrive; they have not just different volumetric flow (F_1, F_2), like in the previous cases, but also different compositions (x_1, x_2). Therefore, the mixed gas has a different composition, x_3, that needs to be calculated.

More accurately, the model has to solve the following mass balance for every demand node, considering inlet pipes i, outlet pipes j and each species k.

$$\sum_{i=1}^{IN} F_i x_{i,k} = \sum_{j=1}^{OUT} F_j x_{j,k} \quad \forall k \tag{4.12}$$

Two constraints have to be respected:

$$\sum_k x_{i,k} = 1; \ \sum_k x_{j,k} = 1; \tag{4.13}$$

The unknown variable of (4.12) is the molar composition of the gas $x_{j,k}$.

Tracking the composition of the gas withdrawn by the demand nodes of the grid allows to know if the gas has a sufficient heating value in each point of the network or if the hydrogen presence has negatively influenced the energy delivered on customers' devices and appliances.

The gas quality tracking is applied in the next simulations, firstly considering a decentralized injection of hydrogen in different positions of the grid (case 6 and 7) and secondly analyzing the grid in which one of the two natural gas city-gate stations has been substituted with hydrogen (case 8).

4.8. Decentralized hydrogen injection

In this section, the hydrogen injection is treated like a decentralized injection, in the same way the biomethane injection has been considered in the chapter 4.4.

Four positions of injection are considered (figure 4.16):

- Pos. F: between A2 and A9, in the south-eastern region (lowly loaded branch)

- Pos. G: between A5 and A6, in the north-eastern region (lowly loaded branch)

- Pos. H: between A10 and A11, in the southern region (highly loaded branch)

- Pos. I: between A11 and A14, in the south-western region (highly loaded branch), close to REMI B.

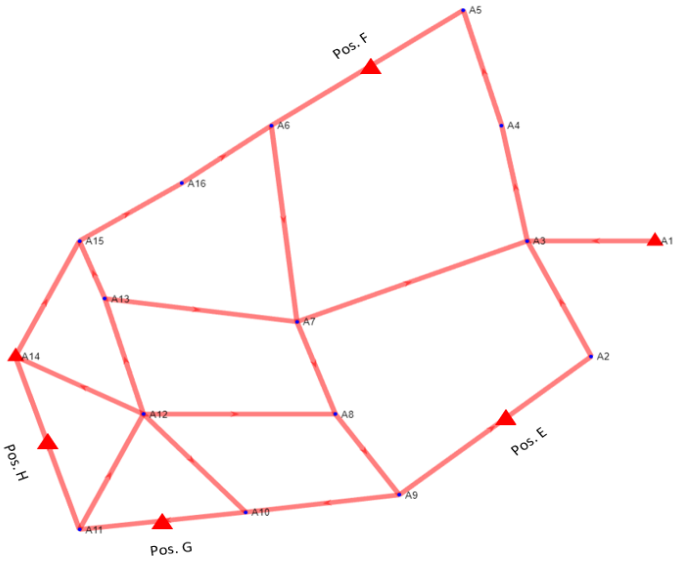

Figure 4.16: Positions of the hydrogen decentralized injection

As in the biomethane case, the comparison between the four positions of hydrogen injection is firstly made at the same flow rate (2200 Sm^3/h, case 6) and then with a sensitivity analysis varying the flow rate (between 500 and 2500 Sm^3/h, case 7). Pressures and velocities of the gas supplied to the withdrawal nodes are studied, like in the previous simulations, but also the composition of the gas in every point is now analysed, as explained in the chapter 4.7. The goal of this section is also to understand if the nodes ranking established by the parameters μ_1 and μ_2, introduced in chapter 4.3, is suitable to choose the position of a hydrogen injection.

Table 4.18: Positions of hydrogen injection (cases 6 and 7)

Position of injection	Nearest nodes	$\eta \left[\frac{Sm^3}{h\,m}\right]$	$\sigma \left[\frac{Sm^3}{h\,m}\right]$	$\mu_1 \left[\frac{Sm^3}{h\,m}\right]$	μ_2 [−]
Pos. F	A2	5,74	5,43	11,17	1,06
	A9	6,22	6,13	12,36	1,01
Pos. G	A5	6,07	4,88	10,95	1,25
	A6	7,17	5,69	12,86	1,26
Pos. H	A10	7,23	9,37	16,6	0,77
	A11	6,39	17,46	23,85	0,37
Pos. I	A11	6,39	17,46	23,85	0,37
	A14 (REMI)	-	-	-	-

4.8.1. Comparison at the same flow rate

In case 6, an injection of 2200 Sm^3/h of hydrogen is applied to the positions F, G, H, I of the grid (REMI C, node A17), in order to study the effect of an injection of the same amount of hydrogen in different positions of the network.

In terms of gas velocity through the pipes, the maximum value is always lower than the upper limit (25 m/s). In cases 6F and 6G, it is reached in the same pipe as in the base case, HP14, but it is reduced because a smaller amount of gas is supplied by REMI B, since there is an additional injection in another point of the grid. In cases 6H and 6I, the maximum velocity is reached in HP24, that is the pipe connected to the decentralized hydrogen supply: here, there is also the gas coming from the natural gas REMI station, so a large amount of gas flows. The gas velocity is particularly high (compared to the other cases) in HP24 in case 6I (20,97 m/s) because the pipe is connected to a REMI (REMI B) and to an industrial node (A11).

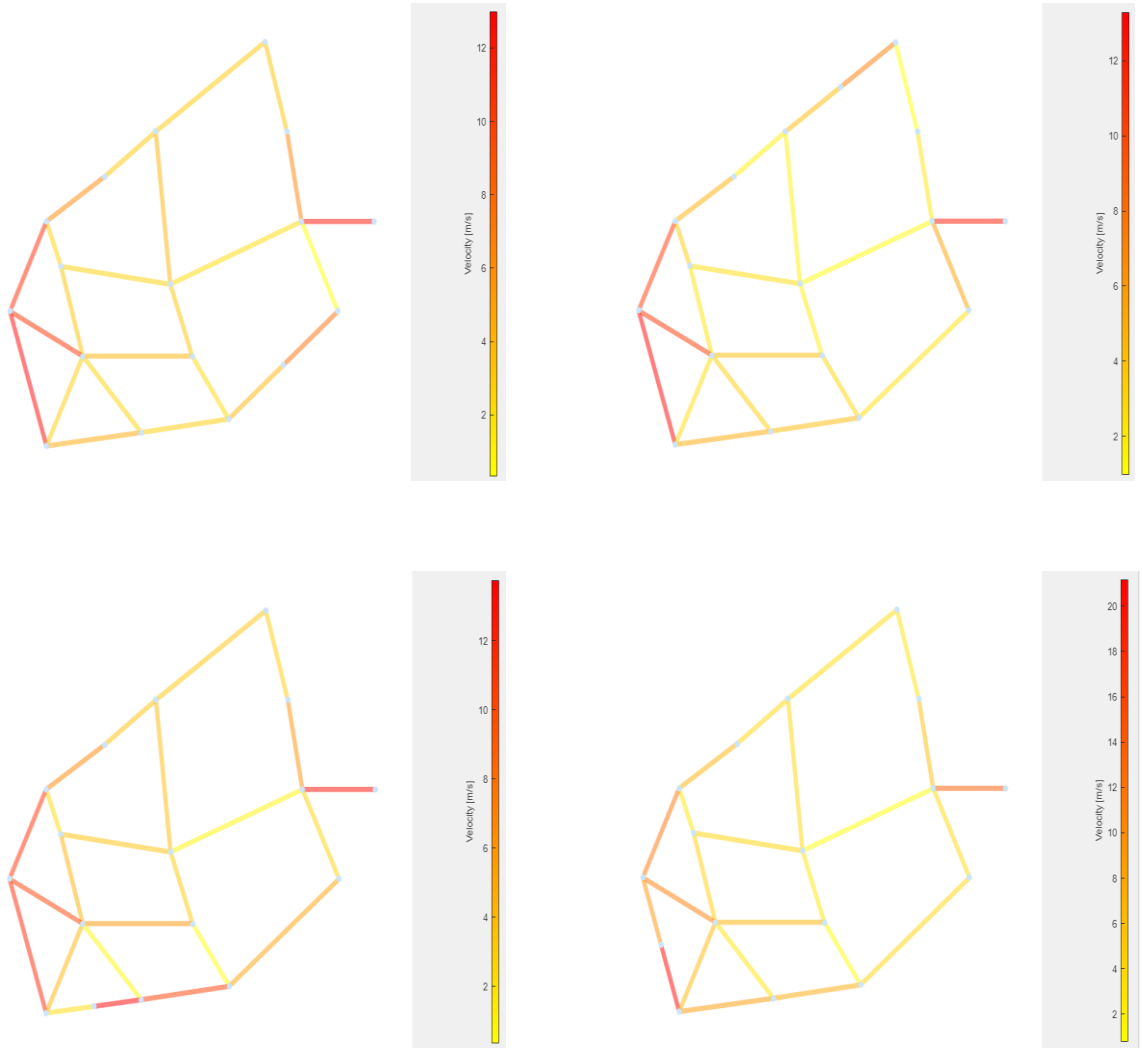

Figure 4.17: Gas velocity in the pipes (case 6F: top-left; case 6G: top-right; case 6H: bottom-left; case 6I: bottom-right)

The maximum pressure drop is always in HP1 due to the length of the pipe and the connection to REMI A, but it is reduced with respect to case 1. The highest pressure drop per unit of length is in HP14 in cases 6F and 6G (as in the base case), while it is in HP24 in case 6I because the largest amount of gas flows through this pipe; in case 6H, it is in HP1, despite the largest volumetric flow is in HP24, because the flow is 100% natural gas in HP1, so the density is higher (and the velocity goes up).

The pressure of hydrogen injection is higher in the cases 6H and 6I than in the other cases. This situation is similar to the one seen in the case of a biomethane injection,

in which the injection pressure was higher when the biomethane was supplied to a highly loaded branch. The consequence is that the cases 6F and 6G, in which hydrogen is injected in lowly loaded branches, have a higher minimum pressure at the demand nodes with respect to 6H and 6I. In particular, hydrogen is injected at a higher pressure in position I and the minimum pressure is reached in this case.

A difference with respect to the biomethane injection in the section 4.4.1 is that the quantity of hydrogen injected does not cause the need for a reduction of the pressure in the natural gas city-gate stations, that is kept at 5 bars. It means that a larger amount of hydrogen could be injected, as it will be shown in the section 4.8.2.

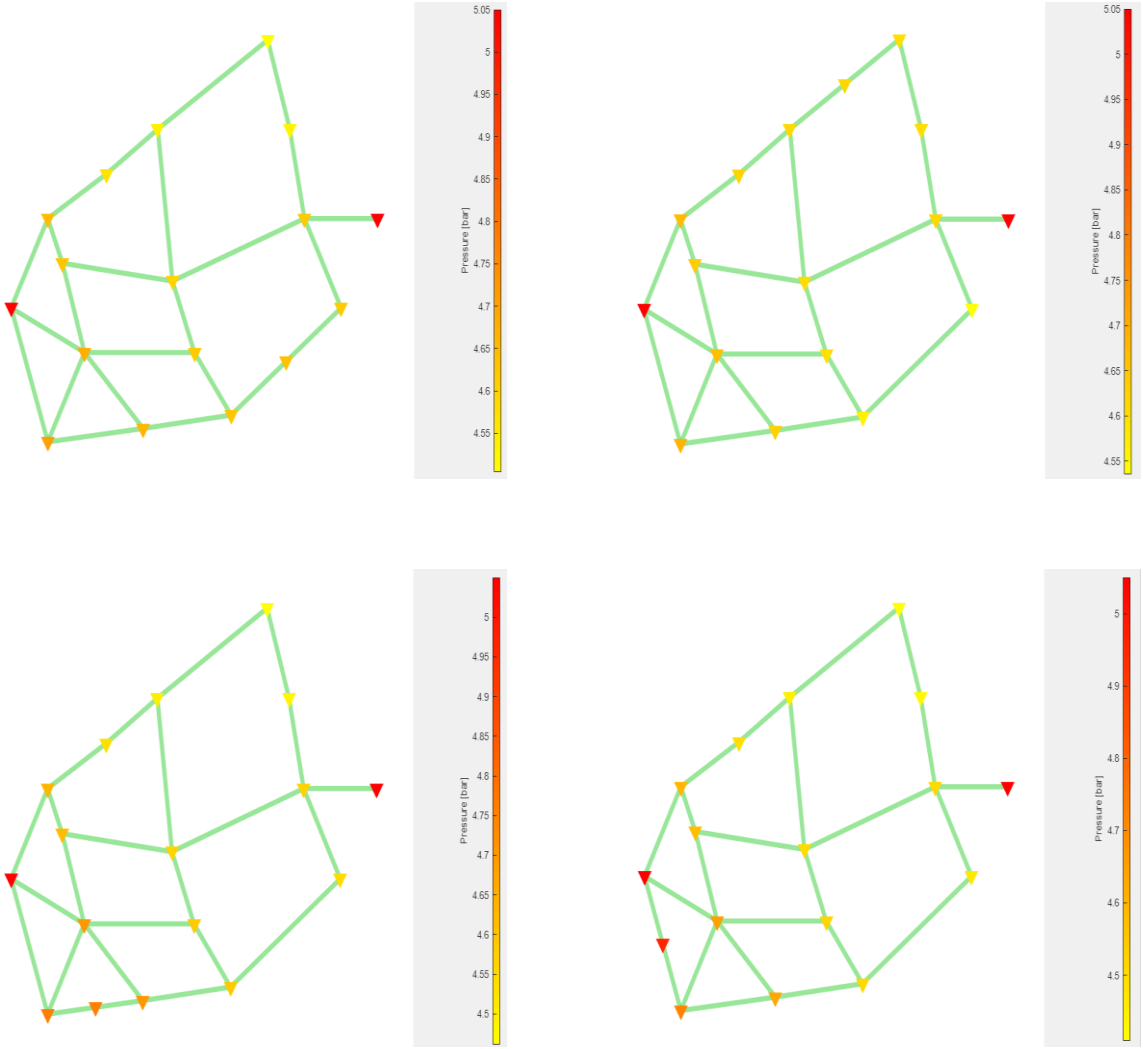

Figure 4.18: Gas pressure at the demand nodes (case 6F: top-left; case 6G: top-right; case 6H: bottom-left; case 6I: bottom-right)

As explained before, a decentralized hydrogen injection requires the gas quality tracking in order to check the energy contained in the gas withdrawn by the demand nodes. In the next figures, the composition of the gas in the network is shown. A white color indicates a 100% hydrogen composition and a red color a 100% natural gas composition.

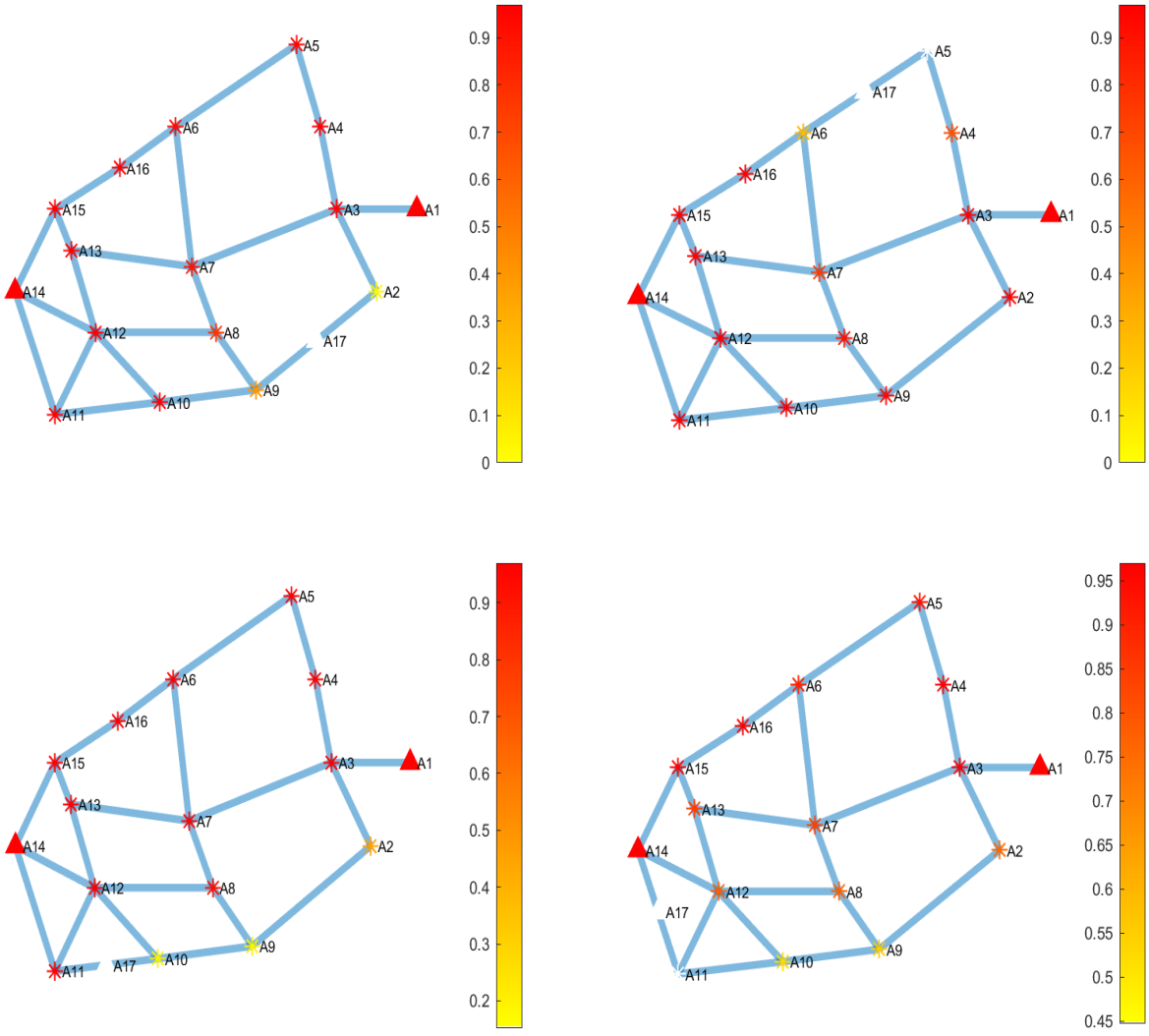

Figure 4.19: Gas quality tracking at the nodes (case 6F: top-left; case 6G: top-right; case 6H: bottom-left; case 6I: bottom-right)

Overall, the power input supplied to the network is 90,8 MW (obtained by equation (4.2)), 86,3% of the base scenario, in all the cases, but the composition of the gas in the demand nodes changes as the position of hydrogen injection varies. When hydrogen is injected in positions F and G, that are in a lowly loaded branch, it influences the composition of the gas withdrawn by six demand nodes in the right region of the network. The same thing happens in the south region in case 6H, even if it is in a highly loaded branch. When the decentralized injection is in position I, a larger number of nodes withdraws a gas that contains hydrogen (Figure 4.20).

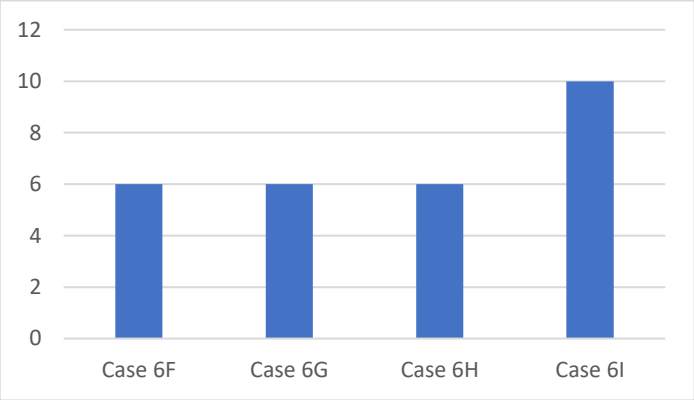

Figure 4.20: Number of demand nodes that receive a gas containing hydrogen (case 6)

The molar fraction of hydrogen in the gas supplied to each node and the percentage of thermal input, compared to the required one, supplied to each withdrawn node is reported in the following tables.

Table 4.19: H_2 molar fraction in the gas and percentage of required power supplied to each node (Case 6F: top-left; case 6G: top-right; case 6H: bottom-left; case 6I: bottom-right)

Node	$\%\frac{F_{H_2}}{F}$	$\%\frac{\dot{Q}}{\dot{Q}_{needed}}$
A2	96%	33%
A3	0%	100%
A4	0%	100%
A5	2%	98%
A6	5%	97%
A7	8%	94%
A8	20%	86%
A9	58%	59%
A10	0%	100%
A11	0%	100%
A12	0%	100%
A13	0%	100%
A15	0%	100%
A16	0%	100%

Node	$\%\frac{F_{H_2}}{F}$	$\%\frac{\dot{Q}}{\dot{Q}_{needed}}$
A2	53%	63%
A3	0%	100%
A4	0%	100%
A5	1%	100%
A6	1%	99%
A7	2%	99%
A8	4%	97%
A9	80%	44%
A10	80%	44%
A11	0%	100%
A12	0%	100%
A13	0%	100%
A15	0%	100%
A16	0%	100%

Node	$\%\frac{F_{H_2}}{F}$	$\%\frac{\dot{Q}}{\dot{Q}_{needed}}$
A2	1%	99%
A3	0%	100%
A4	31%	78%
A5	100%	30%
A6	72%	49%
A7	23%	84%
A8	7%	95%
A9	3%	98%
A10	0%	100%
A11	0%	100%
A12	0%	100%
A13	0%	100%
A15	0%	100%
A16	0%	100%

Node	$\%\frac{F_{H_2}}{F}$	$\%\frac{\dot{Q}}{\dot{Q}_{needed}}$
A2	22%	85%
A3	0%	100%
A4	0%	100%
A5	4%	97%
A6	7%	95%
A7	14%	90%
A8	20%	86%
A9	42%	70%
A10	46%	68%
A11	54%	62%
A12	20%	86%
A13	13%	91%
A15	0%	100%
A16	0%	100%

The tables above show how, keeping the same total volumetric flow supplied to the network as in case 1 (11300 Sm^3/h), the quantity of hydrogen injected (2200 Sm^3/h, 20% of the demand) reduces the energy provided to most of the demand nodes. Therefore, an increase of the natural gas supply with respect to this case is necessary

in order to satisfy the demand of all the withdrawal nodes. The procedure to do it is shown in the next section (4.8.2).

The main results of the simulations of case 6 are summarized in table 4.20.

Table 4.20: Main results of the simulations (case 6)

	Case 1	Case 6F	Case 6G	Case 6H	Case 6I
Closest nodes to the injection	-	A2, A9	A5, A6	A10, A11	A11, A14
Max P loss (pipes) [bar]	0,586 (HP1)	0,356 (HP1)	0,354 (HP1)	0,408 (HP1)	0,466 (HP1)
Max P loss (pipes) [mbar/m]	0,858 (HP14)	0,566 (HP14)	0,591 (HP14)	0,584 (HP1)	0,805 (HP24)
Max F (pipes) [Sm^3/h]	3102 (HP14)	2523 (HP14)	2578 (HP14)	2608 (HP24)	4083 (HP24)
Min F (pipes) [Sm^3/h]	261 (HP7)	62 (HP2)	185 (HP4)	66 (HP8)	146 (HP21)
Max velocity [m/s]	16,02 (HP14)	12,87 (HP14)	13,16 (HP14)	13,61 (HP24)	20,97 (HP24)
P in REMI A and B (A1, A14) [bar]	5	5	5	5	5
P in REMI C (A17) [bar]	-	4,66	4,65	4,75	4,92
Min P (nodes) [bar]	4,329 (A5)	4,55 (A5)	4,58 (A2)	4,51 (A5)	4,45 (A5)
F in REMI A (A1) [Sm^3/h]	3036	2375	2370	2542	2711
F in REMI B (A14) [Sm^3/h]	8264	6725	6730	6558	6389
F in REMI C (A17) [Sm^3/h]	-	2200	2200	2200	2200
Thermal input [MW]	105,2	90,8	90,8	90,8	90,8

4.8.2. Sensitivity analysis

In case 7, the quantity of hydrogen injected in positions F, G, H, I is varied from 500 to 2500 Sm^3/h. The objective of this analysis is to understand how composition,

pressure and velocity vary in the network when the amount of hydrogen is increased and which position of the grid seems more convenient to inject it.

First of all, the energy and the volumetric flow required by the network as a function of the quantity of hydrogen injected are analyzed, firstly keeping the total volumetric flow constant and then keeping the thermal power constant. In particular, the thermal power supplied, the total volumetric flow and the amount of natural gas required by the grid are calculated for the two methods proposed.

An iterative procedure has been used to simulate the case in which the energy supplied to the demand nodes is kept constant (figure 4.21).

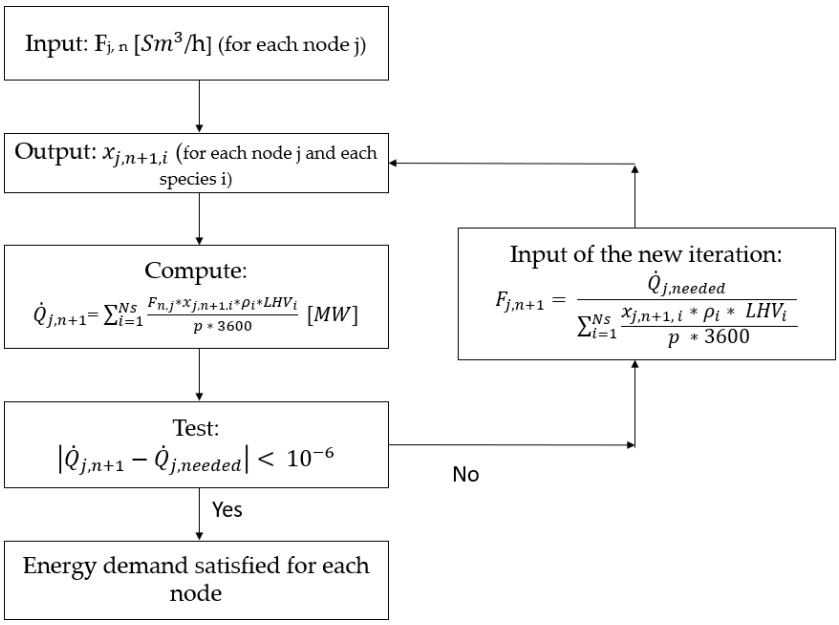

Figure 4.21: Iterative procedure for the constant power method (case 7)

The volumetric flow demand, that is an input of the simulation, and the composition of the gas at each node, that is an output, are changed at every iteration, producing a different thermal power. The iterative process is completed when the thermal power calculated is equal to the one needed (by case 1) in every withdrawal node.

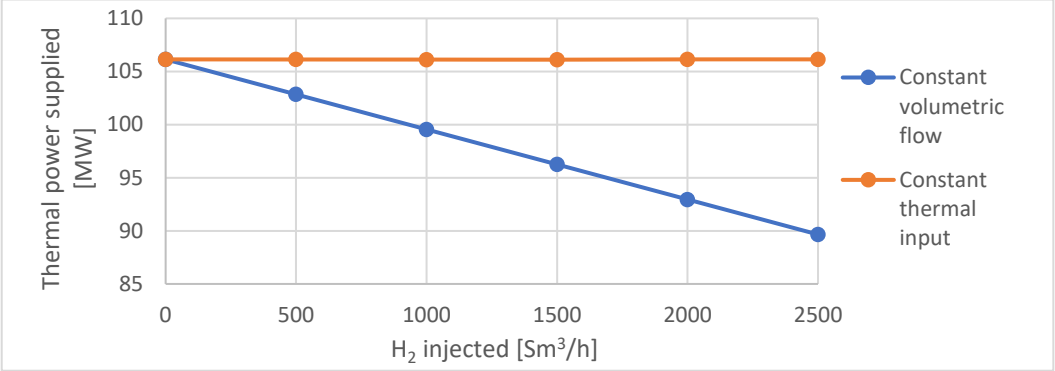

Figure 4.22: Thermal power supplied to the network for the two methods proposed (case 7)

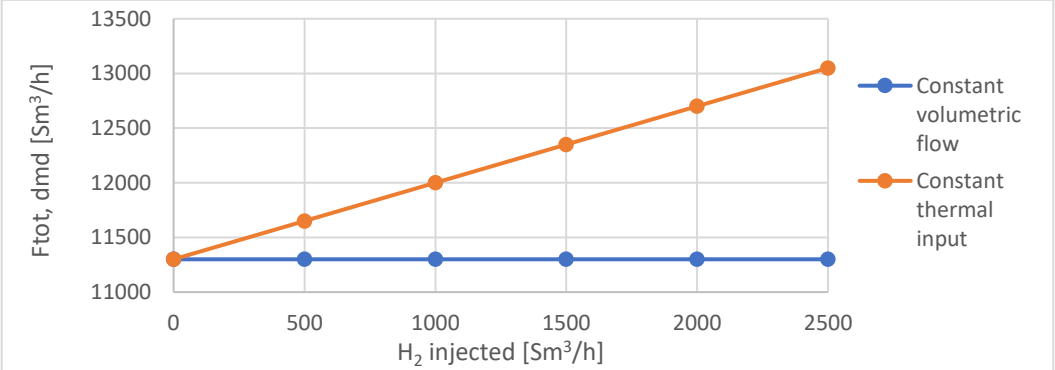

Figure 4.23: Total volumetric flow demand for the two methods proposed (case 7)

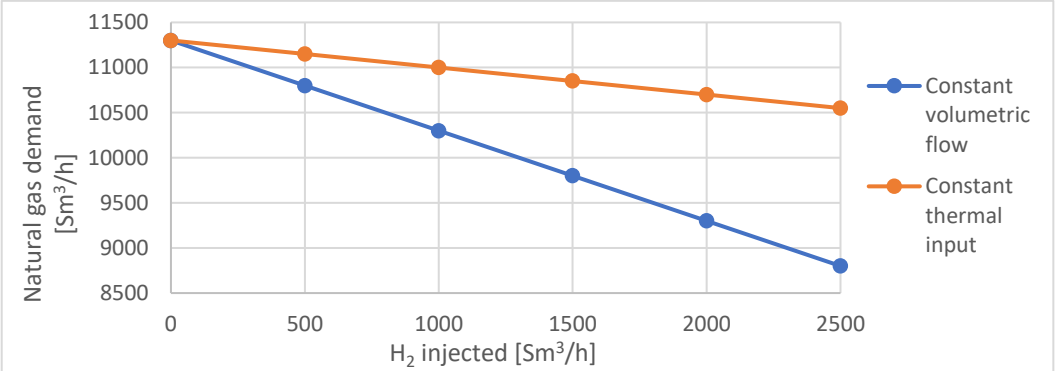

Figure 4.24: Natural gas demand for the two methods proposed (case 7)

The figures above show that, if the total volumetric flow was kept constant, the thermal input would decrease by 15% when 2500 Sm³/h of hydrogen are injected. To deliver the right amount of energy demand by users, the volumetric flow of gas withdrawn increases with the amount of hydrogen injected into the grid. Due to the

low heating value of the natural gas and hydrogen mixture, when 2500 Sm³/h of hydrogen are supplied, the total volumetric gas flow supplied by the network is up to 15% more than in the scenario without hydrogen injection (figure 4.23), but with a 7% decrease of the natural gas demand (figure 4.24).

The following figures show how the maximum hydrogen fraction varies at increasing amounts of hydrogen when it is injected in the four positions F, G, H, I.

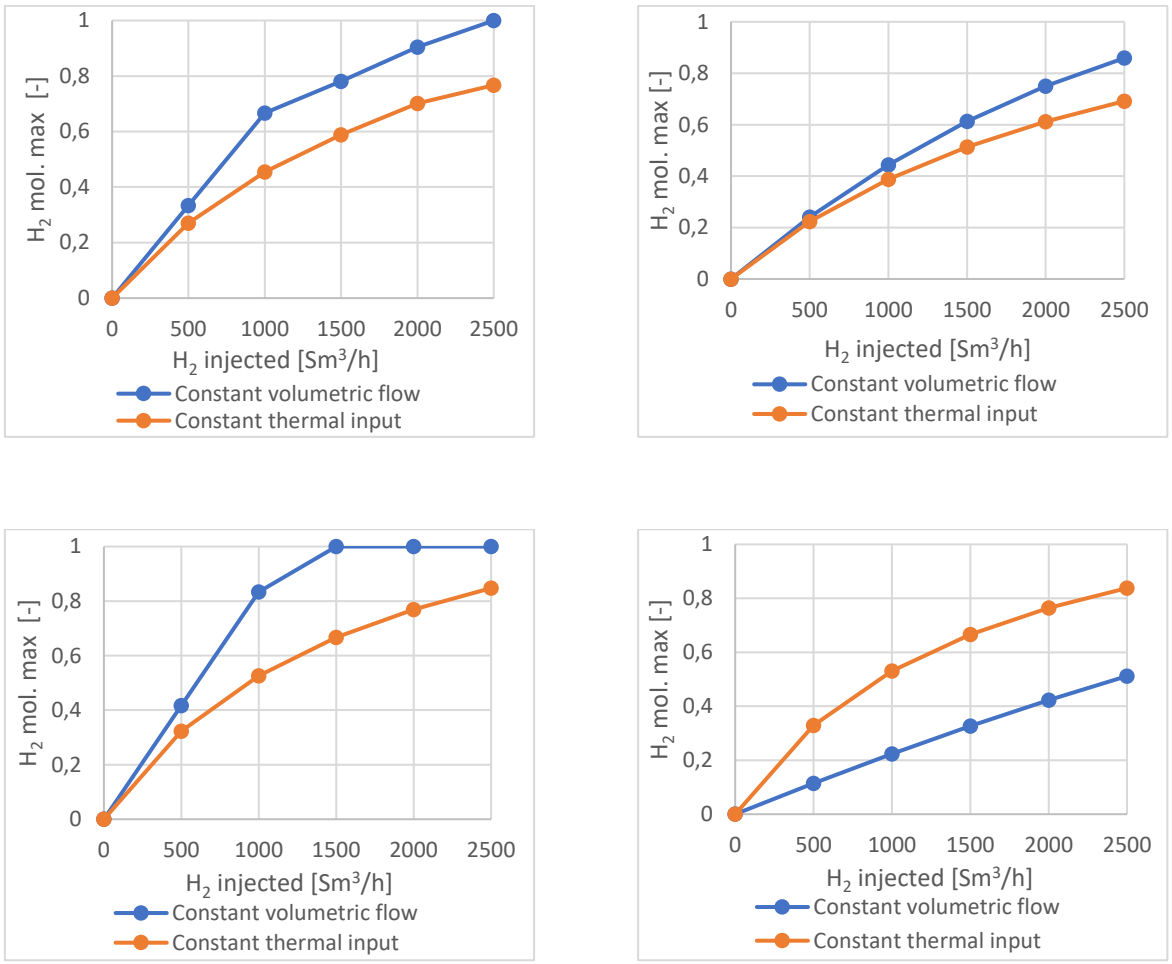

Figure 4.25: Maximum H_2 molar fraction for the two methods proposed (case 7F: top-left; case 7G: top-right; case 7H: bottom-left; case 7I: bottom-right)

The maximum fraction of hydrogen evaluated at the demand nodes increases with the amount of hydrogen injected in all the cases. The higher values are found in the cases 7F and 7G, in which the hydrogen injection is in a lowly loaded branch. The

case 7I is the one in which the gas has a lower hydrogen fraction: it happens because the injection is in a highly loaded area, so a larger number of nodes withdraws a gas containing hydrogen, but its molar fraction is lower in each node.

After that, the trends of the gas maximum velocity, its minimum pressure at the demand nodes and the hydrogen injection pressure as a function of the quantity of hydrogen injected (keeping the thermal power constant) are represented in the four positions.

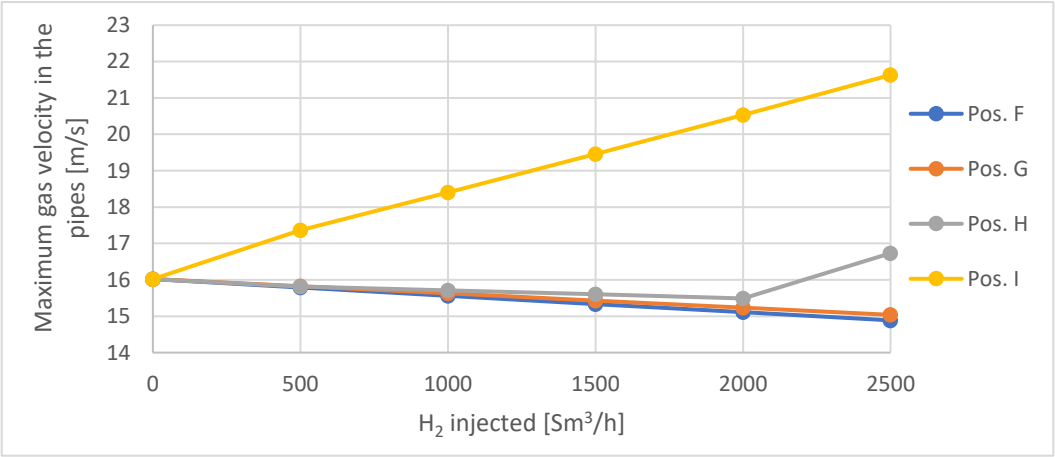

Figure 4.26: Maximum gas velocity in the pipes as a function of hydrogen injected

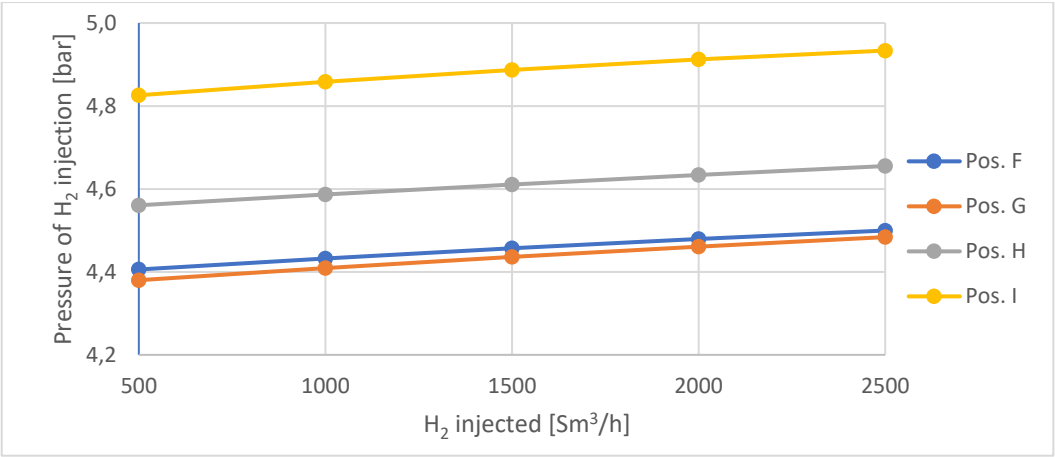

Figure 4.27: Hydrogen injection pressure as a function of hydrogen injected

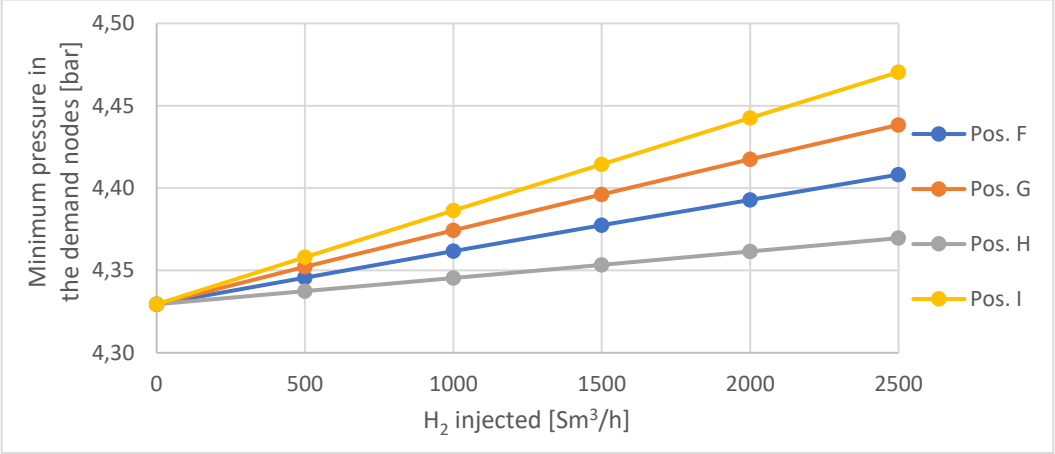

Figure 4.28: Minimum pressure at the demand nodes as a function of hydrogen injected

The figures above show how the injection pressure linearly goes up as the amount of hydrogen injected increases. Consequently, also the minimum pressure in the demand nodes linearly increases. In particular, the case 7I, in which the injection is in the highly loaded branch, is the one in which the higher injection pressures are reached.

The maximum velocity of the gas has a different trend depending on the injection position. In cases 7F and 7G, in the lowly loaded branch, it linearly decreases at higher amounts of hydrogen, while in case 7I linearly goes up; in case 7H, it has a change of trend at 2000 Sm^3/h. The different behaviour is caused by the fact that the velocity does not depend just on the volumetric flow, like in the previous cases, but also on the gas density, that changes in every point of the network.

To better understand what is the maximum quantity of hydrogen that can be injected before velocity and pressure overcome the allowable limits, a larger amount of hydrogen, between 3500 and 6000 Sm^3/h, is injected in positions F, H, I (position G is neglected since it has been observed that the results are very similar to those of position F). So, the maximum gas velocity in the pipes and the pressure of hydrogen injection are investigated again. The goal is to evaluate what is the minimum quantity of the gas at which the velocity of the gas is larger than 25 m/s and the hydrogen injection pressure reaches 5 bars.

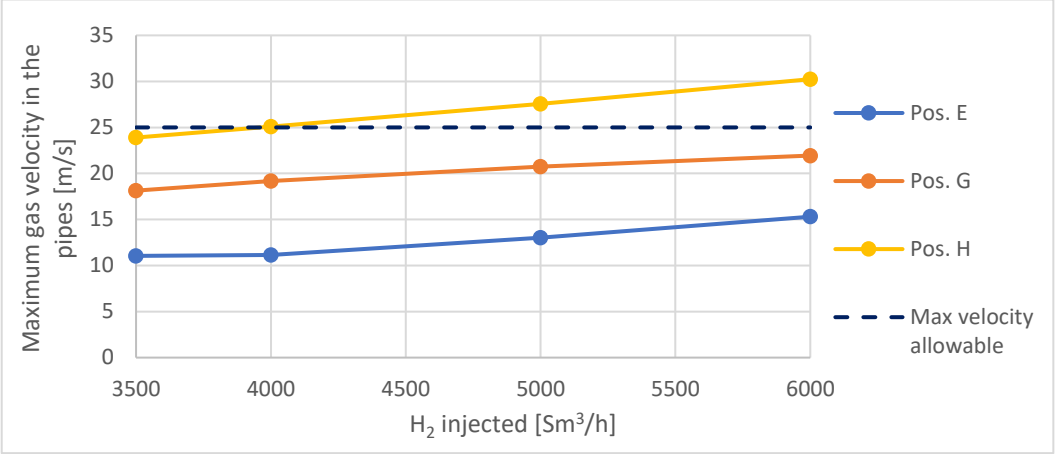

Figure 4.29: Maximum gas velocity in the pipes as a function of hydrogen injected (3500 – 6000 Sm^3/h)

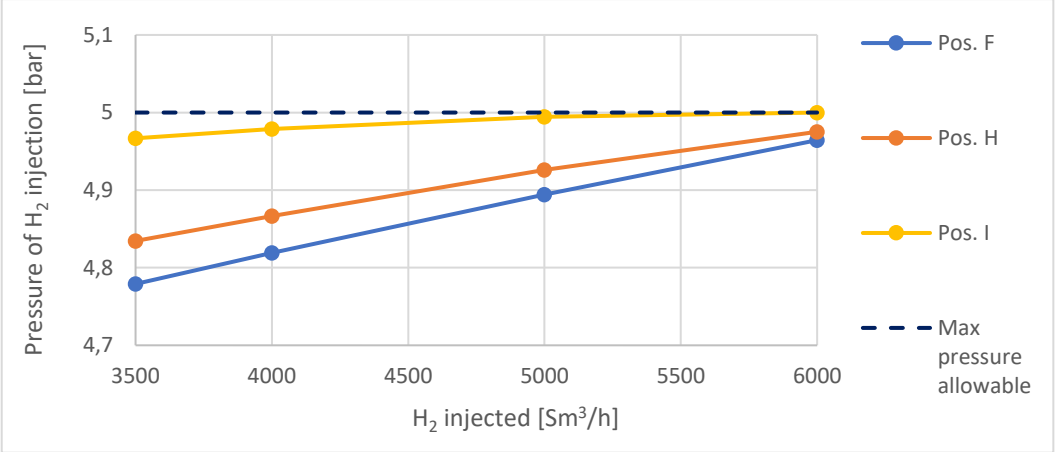

Figure 4.30: Hydrogen injection pressure as a function of hydrogen injected (3500 – 6000 Sm^3/h)

The case 7I is the one in which the lower amount of hydrogen can be injected before the velocity and the injection pressure overcome their allowable limit. In particular, the pipes' diameter should be increased at amounts of hydrogen larger than 4000 Sm^3/h and the pressure would be higher than 5 bars at more than 6000 Sm^3/h of hydrogen injected. In cases 7F (and 7G) a higher quantity of hydrogen can be supplied before overcoming the allowable limits. The case 7H is intermediate between the cases 7F and 7I, both velocity and pressure are below the allowable limits until 6000 Sm^3/h.

These results agree with the nodes ranking seen in chapter 4.3, since, as in the biomethane case, a position of injection near the node A11 (positions H and I) appears to be the worst place, meaning that it is the case in which the lower amount

of hydrogen can be injected before the need for an intervention in the network. The right region of the network (positions F and G) seems to be more convenient for a decentralized injection (from the point of view of the DSO), as expected by the ranking determined by the parameters discussed in chapter 4.3.

4.9. Grid with one NG supply and one H_2 supply

The last case examined (case 8) is the network in which a city-gate station supplies natural gas to the grid and the other one supplies hydrogen. In particular:

- Case 8a: hydrogen is injected in REMI A, natural gas is injected in REMI B.
- Case 8b: natural gas is injected in REMI A, hydrogen is injected in REMI B.

In these cases, the hydrogen supply is not treated as a decentralized injection, in which the flow rate is fixed (as in chapter 4.7), but the injection is at the nominal pressure of 5 bars (like the natural gas city-gate station).

The first considerations are on the gas quality tracking, analysing how the two gases mix in the network, in the case in which the total volumetric flow rate remains the same as the one of case 1 (11300 Sm^3/h).

In case 8a, the diameter of pipe HP1 has been increased to 120 mm in order to keep the gas velocity below 25 m/s.

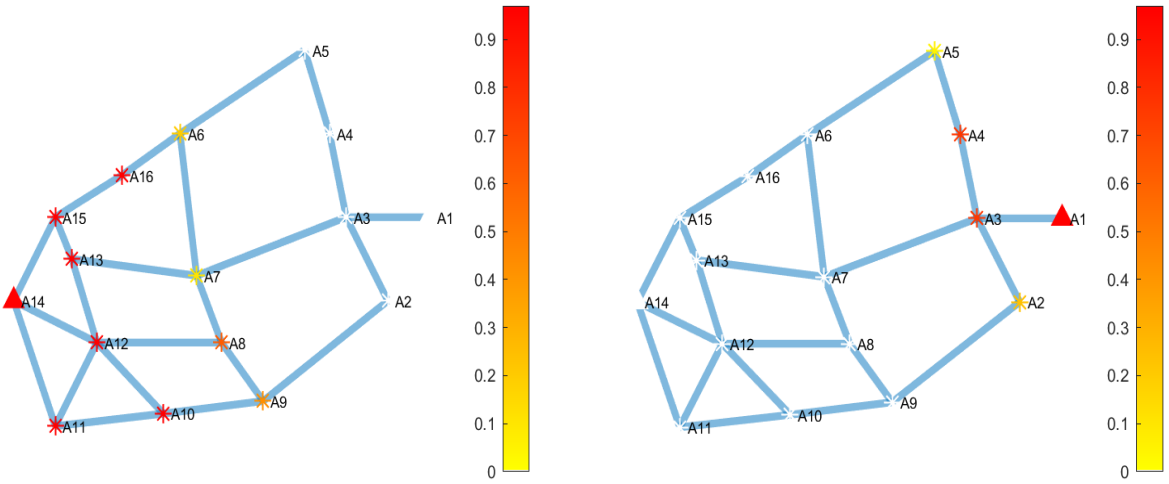

Figure 4.31: Gas quality tracking at the demand nodes when the volumetric flow rate is constant in case 8a (left) and in case 8b (right)

In case 8a, when the hydrogen is injected in the right region of the network, in which a lower number of nodes is present, the quantity of hydrogen injected at 5 bars is smaller than in case 8b, in which the injection is in a highly loaded branch. The low density of the hydrogen allows it to reach all the nodes in the grid and most of them receive a gas composed of 100% H_2. Therefore, the thermal power supplied to the grid is lower in case 8b. Overall, it is supplied the 63% of the total power needed in case 8a and the 39% in case 8b (table 4.26).

Table 4.21: H_2 molar fraction in the gas and percentage of required power supplied to each node (case 8, constant volumetric flow rate)

	Case 8a		Case 8b	
Node	$\%\frac{F_{H_2}}{F}$	$\%\frac{\dot{Q}}{\dot{Q}_{needed}}$	$\%\frac{F_{H_2}}{F}$	$\%\frac{\dot{Q}}{\dot{Q}_{needed}}$
A2	85%	30%	52%	47%
A3	100%	30%	0%	85%
A4	100%	30%	0%	85%
A5	81%	30%	61%	34%
A6	38%	44%	93%	30%
A7	64%	38%	82%	30%
A8	0%	75%	100%	30%
A9	0%	61%	100%	30%
A10	0%	100%	100%	30%
A11	0%	100%	100%	30%
A12	0%	100%	100%	30%
A13	0%	100%	100%	30%
A15	0%	100%	100%	30%
A16	0%	100%	100%	30%

In order to supply the energy required to each withdrawal node, the volumetric flow rate entering the grid has to be increased, as it has been done in the previous sections. The difference, with respect to chapter 4.7, is that the quantity of hydrogen supplied to the grid is not imposed, but its injection pressure is decided.

In theory, the injection pressure of hydrogen could be kept at 5 bars as in the case of a natural gas injection. The problem is that the velocity would be very high, as in the previous cases, when hydrogen is injected. The diameter increase would not be enough to keep the velocity under the allowable limit in this case because, at fixed pressure, a larger hydrogen flow would be introduced because of the larger passage area. So, the velocity would have two opposite effects: the larger diameter should decrease it, but the higher amount of flow should increase it.

The solution is to increase the diameter of the pipes connected to that station and, at the same time, to decrease the pressure of the hydrogen REMI station, in order to limit the quantity of hydrogen introduced. In this way, the velocity is kept below the limit of 25 m/s in all the pipes.

In particular, the adjustments made are:

- In case 8a, the pressure of hydrogen injection (REMI A) is decreased to 4,6 bars and the diameter of the pipe HP1 is increased to 170 mm (57% increase).
- In case 8b, the pressure of hydrogen injection (REMI B) is decreased to 4,4 bars; the diameter of the pipe HP14 is increased to 155 mm and the one of HP22 and HP23 is increased to 145 mm (respectively 43% and 34% increase).

The larger diameter increase in case 8a is due to the fact that there is only one pipe connected to the hydrogen station. In case 8b, the diameter of HP14 is larger than the one of HP22 and HP23 because HP14 connects the hydrogen station to A11, that is an industrial node, so a higher amount of gas flows through that pipe.

As a consequence of the choice of the hydrogen injection pressure, the pressure at the demand nodes is higher in case 8a than in case 8b. However, the minimum pressure is always in the node A5 (4,36 bars in case 8a and 4,05 bars in case 8b).

The maximum pressure drop of the gas is around 9% in case 8a (in HP23) and around 17% in case 8b (in HP1), therefore it occurs in the pipes in which natural gas flows.

The maximum velocities of the gas always occur in the pipes connected to the hydrogen supply, where the larger amount of gas flows, but it is kept below 25 m/s with the adjustments explained before.

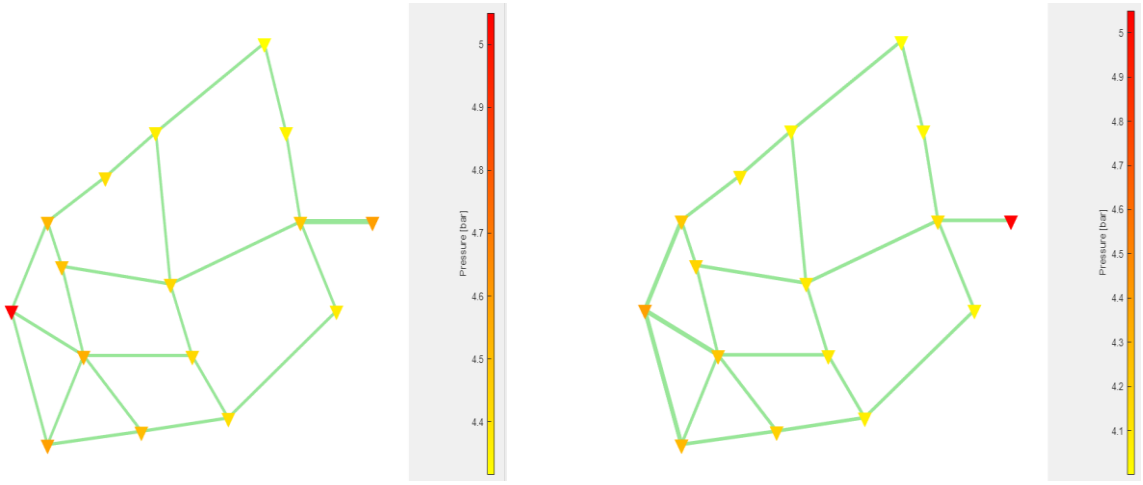

Figure 4.32: Gas pressure at the demand nodes in case 8a (left) and in case 8b (right)

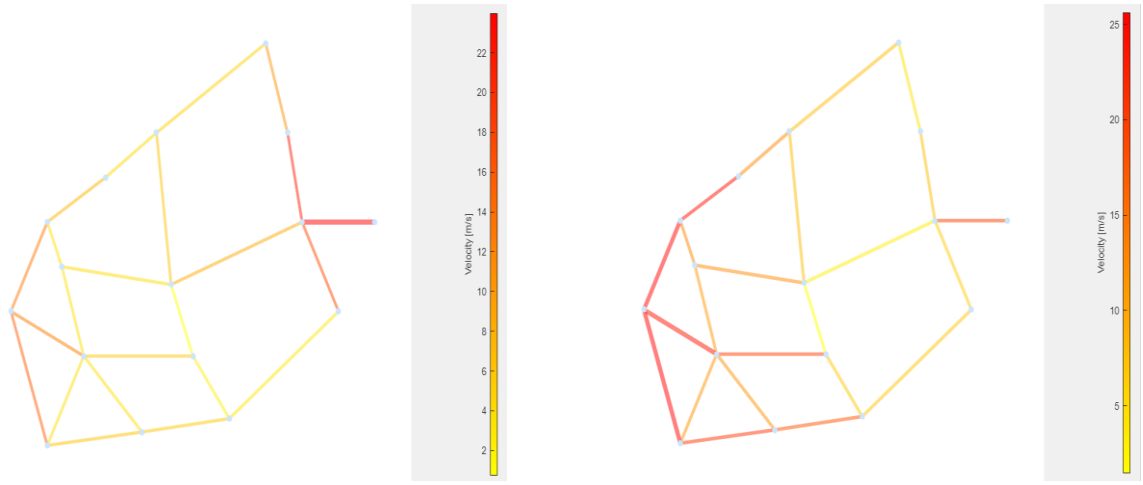

Figure 4.33: Gas velocity in the pipes in case 8a (left) and in case 8b (right)

As explained before, this simulation has been made keeping the thermal power supplied to the grid constant. Therefore, each demand node receives the right amount of energy, thanks to the quality tracking of the grid. With respect to the case in which the volumetric flow remains the same as the one of case 1 (figure 4.31), the composition of the gas in the network changes (figure 4.34).

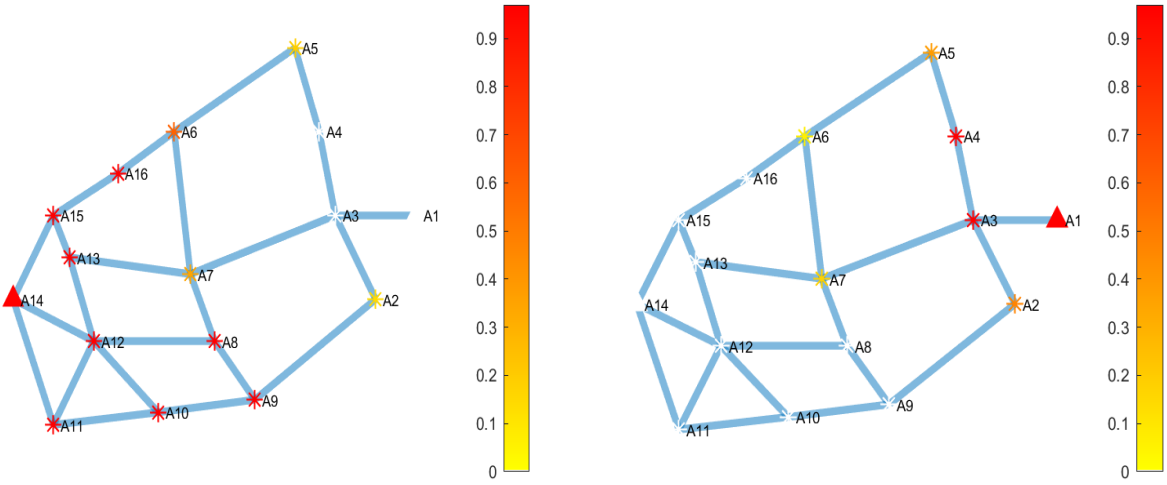

Figure 4.34: Gas quality tracking at the demand nodes when the thermal power is constant in case 8a (left) and in case 8b (right)

In case 8a, hydrogen is present in the gas withdrawn by six demand nodes (they were eight in the case of constant volumetric flow), whereas it is present in twelve nodes in case 8b (they were fourteen, so all the nodes, in the case of constant volumetric flow). The reason why this number goes down lies in the adjustments made to keep the velocity below the allowable limits when the volumetric flow is increased. The decrease of the pressure of hydrogen injection reduces its capability to travel along the network and so it becomes more difficult to reach the opposite side of the grid. Therefore, a lower number of nodes withdraw a gas containing hydrogen (figure 4.35).

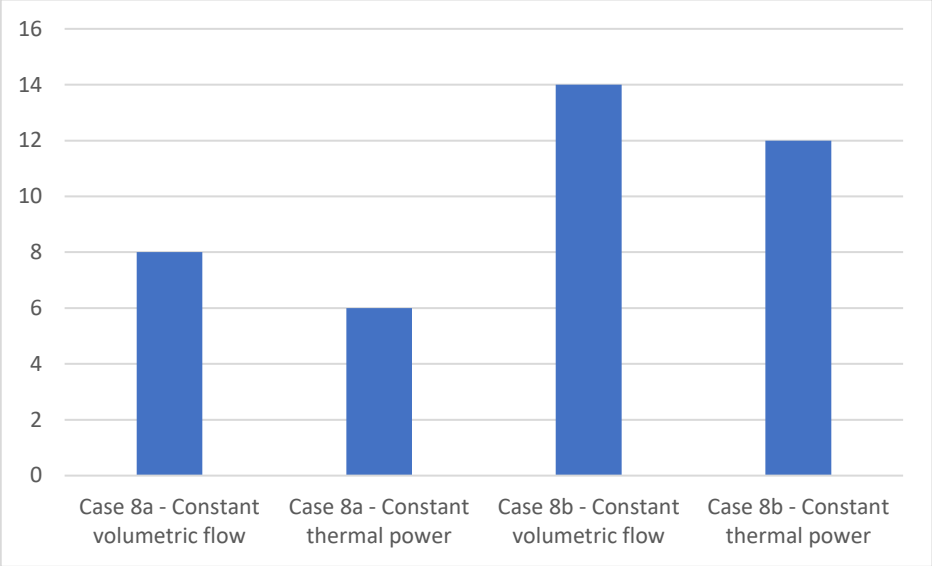

Figure 4.35: Number of demand nodes that receive a gas containing hydrogen (case 8)

In case 8a, the total volumetric flow is 18900 Sm^3/h (58% H_2), that is 67% higher than in case 1 and half of the flow injected in case 4c. The natural gas supplied is 71% of the one in case 1.

In case 8b, the total volumetric flow is 28566 Sm^3/h (87% H_2), that is 2,5 times higher than case 1 and 25% lower than case 4c. The natural gas supplied is 32% of the one in case 1.

The big difference in the amount of hydrogen injected among the two cases is because of the reasons explained before: the quantity of gas needed in the left region of the network is larger due to the higher energy demand, so the case 8b a lot of hydrogen injected in REMI B. Therefore, this case is the one in which a lower quantity of natural gas is needed to supply the grid, but the amount of hydrogen that has to be available is very high.

In table 4.27, the results of simulations 8a and 8b and the comparison with case 1 (100% natural gas) and case 4c (100% hydrogen) are reported.

Table 4.22: Main results of the simulations (case 8)

	Case 1	Case 4c	Case 8a	Case 8b
Max P loss (pipes) [bar]	0,586 (HP1)	0,154 (HP2)	0,461 (HP23)	0,841 (HP1)
Max P loss (pipes) [mbar/m]	0,858 (HP14)	0,286 (HP3)	0,802 (HP14)	1,202 (HP1)
Max F (pipes) [Sm^3/h]	3102 (HP14)	14655 (HP1)	10909 (HP1)	9342 (HP14)
Min F (pipes) [Sm^3/h]	261 (HP7)	361 (HP7)	135 (HP7)	252 (HP4)
Max velocity [m/s]	16,02 (HP14)	24,24 (HP3)	23,75 (HP1)	24,75 (HP14)
P in REMI A (A1) [bar]	5	5	4,6	5
P in REMI B (A15) [bar]	5	5	5	4,4
Min P (nodes) [bar]	4,33 (A5)	4,75 (A5)	4,36 (A5)	4,04 (A5)
F in REMI A (A1) [Sm^3/h]	3036	14655	10909	3610
F in REMI B (A14) [Sm^3/h]	8264	22914	7991	24956
Thermal input [MW]	105,2	105,2	105,2	105,2

5 Conclusions and future development

The energy transition of the last decades has generated an ever-greater interest on the introduction of renewable fuels into the energy market, with the objective of reducing and replacing the use of high-carbon fuels. Among the renewable fuels, this thesis has evaluated the use of biomethane and hydrogen, investigating, in particular, their impact on existing infrastructures and on distribution grids.

The first part of this work analyses the state of the art of the injection of biomethane and hydrogen in the pipelines and the potential problems connected to this kind of technology, together with the current uses and an outlook of the final uses of these alternative gases in the next years.

Regarding the biomethane, the following considerations on this analysis can be made:

- The biomethane has the advantage of being completely compatible with the natural gas grid, so it can be injected at the transmission and the distribution level without any change on the infrastructures. Moreover, it can be used by end-use systems (houses, industries, vehicles) without noticing any difference with respect to natural gas.
- Today, biomethane represents a small part of the natural gas demand (about 0,1%), but its market is rapidly growing, also due to the support of an increasing number of policies. The European countries, in particular Germany and France, together with the North America, are the ones that have exploited more the potential of the biomethane industry, but some countries from other parts of the world, such as Brazil and India, are catching up quickly.

With respect to the analysis on the hydrogen, the following main aspects can be evidenced:

- The projects of hydrogen blending in the natural gas grid have recently started in a lot of countries in the world. In most of them, the fraction of

hydrogen blended in the gas is still limited (1%, 2%, 5%), but a higher fraction of hydrogen has been injected in some trials, up to 20%. However, the number of projects is rapidly increasing and some projects that plan to build 100% H_2 grids in the next years have already been published.

- Unlike biomethane, the hydrogen properties largely vary with respect to those of natural gas: hydrogen is a much lighter gas and its combustion parameters are different from those of natural gas. Therefore, transport, storage and use of hydrogen ask for modifications on the infrastructures with respect to when natural gas is used.
- Durability and integrability of existing natural gas pipelines can be affected by hydrogen presence because it degrades mechanical properties of steel (embrittlement). Thus, the fraction of hydrogen that can be injected into the grid without adjustments of the infrastructures is limited. Some studies consider the limit between 10% and 25%, depending on the pressure of the gas transported. Regarding plastic pipelines, so at the distribution level, hydrogen has no significant degradation, therefore there is not a limit of the hydrogen fraction contained in the gas.
- Most of the existing utilities, such as gas turbines and gas engines, can work without the need for adjustments at low levels of hydrogen blending in the natural gas, up to 5% or 10% depending on the utility. It has been demonstrated that domestic appliances can be safely used with hydrogen concentrations up to 30%.

In the second part of this work, a simulation model has been implemented in order to analyse the effect of the presence of the alternative gases in a natural gas network.

First, several assumptions concerning the fluid-dynamics of compressible flows have been validated against more accurate models, with the following results:

- ISO-12213 establishes the standard requirements for the calculation of the compressibility factor z, accounting for the non-ideality of the gas by means of an implicit equation. For the natural gas (and biomethane), it has been demonstrated that some explicit correlations (AGA, Papay) and an Excel tool (Refprop) can be good alternatives at the distribution level, showing low discrepancies (0,07% for AGA, 0,28% for Papay, 0,02% for Refprop) in the pressure range of the distribution lines ($p < 5$ bar).
- The blending of hydrogen in the natural gas has a strong influence on the value of z. At the distribution level, Papay and Refprop accurately describe the non-ideality of the gas for all the fractions of hydrogen in the gas (10%, 20%, 50%, 100%), whereas AGA is not accurate for significant fractions of hydrogen (50%, 100%).

- The Hofer explicit approximation of the Colebrook-White equation is the reference for the friction factor *f* calculation for all the levels of hydrogen in the gas, whereas the other correlation examined, the Chodanovic-Odischarija, is not accurate for a gas containing more than 50% of hydrogen.

After having defined the fluid dynamics of the model, the grid structure of the network studied has been created using a Matlab program. Several simulations have been made, starting from a 100% natural gas grid and then adding injections of biomethane and hydrogen in different positions of the grid and with different flow rates.

Considering biomethane, the following results are obtained:

- Biomethane is assimilable to natural gas. Therefore, its injection does not influence the velocity of the gas through the pipes or the gas composition at the demand nodes. Thus, gas quality tracking is not required.
- The main concerns about biomethane injection regard the pressure of the gas in the network. If the injected amount is higher than the load of the branch it insists on, a pressure issue is reached ($p > 5$ bar). The maximum pressure is overcome as the exceeding biomethane amount is forced to flow towards the main injection point. To avoid it, an intervention of the DSO (Distribution System Operator) is necessary in order to decrease the pressure of injection of the natural gas and keep the pressure level lower than the limit in all the points of the grid.
- The factors that influence the biomethane injection are the position of injection and the quantity supplied to the network. For low amounts (up to 2000 Sm^3/h, 18% of the total gas demand), there is no need for an intervention on the grid, independently on the position. When a larger flow of biomethane is injected, depending on the place of injection, management of the grid is required. From this point of view, the decentralized injection should be placed next to a large customer (like an industry) and in a lowly loaded branch (low concentration of nodes near the customer).
- When the pressure at the natural gas stations is lowered, the pressure level in all the demand nodes also decreases. Considering the same amount of biomethane injected in different places of the network, the pressure level in the network is lower when the biomethane is injected in an unfavourable position of the grid, near a REMI station or in a highly loaded branch.

Regarding hydrogen, the following results are obtained:

- The different properties of hydrogen, compared to natural gas, imply that the injection of hydrogen does not only influence the pressure of the gas at

the nodes, like biomethane, but also the velocity of the gas through the pipes. Moreover, in the case of a decentralized injection, gas quality tracking is required because the composition of the gas changes after the mixing between natural gas and hydrogen and it is necessary to know the heating value of the gas supplied to the withdrawal nodes.

- The analysis on the presence of different fractions of hydrogen (5%, 10%, 20%, 50%, 100%) in the gas supplied to the network shows that the lower heating value (in [MJ/Sm^3]) of the mixture linearly decreases as the fraction of hydrogen goes up. Therefore, the volumetric flow needed in order to keep the thermal input constant has to increase (non-linearly). Because of this fact, without any further modification to the network parameters, the pressure drops through the pipes increase, as well as the velocity, whereas the gas pressure at the demand nodes decreases.
- When the network is supplied by 100% H_2, the volumetric flow rate entering the grid has to increase by 3,4 times compared to the natural gas case in order to keep the thermal power supplied to the withdrawal nodes constant. The large volumetric flow through the pipes leads to a problem concerning the gas velocity, that overcomes the allowable limit (25 m/s) in the tubes connected to the injection points (in which the volumetric flow is larger). A possible solution, used in this work, is to add a tube in parallel to the ones in which the velocity problem is more critical, so that the passage area increases and the gas is slowed down. In particular, the section has been increased by four times in the pipe connected to the injection point in the right area of the network, whereas the section of the three pipes linked to the station in the left side of the network has been doubled. As a result, the pressure of the gas at the demand nodes is higher than in the natural gas case, despite the higher volumetric flow that would cause larger pressure drops, reduced by the diameter increase.
- Like the biomethane, a decentralized hydrogen injection is influenced by the position of injection and the quantity supplied to the network. From the point of view of the pressure, a larger quantity, compared to biomethane, can be injected before needing an intervention of the DSO on the network to keep the pressure lower than 5 bar. In fact, until 6000 Sm^3/h of hydrogen supplied (39% of the total gas demand) the pressure is below the allowable limit in all the injection positions analyzed. Also, the velocity of the gas through the pipes does not create problems until large amounts of hydrogen are injected (depending on the positions); once it becomes higher than 25 m/s, an increase of the diameter of the pipes is necessary.
- When natural gas and hydrogen mix in the network, the density and the heating value of the gas can be different in each withdrawal node. Therefore,

the gas quality tracking becomes crucial when a decentralized hydrogen injection is present. It is fundamental to control not only that the right amount of gas enters the grid, in order to keep the thermal power introduced constant, but also that the energy supplied to each node satisfies the demand. In the network considered, it has been calculated, by an iterative procedure, that, as the amount of hydrogen injected increases, the total volumetric flow needed by the network linearly goes up. Every 500 Sm^3/h of hydrogen supplied, the total gas demand increases by 350 Sm^3/h (with respect to the case without decentralized injection), resulting in a decrease of the natural gas demand of 150 Sm^3/h, regardless of the position of injection.

- When the hydrogen supply is not treated like a decentralized injection, so at a fixed flow rate, but it enters the grid at a fixed pressure (like natural gas), the same problems about velocity can occur. The diameter increase can be insufficient to fix the problem, since a larger quantity of gas would be introduced, so the other adjustment that needs to be made is to decrease the injection pressure, in order to limit the amount of hydrogen entering the grid and, so, keeping the velocity below the allowable limits.

Furthermore, some parameters that aim to rank the demand nodes, in order to do a priori evaluation on which positions of the network are more convenient to place a decentralized injection (from the point of view of the need for an intervention of the DSO) have been introduced. The goal is to generalize these parameters to the real grids, composed of thousands of nodes. The parameters considered, η and σ, consider, for each withdrawal node, the gas demand, the distance from the other nodes and its distance from the natural gas injection stations. Two ways to link these two parameters have been proposed, represented by μ_1 and μ_2. The following considerations can be made:

- By the analysis made in different positions of injection of hydrogen and biomethane, the parameter that seems to have a more significant influence is σ, that is an indicator of the distance of the node taken in consideration by the REMI stations. The other parameter, η, that indicates the flow rate withdrawn by the node considered weighted on the distance from the other nodes, is also important, but it has a minor impact on the choice of the injection position. This fact has been demonstrated, for example, by the injection near the nodes A2 and A11: A2 has the lowest value of η (that should be maximized) among all the nodes and one of the lower values of σ (that should be minimized, so it is good), and the analysis shows that it is one of the best nodes (from the point of view of the DSO) near which placing the decentralized injection; A11 has the highest value of σ and, in fact, it seems to be the worst node in which injecting the alternative fuel.

- Two ways of linking η and σ have been presented, indicated by $\mu_1$and μ_2. Among them, even if they provide similar results, the one that seems more suitable is μ_1, that sums η and σ. This fact can be understood by the node A4: according to μ_2, it should be the best node for an injection, but the analysis has shown that a larger amount of alternative gas can be injected near A2 and A6, that agrees with the ranking of the nodes based on μ_1.

The major limitations of this work regard the fact that a simplified grid in a stationary condition has been analysed. Therefore, some improvements and additional cases should be investigated in future development:

- Investigation of more complex grids (thousands of nodes) in order to generalize the observed behaviours in presence of more possible pathways for the gas.
- Analysis of a non-stationary condition, varying the demand of gas in time, in order to simulate the actual amount of gas (and heating value) delivered on a single customer during a day.
- Presence of more decentralized injections, in order to assess if an even more distributed supply is either helpful or detrimental.
- Generalization of the parameters used to do a priori evaluation on which positions of the network are more convenient to place a decentralized injection, taking into account the mesh of the grid, the demand profile of the nodes, the possibility to have more than one decentralized injection.

Bibliography

[1] European Commission, [Online]. Available: https://climate.ec.europa.eu/eu-action/climate-strategies-targets/2050-long-term-strategy_en. [Accessed November 2022]

[2] International Energy Agency, "IEA", [Online]. Available: https://www.iea.org/reports/net-zero-by-2050. [Accessed November 2022].

[3] Snam, Global gas report 2022 [Online]. Available: https://www.snam.it/en/energy_transition/reports/global_gas_report. [Accessed November 2022].

[4] D.M. 16-04-2008, Regola tecnica per la progettazione, costruzione, collaudo, esercizio e sorveglianza delle opera e dei sistemi di distribuzione e di line dirette del gas naturale con densità non superiore a 0.8.

[5] International Energy Agency, "IEA", [Online]. Available: https://www.iea.org/reports/outlook-for-biogas-and-biomethane-prospects-for-organic-growth/an-introduction-to-biogas-and-biomethane. [Accessed November 2022].

[6] International Energy Agency, "IEA", [Online]. Available: https://www.iea.org/reports/energy-technology-perspectives-2020/etp-model. [Accessed November 2022].

[7] Gas Infrastructure Europe, "GIE", [Online]. Available: https://www.gie.eu/publications/maps/european-biomethane-map/. [Accessed November 2022].

[8] HYGAS report, "Pipeline gas from coal-hydrogenation (IGT hydrogasification process", 1975.

[9] H21 website, [Online]. Available: https://h21.green/. [Accessed November 2022].

[10] HyDeploy, "HyDeploy: the UK's first hydrogen blending deployment project", [Online]. Available: https://hydeploy.co.uk/hydrogen/. [Accessed November 2022].

[11] Hydrogen Central, "E.ON, Avacon and DVGW announce 20 percent hydrogen in the german gas network for the first time", [Online]. Available: https://hydrogen-central.com/eon-avacon-dvgw-20-percent-hydrogen-german-gas-network/. [Accessed November 2022].

[12] ATCO, "Fort Saskatchewan Hydrogen blending project", [Online]. Available: https://gas.atco.com/en-ca/community/projects/fort-saskatchewan-hydrogen-blending-project.html. [Accessed November 2022].

[13] Grande Region Hydrogen, "MosaHYc", [Online]. Available: https://grande-region-hydrogen.eu/en/projects/mosahyc/. [Accessed November 2022].

[14] Snam, "Snam: Europe's first supply of hydrogen and natural gas blend into transmission network to industrial users", [Online]. Available: https://www.snam.it/en/Media/Press-releases/2019/Snam_Europe_first_supply_hydrogen_natural_gas_blend.html. [Accessed November 2022].

[15] Snam, "Snam: hydrogen blend doubled to 10% in Contursi trial", [Online]. https://www.snam.it/en/Media/news_events/2020/Snam_hydrogen_blend_doubled_in_Contursi_trial.html. [Accessed November 2022].

[16] Snam, "Snam, RINA e Gruppo GIVA: effettuato primo test al mondo con un mix di gas naturale e idrogeno al 30% nella lavorazione dell'acciaio", [Online]. https://www.snam.it/it/media/comunicati-stampa/2021/Snam_RINA_Gruppo_GIVA_primo_test_al_mondo_mix_gas_naturale_idrogeno_acciaio.html. [Accessed November 2022].

[17] Società Gasdotti Italia (SGI), "HyBRIDS", [Online]. https://www.gasdottitalia.it/en/content/hybrids-project. [Accessed November 2022].

[18] Australian Gas Infrastructure Group, "Hydrogen Park South Australia", [Online]. https://www.agig.com.au/hydrogen-park-south-australia. [Accessed November 2022].

[19] SGN Natural Gas, "H100 Fife", [Online]. https://www.sgn.co.uk/H100Fife. [Accessed November 2022].

[20] Engie, "The GRHYD demonstration project", [Online]. https://www.engie.com/en/businesses/gas/hydrogen/power-to-gas/the-grhyd-demonstration-project. [Accessed November 2022].

[21] Compressor Tech2, "Enbridge hydrogen blending project now operational", [Online]. https://www.compressortech2.com/news/enbridge-hydrogen-blending-project-now-operational/8017456.article. [Accessed November 2022].

[22] J. Leicher, J. Schaffert, H. Cigarida, "The impact of hydrogen admixture into natural gas on residential and commercial gas appliances", *Energies* 2022, 15, 777.

[23] G. Pluvinage, J. Capellle, M. Hadj Meliani, "Pipe networks transporting hydrogen pure or blended with natural gas, design and maintenance", *Engineering failure analysis* 106, 2019

[24] ASME B31G. 12-2019 "Hydrogen piping and pipelines ASME codes for pressure piping", American Society of Mechanical Engineers, 2019.

[25] H. Wang, Z. Tong, G. Zhou, C. Zhang, H. Zhou, Y. Wang, W. Zheng, "Research and demonstration on hydrogen compatibility of pipelines: a review of current status and challenges", *International journal of hydrogen energy 47* (2022), 28585-28604.

[26] H. Kyriakopoulou, P. Karmiris-Obratanski, A. Tazedakis, "Investigation of hydrogen embrittlement susceptibility and fracture toughness drop after in situ hydrogen cathodic charging for an X65 pipeline steel", *Micromachines* 2020, 11(4),430.

[27] M.-H. Klopffer, P. Berne, E. Espuche, "Development of innovating materials for distributing mixtures of hydrogen and natural gas. Study of the barrier properties and durability of polymer pipes", *Oil and gas science and technology,* 2015, 70 (2), pp. 305-315.

[28] IEE Fraunhofer, "The limitation of hydrogen blending in the European gas grid", 2022.

[29] HyGrid project, "Industrial specifications for a system to recover hydrogen from natural gas grids", 2016.

[30] J. Jaworski, P. Kulaga, T. Blacharski, "Study on the effect of addition of hydrogen to natural gas on diaphragm gas meters", *Energies* 2020, 13, 3006.

[31] M. Dell'Isola, G. Ficco, L. Moretti, J. Jaworski, P. Kulaga, E. Kukulska-Zajac, "Impact of hydrogen injection on natural gas measurement", *Energies* 2021, 14, 8461.

[32] Hy4Heat Project closure report, "Hydrogen odorant and leak detection, part 1", 2020.

[33] IEA, "Global Hydrogen Review 2022", [Online]. https://www.iea.org/reports/global-hydrogen-review-2022. [Accessed November 2022].

[34] IEA, "Global Hydrogen Review 2021", [Online]. https://www.iea.org/reports/global-hydrogen-review-2021. [Accessed November 2022].

[35] D. Matko, G. Geiger, W. Gregoritza, "Pipeline Simulation Techniques", *Mathematics and Computers in simulation*, no. 52, pp. 211-230, 2000.

[36] A. Herràn-Gonzàlez, J. De La Cruz, B. De Andrès-Toro, J. Risco-Martìn, "Modeling and simulation of a gas distribution pipeline network". *Applied Mathematical Modelling*, no. 33, pp. 1584-1600, 2009.

[37] M. Schmidt, M. C. Steinbach, B. M. Willert. "High detail stationary optimization models for gas networks". *Optim Eng* (2015) 16:131-164.

[38] National Institute of standards and technology, "NIST".

[39] ISO 12213-2, "Natural gas – Calculation of compression factor, part 2: calculation using molar-composition analysis", Second edition, ISO 2006.

[40] P. Brenner, S. Grubdel, C. Himpe, C. Huck, T. Streubel, C. Tischendorf, "Gas Network Benchmark Models".

[41] UNI 9165:2004, Reti di distribuzione del gas – Condotte con pressione massima di esercizio minore o uguale a 5 bar – Progettazione, costruzione, collaudo, conduzione, manutenzione e risanamento

List of Figures

List of Tables

List of symbols

Variable	Description	SI unit
T	Temperature	K
p	Pressure	Pa
d	Density	kg/m^3
H_S	Gross calorific value	MJ/m^3
WI	Wobbe Index	MJ/m^3
S_L	Laminar combustion velocity	m/s
φ	Equivalence ratio	-
λ	Air excess ratio	-
th	Nominal wall thickness	m
V	Potential	V
S	Minimum yield stress	Pa
F	Strength design factor	-
E	Weld factor	-
G	Temperature derating factor	-
H_f	Material performance factor	-
t	time	s
u	Axial velocity	m/s
x	Axial coordinate	m
f	Darcy friction factor	-
θ	Inclination angle	rad
e	Specific energy	J/kg
P	Perimeter	m
A	Cross-section area	m^2
Z	Compressibility factor	-
MM	Molecular weight	kg/kmol
R	Universal gas constant	J/mol/K
F	Standard volumetric flow rate	Sm^3/s
L	Length	m
g	Gravitational acceleration	m/s^2
Tc	Critical temperature	K
p_c	Critical pressure	bar

T_{pc}	Pseudo-critical temperature	bar
p_{pc}	Pseudo-critical pressure	bar
T_{pr}	Pseudo-reduced temperature	-
p_{pr}	Pseudo-reduced pressure	-
x_i	Molar fraction	-
y_i	Mass fraction	-
Re	Reynolds number	-
ε	Roughness	m
k	Thermal conductivity	W/m/K
LHV	Lower heating value	MJ/kg
$\dot{m}$	Mass flow rate	kg/s
π	Pi	-
$\dot{Q}$	Thermal power	W
N_d	Number of demand nodes	-
η	Parameter for the nodes ranking	$Sm^3/s/m$
σ	Parameter for the nodes ranking	$Sm^3/s/m$
μ_1	Parameter for the nodes ranking	$Sm^3/s/m$
μ_2	Parameter for the nodes ranking	-

List of acronyms

Name	Description
Max	Maximum
Min	Minimum
IEA	International Energy Agency
ISO	International Organisation for Standardisation
UNI	Ente Nazionale Italiano di Unificazione
REMI	Cabina di Regolazione e Misura
AGA	American Gas Association
DSO	Distribution System Operator
MOP	Maximum Operating Pressure
P2G	Power-To-Gas
SMR	Steam Methane Reformer

Acknowledgments

Ringrazio profondamente i professori Giulio Guandalini e Paolo Colbertaldo per avermi seguito costantemente e con grande pazienza nella realizzazione di questa tesi, per avermi sempre stimolato e suscitato interesse negli argomenti trattati. Grazie anche per avermi permesso di lavorare con la dovuta calma e serenità, senza mai mettermi alcuna pressione. Grazie anche a Federico per la sua disponibilità nell'aiutarmi a risolvere i problemi affrontati in Matlab.

Grazie alla mia famiglia per avermi sempre supportato in questi cinque anni, per avermi permesso di portare avanti i miei studi senza chiedere nulla in cambio e senza mai mettermi alcun tipo di pressione sui risultati da ottenere.

Un grande ringraziamento va a tutti i miei amici, per essere sempre stati in grado di farmi svagare e farmi staccare la testa dagli impegni universitari, e a tutti i miei compagni di studio, quelli con cui ho condiviso tutto il percorso e quelli con cui ho passato solo gli ultimi mesi, senza i quali le lunghe giornate passate in università sarebbero risultate infinitamente più pesanti. Un grazie soprattutto a Ribo, Tommi e Marco, fedelissimi compagni di studio con cui ho condiviso lunghe sessioni di studio, ansie e gioie.

Infine, grazie al Politecnico, per avermi sempre messo a dura prova e per avermi preparato ad affrontare il mondo.